# Progressive damage analysis of CFRP Laminate with circular cutouts under flexural loading

S.Gurucharan

A Thesis Submitted to

Indian Institute of Technology Hyderabad

In Partial Fulfillment of the Requirements for
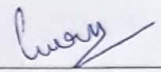
The Degree of Master of Technology



भारतीय प्रौद्योगिकी संस्थान हैदराबाद
Indian Institute of Technology Hyderabad
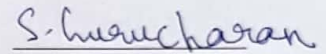
Department of Mechanical Engineering
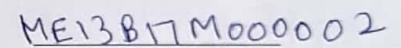
June 2018

# Declaration

I declare that this written submission represents my ideas in my own words, and where ideas or words of others have been included, I have adequately cited and referenced the original sources. I also declare that I have adhered to all principles of academic honesty and integrity and have not misrepresented or fabricated or falsified any idea/data/fact/source in my submission. I understand that any violation of the above will be a cause for disciplinary action by the Institute and can also evoke penal action from the sources that have thus not been properly cited, or from whom proper permission has not been taken when needed.
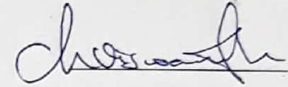
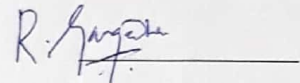(Signature)

S. Gurucharan

(Student Name)

ME13B17M000002

(Roll Number)

# Approval Sheet

This Thesis entitled Progressive damage analysis of CFRP Laminate with circular cutouts under flexural loading by S.Gurucharan is approved for the degree of Master of Technology from IIT Hyderabad
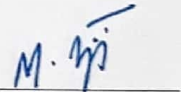
(Dr. Viswanath Chinthapenta, Assistant Professor) Examiner
Dept. of Mechanical and Aerospace Engineering
IIT Hyderabad

(Dr. Gangadharan Raju, Assistant Professor) Examiner
Dept. of Mechanical and Aerospace Engineering
IIT Hyderabad

(Dr. Syed Nizamuddin Khaderi, Assistant Professor) Examiner
Dept. of Mechanical and Aerospace Engineering
IIT Hyderabad

(Dr. M. Ramji, Associate Professor) Adviser
Dept. of Mechanical and Aerospace Engineering
IIT Hyderabad

(Dr. S. Suriya Prakash, Associate Professor) Chairman
Dept. of Civil Engineering
IIT Hyderabad

# Acknowledgements

# Dedication

To family, teachers and friends

# Abstract

Application of a flexural or bending load on a Carbon fiber reinforced polymer(CFRP) specimen leads to both tensile and compressive stress state across the thickness of the specimen thereby resulting in a more complex damage behavior as the tensile and compressive failure modes of a composite material are different. Study of damage behavior of specimen includes location of damage initiation, damage propagation, various types damage modes and their interactions, prediction of damage initiation load and final failure load. Damage behavior of the CFRP specimen has to be studied for its efficient and sustainable design. In the present thesis, damage behavior of pristine CFRP specimen (without hole), specimen with both single circular hole and multiple circular holes having three different configurations (two hole longitudinal (2HL), two hole transverse (2HT) and two hole diagonal (2HD)) was studied both experimentally and numerically under four point flexural loading. The layup sequence of the CFRP specimen having Unidirectional (UD) $[0]_{16}$ and Quasi-isotropic $[-45/0/45/90]_{2s}$ are studied. Two-dimensional Digital Image correlation(DIC) technique was employed for capturing the in-plane displacement and strains across the thickness of the specimen.

Finite element (FE) based Progressive damage analysis(PDA) the CFRP specimen was performed. In the progressive damage model, Hashin's failure criteria was implemented for the prediction of damage initiation of both fiber or matrix at a lamina level, material property degradation model was implemented for modelling damage evolution in the specimen and cohesive zone model was implemented for predicting the intiation and propagation of interlaminar delamination between layers of the specimen. Damage behavior of the specimen obtained from experiment was compared with the results obtained from PDM for validation. Additionally, the variation of load vs displacement, longitudinal strain distribution over the thickness face of the CFRP specimen obtained both experimentally and numerically were studied and the corresponding plots obtained from both were compared.Finally, the load carrying capacity of pristine specimen, specimen with single hole and specimen with multiple holes with three different configurations (2HL,2HT and 2HD) were compared and it was also seen which type of specimen according to the two lay up sequences which are unidirectional $[0]_{16}$ and Quasi $[-45/0/45/90]_{2s}$ was more stiffer and stronger.

# Contents

# List of Figures

# List of Tables

# Chapter 1

# Introduction and Literature Review

## 1.1 Introduction

Composite is a material which is formed by combining two or more constituent materials with significantly different physical and chemical properties on a macroscopic scale such that it has different characteristics and properties from the individual constituent components. Generally there are two constituent materials which form the composite namely reinforcement and matrix. Fiber reinforced composite is a type of composite where the reinforcement is fiber. The role of fiber is to provide stiffness and strength to the composite and this stiffness and strength is more than those of the individual fibers itself. Thereby fiber is the constituent of the composite which resists any external load. The role of the matrix is to bind the fibers together, transfer the load between fibers and protect the fibers from being degraded to the environment. Composites can be classified into different types according to the type of reinforcement material, matrix material and arrangement of the reinforcement in the matrix. A lamina or ply is a typical sheet of composite material which consists of many fibers embedded in a matrix material. A laminate is a collection of lamina stacked so as to achieve the desired thickness, stiffness and strength.



<div align="center">(a)        (b)</div>

<div align="center">Courtesy: www.compositestoday.com</div>

Figure 1.1: a) Composite used in fuselage of aircraft b)Composite fuel tank constructed by NASA and boeing

There is a huge demand on aircraft and automobile industries, which are very high profit industries, to reduce the weight of their products but by not also compromising much on the strength and stiffness so as to reduce fuel usage and reduce the emission of pollutants into the environment, thereby making the products more environment friendly.Since, composites are found to have improved engineering properties than conventional materials such as metals such as stiffness/weight ratio, strength/weight ratio, fatigue life, thermal properties and corrosion resistance, they can serve the above purpose. Composites nowadays also find applications in other industries such as marine, civil , military etc. Figure 1.1 shows composites being used in the fuselage of a Boeing 787 aircraft. Nowadays, composites are fast replacing metals in most of the aircraft parts. Figure 1.2 shows the percentage of materials used in the parts of an aircraft. From the figure it is seen that composite material is used in exactly half the parts of an aircraft.
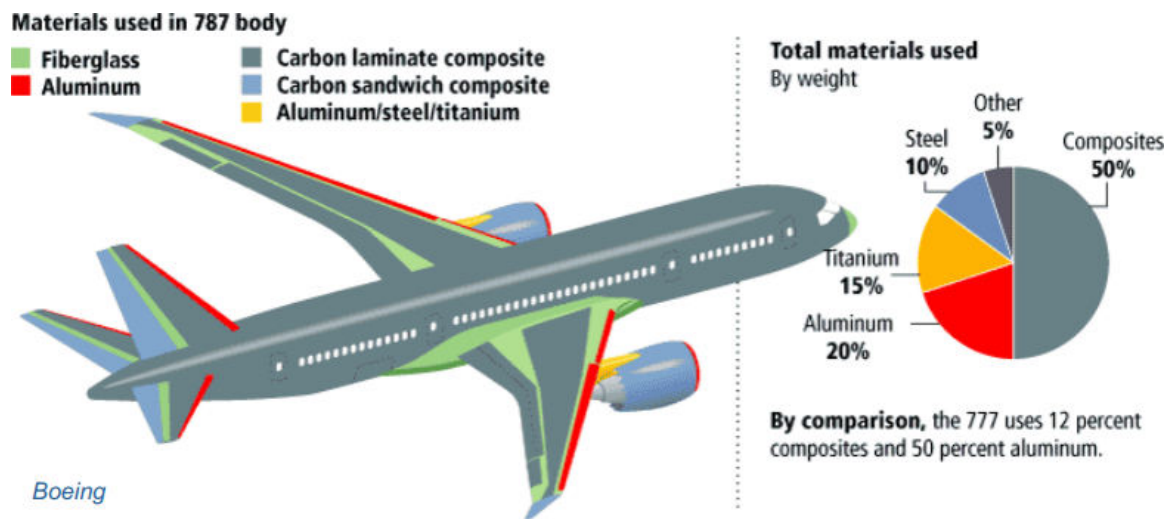
Figure 1.2: Percentage of different materials used in fuselage of Boeing 787 aircraft
Courtesy: www.boeing.com

Flexural or bending load can be applied on a structure in two ways, either by applying a pure moment along an axis which is perpendicular to longitudinal axis of the structure or by applying an transverse load to a structure, which is, a load which is perpendicular to the longitudinal axis of the structure. As shown in Figure 1.3, when flexural load or moment is applied to a structure, the structure bends in such a way that there will be an axis along the where there is be no deformation and this axis is known as neutral axis. In an homogeneous structure, neutral axis will pass through the centroid of the structure. The region above the neutral axis will be in compression and the region below the neutral axis will be in tension. Thereby, there will be both compressive and tensile stress state present across the thickness of the specimen. At any cross section of the structure, there will be a linear variation of strain along the width of the structure with the value of strain at any point on the neutral axis being zero.

Parts of structures which are being used in industry are also subjected to flexural loading. For example, take the case of wings of an aircraft. The loads which act on it are force due to weight of the aircraft itself which acts vertically downwards and the lift force due to wind pressure which acts vertically upwards. This particular scenario can be modeled in such a way that the wing can be treated as a beam, body of the aircraft can be treated as support to which the beam is fixed, force
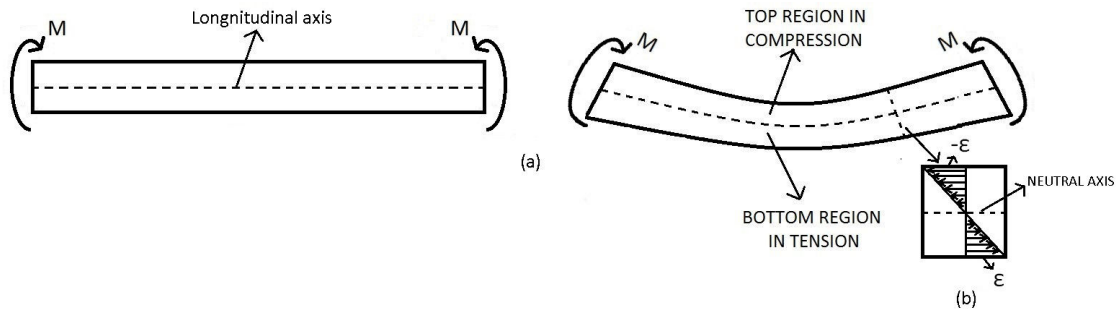
Figure 1.3: a) Deformation of structure when subjected to pure bending (b) Variation of strain along the width of the structure through any cross section

due to weight of aircraft and lift force can be treated as distributed loads acting throughout the length of the beam. While the aircraft is taking off, the lift force is more than the force due weight of the aircraft and therefore the wings bends upwards, due to which the top most part of the wind will be under compression and the bottom most part of the wind will be under tension. Diagram of bending of wings during take off is shown in Figure 1.4 While the aircraft is landing, the force due to weight of the aircraft is more than the lift force and therefore the wings bends downwards, due to which the top most part of the wind will be under tension and the bottom most part of the wind will be under compression.
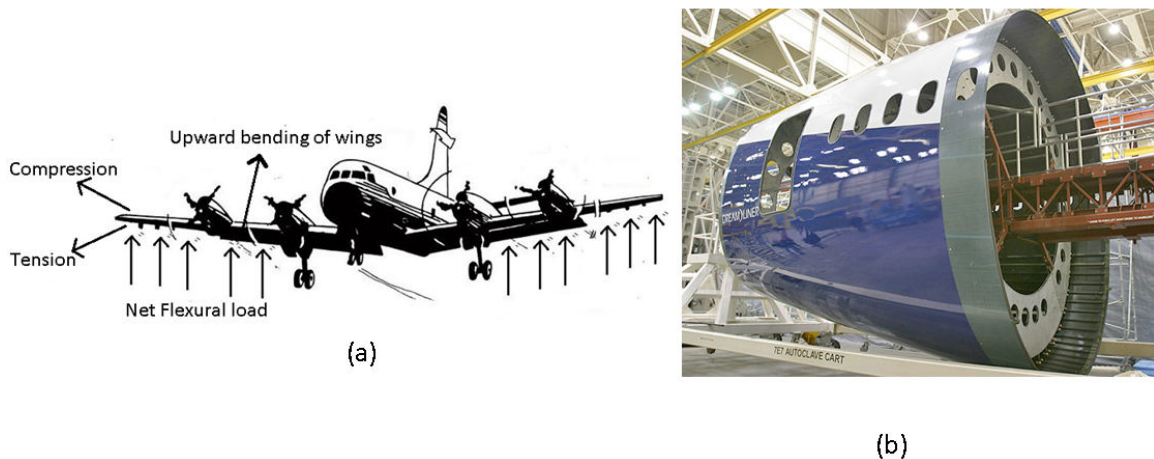


Figure 1.4: a) Bending of wings of an aircraft during takeoff b) Cutouts introduced in fuselage of Boeing dreamliner aircraft
Courtesy: google images with modifications in image (a)

As the flexural load applied to the composite structure increases, certain damage mechanisms which does not involve only fiber initiates and propagates in the structure. But these damage mechanisms do not reduce the load carrying capacity of the composite structure. The load at which damage initiates in the structure is known as failure initiation or first ply failure load. At a critical value of load applied, the fibers in the composite structure starts breaking and that is when the load carrying capacity of the structure reduces and the structure finally fails. This critical load is known as the final failure load or ultimate load. Damage mechanisms in a composite laminate can

be of interlaminar or intralaminar level. Interlaminar damage include delamination, which is the separation of layers of the laminate. Intralamainar damage include, fibre breakage, matrix cracking and fiber kinking. All these mentioned damage mechanisms will be explained in detail later in this chapter. Cutouts or holes are required in structures due to functional requirements like wiring, assembly, piping, visual inspection etc. With the presence of holes in the structure, damage becomes more severe as the holes act as a stress riser.In most of the cases, multiple holes are required in the structure and due to the interaction of these holes, damage becomes even more severe. There are cases where the the structure is to loaded in more than one direction and because of this, it requires high strengths in one than one direction. To satisfy this, the orientation of the fibres in the laminae or plies of the composite laminate are changed to different angles. Examples of such types of laminates include cross-ply laminate, angle ply laminates, quasi-isotropic laminates. Cross-ply laminate is a type of laminate where the plies in the laminate are oriented either at 0 or 90 degrees, for example [0/90/0/90/0] Angle-ply laminate is a type of laminate where plies of the material are oriented at an angle and negative of the angle, for example [45/-45/-30/30]. Quasi-isotropic laminates are laminates where the plies are oriented in such a way that the relative angle between any two consecutive plies are same and the resultant laminate is isotropic, for example $[45/0/-45/90]$. Study of damage behavior of the composite structure involves determination of load at which damage initiates in the structure, location at which damage initiates, how the damage propagates, various types of damage mechanisms which occur and their interactions and determination of final or ultimate failure load. In order to design the structure efficiently so that it can sustain load upto its full capacity and thereby exploiting the full advantage of composites over conventional materials, it is required to perform progressive damage analysis of a composite laminate having holes and of different lay-up sequences. This particular type of design is known as damage tolerant design.

## 1.2 Literature Review

Various research studies have been done on effect of flexural loading on composites, damage behavior of composites under flexural loading. Researchers have tried to study damage behavior for different configurations of flexural loading through certain experimental methods and also through some numerical methods like the conventional finite element method. Certain analytical models were developed to predict initiation and evolution of failure. Studies were done for composite laminates having no hole, having single hole of circular, elliptical or square shape, and also having multiple holes. This section summarizes the various studies which have been done on mechanical and damage behavior of composite laminates under flexural loading.

### 1.2.1 Composites without hole

In 1989, J.K.Chen[1] tried to investigate the elastic-plastic response of interlaminar stresses in boron-aluminum metal-matrix composites composite laminates due to bending and torsion. The plasticity model used is a general three-dimensional orthotropic yield criterion, which is quadratic in stresses, in conjunction with incremental flow theory. The results, including bending moment-curvature relations, growth of plastic zones, and distribution of interlaminar stresses, are presented.In 1991, P.D.Copp [2] performed failure analysis of carbon-carbon composite materials under three point bending. Here, damage initiation and failure mechanisms in woven uncoated carbon-carbon com-

posite laminates were determined experimentally through three point bending test. A linear finite element analysis was conducted to predict damage initiation analytically in the tested specimens. Tsai-Wu failure criteria was employed for this purpose. Finally, comparison of experimental and analytical predictions were made. Failure modes and damage initiation sites were also determined for different length to depth ratios.In 1992, J.N.Reddy [3] developed a finite element computational procedure to find linear and non-linear first-ply failure loads of composite laminates subjected to in-plane and transverse loads. The finite element model is based on first-order shear deformation theory and several phenomenological failure criteria. Linear and non-linear first-ply failure loads are computed for a uniformly distributed transverse load, a concentrated transverse load acting at the centre of the plate, and a uniformly distributed in-plane edge load for simply supported and clamped boundary conditions. In 1993, Sheng Liu [4] tried to fundamentally study the interaction between matrix cracking and delamination propagation in composite structures resulting from transverse loadings. An analytical model was developed which consists of a stress analysis for calculating stresses and strains in the composites, and a failure analysis for predicting matrix cracking and delamination growth.This particular study was also performed through non-linear finite element method. Experiments were also performed to verify the model proposed and numerical calculations. Also in 1995, T.Y.Kam [5] presented an analytical method which was developed from Von Karman-Mindlin plate theory and Ritz method to study the non-linear behaviors and first ply failure strengths of centrally loaded composite plates with semi-clamped edges. This method was also used to construct nonlinear load-deflection curves of composite plates and also to predict the first-ply failure loads based on various commonly used strength of material type failure criteria.Also, Experiments on laminated composite plate was performed to identify the first ply failure loads using acoustic emission technique and also to construct the load-displacement curve. The experimental results were used to investigate the capabilities of the analytical method used to predict the first-ply failure load and nonlinear behavior of the laminated composite plates. In 1997, G.S.Padhi [6] presented an analytical method to study the non-linear behaviour, first ply failure and ultimate collapse of laminated composite plates of three different aspect ratios with clamped edges,subjected to transverse pressure. Here, Hashin's and Tsai Wu failure criteria was used to predict failure initiation. For predicting failure propagation, stiffness reduction is carried out at the Gauss points of the finite element mesh depending on the mode of failure. This model was incorporated into a Finite element program. The results predicted by this model is compared with experimental data for validation. In 2001, L.Dufort [7] provided an experimental evidence of cross section warping in beams under three point bending through a suitable optical method. This method was used to measure the whole displacement field onto one of the lateral surfaces of two short composite beams. The corresponding displacement field and and warping of cross section was also studied through a higher order analytical method which accounts for variable shear stress and strain through the thickness and also by performing a finite element simulation and the results obtained from these two approaches were compared with the experimental results for validation. In 2003, P.Feraboli, [8] predicted the interlaminar shear strength of unidirectional, cross-ply and quasi-isotropic composite laminates loaded under four point bending. This was done by developing various finite element analysis using a commercial finite element package, allowing for better insight on the mechanics of delamination in four-point bending. The profile of the shear stress through the thickness and its variation along the length, the distribution of the shear stress across the width, the location of

delamination initiation and propagation and maximum interlaminar shear strength and the shear stress contour were studied through the analysis. These results obtained were validated with an experimental database which was gathered through the known modified version of the ASTM D2344 short beam test.

In 2004, F.Bosia [9] studied the through-the-thickness deformation of laminated composite plates subjected to out-of-plane line and concentrated load both experimentally and numerically using different span to depth ratios and aspect ratios of specimen. Experimental inspection of the specimens is carried out by combining two different techniques: embedded fibre Bragg grating sensors for internal strain measurements and surface-mounted resistive strain gauges for surface strain measurements at selected locations To eliminate the contribution due to the strain concentration in the vicinity of the loading point and highlight that due to shear effects, measurements are carried out at various distances from the load application by displacing the specimens in the loading frame. Numerically, the strains are calculated through finite-element simulations using both laminated-shell and solid elements and finally, the results obtained from these simulations are compared to the experimental results. In 2006, A.Turon, [10] proposed a thermodynamically consistent damage model in the context of damage mechanics for the simulation of progressive delamination in composite materials under variable-mode(modeI+modeII) loading.A novel constitutive equation is developed to model the initiation and propagation of delamination and this model is implemented in a finite element formulation. The numerical predictions are compared with the experimental data obtained from standard tests like double cantilever beam (DCB) test for mode I loading, the end notched flexure (ENF) test for mode II loading, and mixed-mode bending (MMB) test for modeI+modeII . Also in 2009, M.Mulle [11] employed two advanced experimental optical techniques to analyze the mechanical behavior of a composite structure submitted to bending tests by considering a beam type specimen. In one optical measurement technique, several optical fibre Bragg grating sensors have been embedded in various levels of the ply stack of the composite laminate to measure the interior strains through the thickness of the specimen. The other technique is called the 3-D Digital image correlation technique which was used to measure the surface strains along the thickness of the specimen. Also the variation of load with displacement was studied experimentally using these two techniques. Also the mechanical behavior was studied by performing Finite element simulations and the strain and load-displacement variations obtained from the simulations were compared with that obtained from the two experimental techniques. In 2010, Zhou Hong Wei, [12] experimentally investigated the damage initiation, damage growth and meso scale changes in glass fibre reinforced composites with different orientations of fibres through Scanned electron microscopy(SEM) by carrying out three point bending tests and . The dependence of mechanical parameters on the orientation angles of fibers are also analyzed. In 2010, Luca Motoc [13] aimed to approach the failure mechanisms for a polymeric multiphase composite subjected to three point bending. The multiphase polymeric composites contained five layers, each of them containing dilute particles embedded into different volume fraction into a polymeric matrix along with long, random glass fibers. A micromechanical based approach was be used during the modeling step to size the stress and strains on the outer layers of the particle, polymeric resin and on the long,random glass fibers. The failure mechanisms of the laminates were also studied by testing the specimens experimentally under three-point bending and the results obtained from experiments and the micromechanical model were compared.

In 2011, E.Nelson [14] performed multiscale nonlinear progressive analysis of composite laminate

under bending using multicontinuum theory(MCT) which experiences delamination as a primary failure mode. The analysis treats the fibre and matrix constituents of a lamina as separate but linked constituents. Fibre and matrix failure including delamination are modeled independently using stress based failure criteria formulated in terms of constituent stresses generated through MCT decomposition. This MCT analysis was coupled with nonlinear damage progression in a finite element setting. A comparison of element formulations involving 3D elements and layered solid and shell elements are also presented. Finally comparison of results of the MCT model and experiment are made. In 2012, H.Ullah [15] studied the deformation and damage behavior of woven Carbon fibre reinforced polymer(CFRP) composite material under high-deflection three point bending. Experimental tests were carried out to characterise the behaviour of a woven CFRP material under large-deflection bending. Two-dimensional finite element (FE) models were also implemented for the same. Single and multiple layers of bilinear cohesive-zone elements are employed to model the onset and progression of inter-ply delamination process. In 2013, M.Allel [16] tried to study the failure process of composite laminate loaded under three point bending and tried to predict its ultimate strength by seeking a law through mesoscopic approach. Tests on two particular types rectangular plates according to the conventional standards were made and this in order to validate our approach, the calculation has been implemented in a nonlinear finite element code. In 2015, P.F.Liu [17] studied the intralaminar damage behavior and interlaminar delamination carbon fiber composite specimens of three different fibre orientations which are $[0_{16}//0_{16}]$, $[30_{16}//30_{16}]$, and $[15/15]_{3s}//[15/15]_{3s}$ with initial interlaminar cracks through three-point bending mechanical experiments and acoustic emission (AE) tests of composite specimens. The effects of the layup patterns, the loading conditions, and the initial interlaminar crack length on the intralaminar damage and interlaminar delamination behaviors of composite laminates were comparatively studied by analyzing the response process of the AE characteristic parameters including the amplitude, energy, and counting. Also in 2015, M.Meng [18] investigate the effect of fibre lay-up on the initiation of failure of laminated composites loaded under three point bending by developing a three dimensional finite element analysis. The investigation was also done through an analytical method which involved study of deformation behavior through 3D classical laminated plate theory and by implementing Tsai-Wu failure criteria to predict failure initiation. Carbon fibre reinforced composites of three different fibre orientation which are unidirectional $[0]_{16}$, cross-ply $[0/90]_4$, and angle ply $[45]_{4s}$ were manufactured and tested under three point bending and therby the failure behavior of the specimens were observed. The analytical solution was compared with the Finite element analysis results. Also in the same year, EA Patterson [19] investigated the resultant damage modes in delaminated carbon fibre reinforced plastic(CFRP) composite laminates subjected to four point bending. The stereoscopic three dimensional Digital Image Correlation (DIC) method was used to measure full-field deformations and to evaluate maps of surface principal strains in the laminates. The size of delamination and shapes of delamination which include circular and elliptical delamination was also investigated. Also in the same year, C.Marsden [20] experimentally studied the initiation and evolution of intralaminar microcracking in cross-ply thin carbon-epoxy laminates through four-point bending fatigue testing.

In 2016, Murat Koc [21] investigated the failure behavior of fibre reinforced composites having different fibre lay-ups under four point bending First, the tests were modeled analytically using the classical lamination theory (CLT). The maximum allowable moment resultants of off-axis laminate as well as balanced and symmetric angle-ply composite laminates as a function of fiber orientation

angle were obtained using Tsai-Wu, maximum stress, maximum strain, Hashin, Tsai-Hill, Hoffman, quadric surfaces, modified quadric surfaces, and Norris failure criteria. Second, the same tests are simulated using the finite element method (FEM). An analysis is conducted for optimal positioning of the supports so as to ensure that intralaminar failure modes dominate interlaminar (delamination) failure mode. A test setup is then constructed accordingly and experiments were conducted. The correlation of the predicted failure loads and the experimental results was discussed. In 2017, J.Kim [22] investigated the failure prediction of composite laminates with two different fibre lay ups which are un-symmetric cross-ply $[0/90]_8$ and quasi-isotropic $[0/45/90]_{2s}$ under bending. The non-linear finite element analysis using Arc-length method was performed. 2D strain-based interactive failure theory that is more accurately final failure of composite laminate under multi-axial loading was applied to predict the final failure of composite laminates under bending. In order to compare the accuracy of the failure predictions, a 3-point bending test are performed for both lay-up sequences. Also, it is compared with the other failure criteria such as maximum strain, maximum stress and Tsai-Wu theories.

### 1.2.2 Composites with single/multiple holes

In 1990, C.B.Prasad [23] performed an analytical investigation of the effects of circular and elliptical holes on the moment distributions of symmetric composite laminates subjected to pure and cylindrical bending. A general, closed form solution for the moment distribution for the moment distribution of an infinite anisotropic plate is derived and this solution is used to determine stress distribution both on hole boundary and throughout the plate. In 1991, RD Bradshaw [24], investigated the failure of composite laminated plates with three different stacking sequences with centrally located circular holes under four-point bending. Point stress and average stress criteria were developed to determine the failure loading by predicting failure initiation for any hole size. In 1995, Y.W.Kwon [25] investigated the failure modes and failure strengths of laminated graphite fibre/epoxy matrix composite plates without and with hole subjected to four point bending. A series of four-point bending experimental tests were conducted for these plates. Finite element analyses simulations were performed to compute stress distributions around holes and failure strength of these composite plates and the results obtained from the simulations were compared with that of experiment. Also in 1995, T.K.Paul [26] analytically performed flexural analysis of laminated composite plates containing two elliptical holes using higher-order shear deformation theory. This finite element formulation was used for the analysis of in-plane stresses of a simply supported laminated square plate containing two elliptical holes under transverse sinusoidal loading. The variation of the stress concentration factor with respect to plate thickness, hole size and distance between holes was also studied. Also in the same year, Y.Zhao [27] analyzed the strength of notched laminated composites under bending by implementing two failure models in finite element method which include a modified point stress model and modified average stress model. The results obtained through this analytical model was validated by performing notched sample experiment.

In 1997, C.Chen [28] determined the stress distribution for a laminated anisotropic composite plate with an elliptical cutout under bending using a combination of complex variable formulations and a variational principle. Through this approach, moment resultants and displacements of anisotropic plates are expressed in terms of complex stress potentials. Also effect of cutout size on stress concentration and moment distribution is also studied. In 2001, T.Shreedhar [29] investigated

the bending behavior of symmetric and anti-symmetric laminated composite shells with a cutout with simply supported and clamped boundary conditions subjected to uniform normal pressure using the finite element method based on a higher-order shear deformation theory.Using this method, distributions of deflection and stresses in the orthotropic laminated shells have been determined. In 2003, S.Temiz [30] performed the stress analysis of composite lamina and laminate without and with holes using finite element method by writing a computer program to solve the problem. In 2005, N.Yahnioglu [31] investigated the stress concentration near the rectangular hole in a composite strip subject to bending by application of uniform loading on the upper face of a strip through exact geometric non-linear equations of elasticity Theory in the plane strain-state. Investigations were carried out by helping of displacement Based Finite element methods and Newton-Raphson Method for linearization of system of non-linear equations. In 2012, S.D.Akbarov [32] investigated the stress concentration around two neighbouring cylindrical holes in rectangular simply supported composite plate loaded by uniformly distributed normal forces on its upper face by formulating the problem within the framework of the three dimensional linearized theory of elasticity. The problem was also solved by performing a three dimensional finite element simulation. The influence of material and geometrical parameters and interaction between the holes on the concentration of stresses around the hole was also studied. In 2013, C.Mao [33] studied the distribution of stresses around the hole of finite composite plate with different stacking sequences having single and multiple circular and elliptical cutouts by means of complex variable method based on classical laminated plate theory. The effects of composite plate size, ellipticity of ellipse, elliptical orientation angle, diameter of circular hole, relative center to center distance between holes and the layups of laminate on the stress distribution around hole is investigated. In 2015, NP Patel [34] analytically investigated the moment distribution in a symmetric cross ply and angle ply laminated composite plate having square hole under different configurations of bending through complex variable formulation and also predicted the failure strength through first ply failure theory. Different configurations of bending include cylindrical bending, bending along X-axis and bending along Y-axis. Effect of size of hole and lay-up sequences on moment distribution and failure strength was studied.

## 1.3   Motivation

As mentioned in the section 1.1, composite structures are widely used in aircraft and automotive industries due to their low strength/weight, stiffness/weight ratio, fatigue life, thermal properties etc. Most of the parts of these composite structures are subjected to flexural loading. An example of wings of an aircraft being treated as a beam fixed at one end and being subjected to a transverse flexural load is also being discussed in Section 1.1. Also other parts of industrial structures such as blades of a helicopter, drive shaft of an automobile and arms of a robot can be modeled as beams which are subjected to flexural loading. On increase of flexural load, certain damage mechanisms which does not involve only fiber and does not reduce the load carrying capacity of composite structure initiates and propagates in the structure. The load at which damage initiates in the structure is known as failure initiation or first ply failure load. Then final failure at a certain critical load occurs through breakage of fibers and this critical load is known as final or ultimate failure load .Composites are orthotropic materials and therefore its material constants will be different along different directions. In addition to this, it also has different tensile and compressive strengths.

Since during flexural loading, there will be both tensile and compressive states present across the thickness of the specimen as discussed in section 1.1, the damage behavior of the structure becomes more complicated under flexural loading and thereby more complex damage mechanisms and their interactions are observed. Therefore it is really essential to study these damage mechanisms in detail. Damage mechanisms in the composite can be of interlaminar level or intralaminar level. The images of various damage mechanisms occurring in a composite laminate obtained through micrograph or Scanned electron microscopy(SEM) method are shown in Figure 1.5.
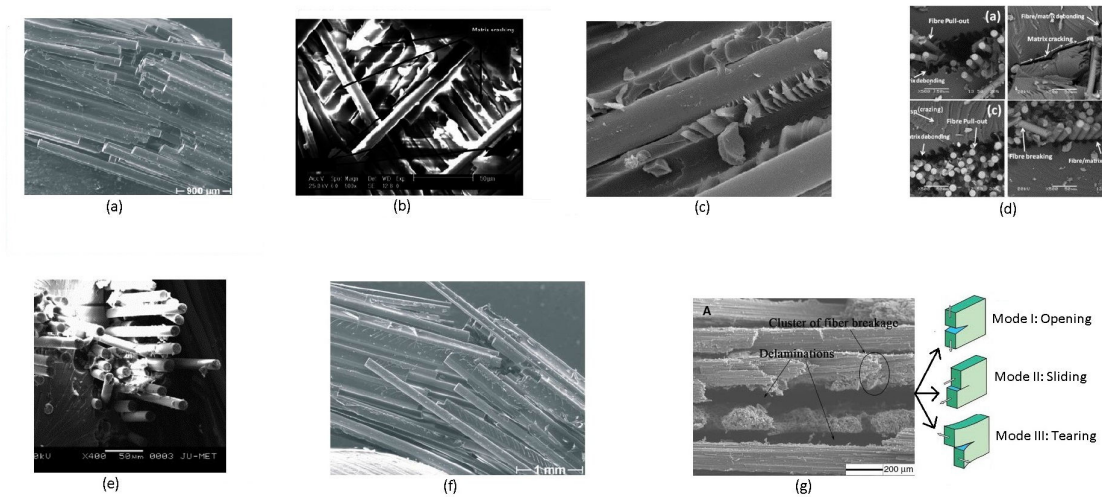


Figure 1.5: a) Fiber breakage b) Matrix cracking c) Fiber Matrix Debonding d) Various intralaminar damage mechanisms e) Fiber pullout f) Fiber kinking g) Interlaminar delamination
Courtesy: google images

Intralaminar damage mechanisms include fiber breakage, fiber kinking, matrix cracking, fiber pullout and fiber-matrix debonding. Since the fibers represent the principal load-bearing constituent of a fiber reinforced composite, fiber breakage through tensile loading can have a severe effect upon both the stiffness and strength of a multi-directional composite and can reduce its load carrying capacity upto a great extent. When fiber composite materials subjected to compression in the fiber direction, localized buckling or microbuckling in fibers occurs and on further buckling, the fibers break and one part of the fiber comes on top of the other fiber which is known as fiber kinking whose SEM image is shown in Figure 1.5(f). Matrix cracking includes splitting, a term referring to long cracks parallel to the fibers, either in the matrix or within the interphase region. This damage mechanism can be tensile, compressive or shear in nature. Matrix cracking is frequently very localized, and often extremely dificult to detect.When the stress in the fiber-matrix interphase exceeds the local strength, the fibers are sheared of the surrounding matrix known as fiber-matrix debonding and pullout of these fibers takes place. Debonding represents, therefore, a very localized mode of failure that is often very difficult to detect using conventional techniques. The amount of debonding present within a composite depends upon the level of surface treatment applied to the fibers during its manufacture. Generally, fibers with low levels of surface treatment tend to debond more easily and the resulting fracture surfaces are usually rough and strongly three dimensional when viewed in a scanning electron microscope . Highly treated fibers debond less and fracture tends to be planar

with cracks propagating directly across fibers. Interlaminar mode of damage includes delamination which is the separation of the adjacent plies in the laminate whose micrograph image is shown in Figure 1.5 (b). The cause of delamination is due to the fact that the transverse strengths or in other words the interlaminar strength parameters are small compared to the other strength parameters. It is the most frequently discussed mode of damage in composite materials. Delamination can be of three types, Mode I delamination is known as opening mode which occurs due to tensile loading , Mode II delamination is known as sliding mode which occurs due to in-plane loading and Mode III delamination is known as tearing mode which occurs due to out-of plane shear. Matrix cracking acts as a precursor to delamination.During critical load on a flexible target, matrix cracking initiates at the lower surface of the target and propagates upwards through the laminate forming planes of delamination. It is essential to study these complex damage mechanisms and the overall damage behavior of the composite structure for its efficient and sustainable design. As discussed in section 1.1, cutouts or holes are essential and unavoidable in the structures due to functional requirements like wiring,piping,assembly, visual inspection etc. Also the stacking sequences in these composite laminates have to be changed to different angles so as for the laminate to have high strengths in more than one direction. Because of this, it is really necessary to study damage behavior of composite structures having holes and of different stacking sequences. This can be done experimentally by fabricating the composite specimens through an available and standard fabrication process, testing them by applying a gradually increasing flexural load and then observing how damage has occurred in the specimen. The study of damage behavior can also be done numerically by performing progressive damage analysis through a reliable progressive damage model and the results obtained from this model can be compared with the experimental results.

## 1.4 Scope

Upto the author's knowledge from the literature review performed, studies on mechanical and damage behavior of composite laminates without cutouts and of different stacking sequences under flexural loading have been done throughly by various researchers both experimentally and through analytical damage models. But for composite laminates with single and multiple cutouts, only the study of mechanical behavior and prediction of damage initiation through some reliable failure criteria has been performed. Study of complete damage behavior which includes failure propagation, occurrence of various damage mechanisms and prediction of ultimate failure load has not been done in these cases. Complete damage behavior of carbon fiber reinforced polymer(CFRP) laminate having single hole and multiple holes of three different configurations which are two hole longitudinal(2HL), two hole transverse(2HT) and two hole diagonal(2HD) can also be studied.

## 1.5 Objective

The objectives of this thesis include:

1) To experimentally study the damage behavior of Carbon fiber reinforced polymer(CFRP) laminate having single hole(1H) and multiple holes of three different configurations which are two hole longitudinal(2HL), two hole transverse(2HT) and two hole diagonal(2HD), which are loaded by four-point bending. The study will be performed for two different stacking sequences for each

of the previously mentioned specimen configurations, which include Unidirectional whose lay-up sequence is $[0]_{16}$ and Quasi whose lay-up sequence is $[45/0/-45/90]_{2s}$. For the purpose of this study, the specimens were fabricated through vacuum bagging process and were tested through four-point bending test. Two-dimensional(2D) Digital Image Correlation technique was employed for capturing the in-plane displacements and strains along the thickness of specimen.

2) To perform progressive damage analysis numerically through a three dimensional progressive damage model implemented in a three dimensional finite element simulation. In the progressive damage model, Hashin failure criteria was employed for prediction of failure initiation, Material property degradation model(MPDM) was employed for modeling of failure evolution and Cohesive Zone Model(CZM) was implemented for delamination modelling between layers of composite laminate.

3) Finally the results obtained from experiments were compared with that obtained from the numerical model for validation.

## 1.6    Thesis layout

Chapter 1 describes fundamentals of composite material and bending phenomena, application of composite structure under flexural loading in aircraft and other industries, definition of damage behavior and reason for studying it in composite laminates with cutouts and having different stacking sequences, review of various studies done on the topic previously by various researchers, motivation, scope and objective of the study.

Chapter 2 describes the experimental study of damage behavior performed on the CFRP specimen without hole, with single hole(1H) and with multiple holes of of three different configurations which are two hole longitudinal(2HL), two hole transverse(2HT) and two hole diagonal(2HD), which are loaded by four-point bending. This includes defining the geometry and flexural loading configuration of the above mentioned specimens, specimen fabrication, Digital Image correlation(DIC) technique and its Principle, experimental testing setup, results obtained from experimental study and its discussion.

Chapter 3 describes the numerical study performed for the previously mentioned specimens by implementing progressive damage model in a finite element package. This includes creation of model of the specimens, meshing and boundary conditions applied,material properties and strength parameters, explanation and flowchart of the progressive damage model implemented in the finite element simulation, Failure initiation prediction through Hashin failure criteria, Failure evolution through Material property degradation model (MPDM) and Delamination modeling through Cohesive Zone Model(CZM), results obtained from numerical study and its discussion, comparison of experimental and numerical results and its discussion.

Chapter 4: Conclusions and recommendations for future work.

# Chapter 2

# Experimental studies involving Digital Image Correlation

## 2.1 Introduction

One of the objectives of this thesis includes performing experimental study of damage behavior of CFRP specimen, with single hole(1H) and with multiple holes of of three different configurations which are two hole longitudinal(2HL), two hole transverse(2HT) and two hole diagonal(2HD), which are loaded by four-point bending. For performing this study, the specimens have to be fabricated through a more accurate and standard fabrication procedure and proper experimental testing of specimens should be done. Also experimental study of specimen without cutout has to be performed at the beginning for a more sequential study. This chapter focuses on the specimen geometry and four-point flexural loading configuration of the previously mentioned types of specimens, fabrication procedure of specimens, detailed description of experimental testing setup and explanation of Digital Image correlation(DIC) technique for capturing capturing the in-plane displacements and strains along the thickness of specimen. Finally the results obtained from this experimental study are shown and discussed.

## 2.2 Specimen Geometry

The specimen geometry and four-point flexural loading configuration for CFRP specimen without cutout is shown in Figure 2.1.The length, width and thickness of the specimen are 250mm,45mm and 3.6mm respectively.The two types of stacking sequences of specimen include Unidirectional $[0]_{16}$ and Quasi-isotropic $[45/0/-45/90]_{2s}$. In the four- point bending configuration, there are two rollers for supporting the specimen which are placed symmetric with respect to the specimen and the distance between them is 70mm. Also there are two rollers for applying load on the specimen which are also placed symmetric with respect to the specimen and the distance between them is 140mm. Four-point flexural configuration is chosen over three-point flexural configuration in our study. This is because our objective is to study the damage behavior of CFRP specimen under pure flexural loading, and in three-point flexural loading, there is both non-zero shear force and bending moment in the portions of specimen between any two rollers. Therefore the whole specimen is subjected to both shear as
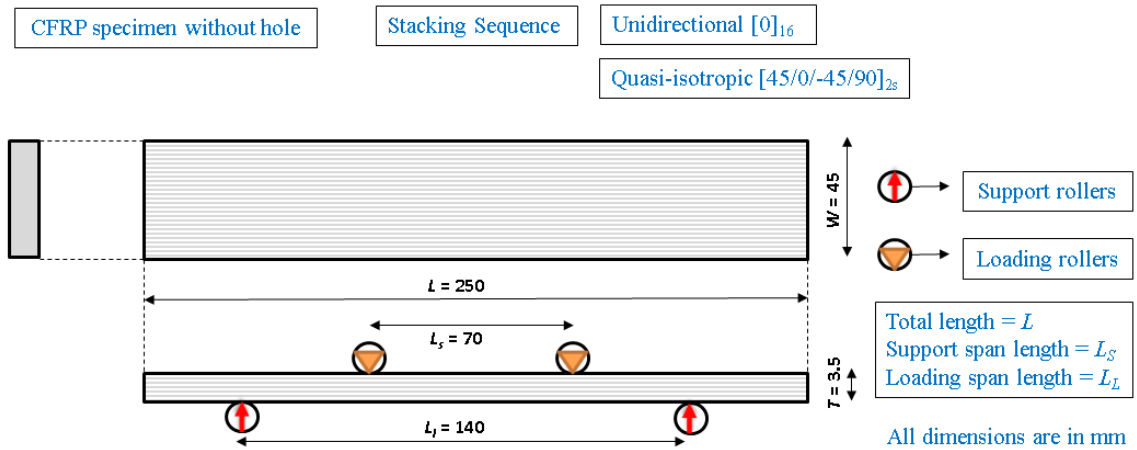
Figure 2.1: Specimen geometry and four-point flexural loading configuration of CFRP specimen without cutout
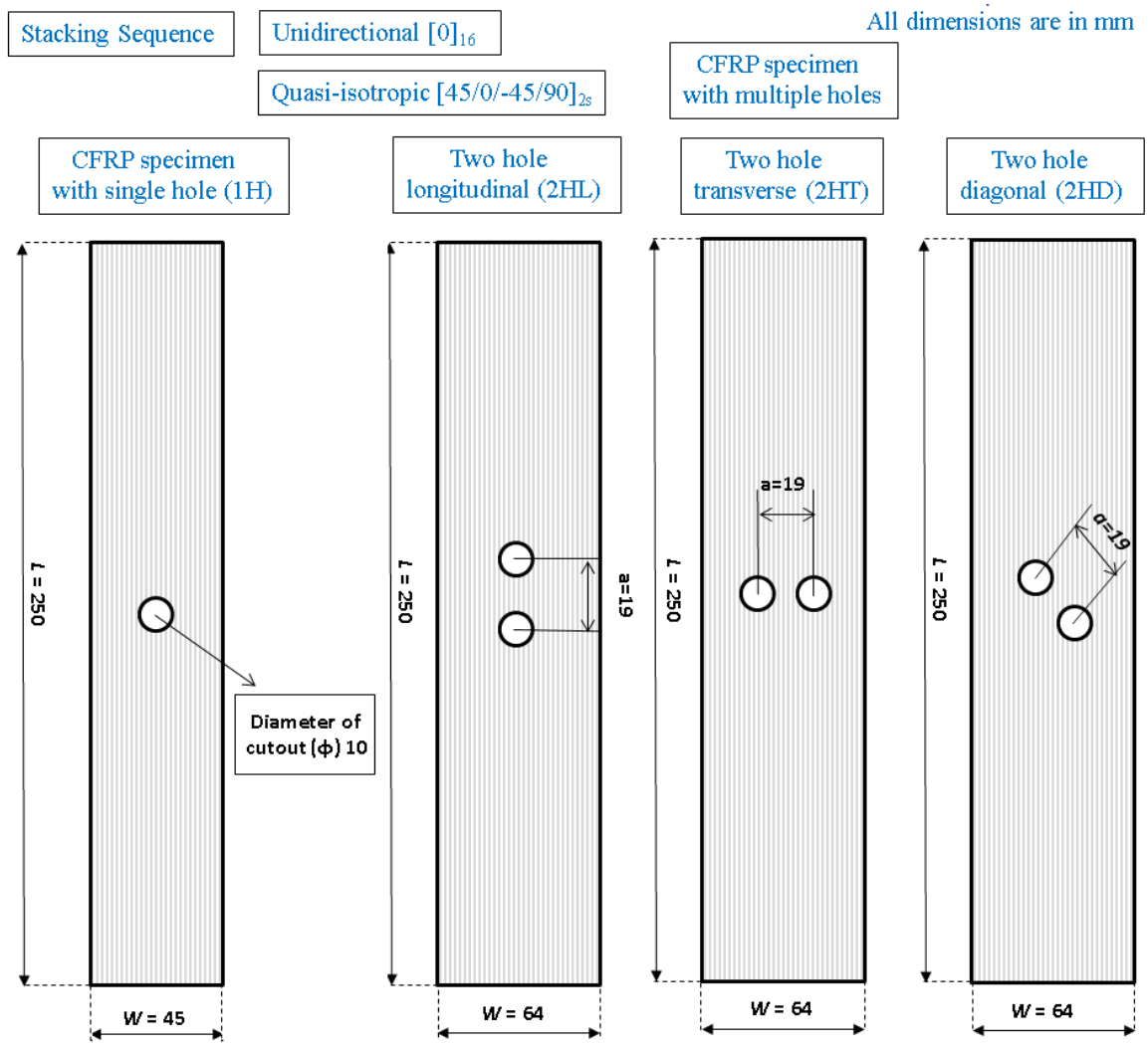


Figure 2.2: Specimen geometry of CFRP specimens with single and multiple cutouts

well as bending which is not desirable in our case. But in four-point flexural loading, there is no shear force in portion of specimen between the two support rollers placed in-between also the bending moment at this portion of the specimen remains constant throughout. Therefore this portion of specimen is under pure bending and therefore in our case, it is desirable to study the damage behavior in this portion of this specimen. By definition of quasi-isotropic laminates, the plies or laminae should be oriented at the same angle relative to the adjacent ply or lamina and the resultant laminate should exhibit isotropy. This means when the laminate is assumed to be a homogeneous material, the elastic properties of the laminate must be same in all directions. In our study, the stacking sequence of the quasi-isotropic laminate is $[45/0/-45/90]_{2s}$ which satisfies the condition for this type of laminate as the relative angle angle between two laminae remains same which is 45 degrees.The dimensions and stacking sequences of CFRP specimen with single and multiple cutouts are shown in 2.2. For CFRP Specimens having single cutout, the dimensions are similar to that of specimen without cutout but additionally there is a circular cutout located centrally in the specimen of diameter 10mm. The diameter of the hole was chosen in such a way that the ratio of width of specimen to diameter of hole to must be greater than 3.5 to avoid high interaction of hole with edge. In this case the width to diameter ratio is 45/10 which is equal to 4.5 and is grater than 3.5. For CFRP specimens having multiple cutouts, the length, thickness and cutout diameter of specimens are same as that of previous specimens but the width of the specimens are 64mm instead of 45mm. For each of the multiple cutout specimens, the distance between the cutouts is 19mm.

## 2.3   Specimen fabrication

The first step to fabrication of specimen from scratch for every type of CFRP specimen involves cutting of carbon fibers of desired sizes and fiber orientations followed by preparation of matrix material. For this, 16 unidirectional carbon fibers of 200 grams per square meter(GSM) were cut for each type of specimen according to the required sizes and orientations as each specimen contains 16 layers. Then the matrix material was prepared by taking resin material whose weight is equivalent to the weight of the fibers and then mixing it with hardener in the ratio 10:1 by weight. The compound used for resin was Araldite CY-930 and for hardener was Araldite HY-951. The resin and hardener were separately heated before mixing so as to remove any air bubbles. After mixing of resin with hardener, the mixture was cooled for some time. It had to be made sure the mixture was not cooled for a long time as reaction of resin with hardener could take place, thereby hardening the matrix mixture. The specimens were fabricated through vaccum bagging technique, which is a technique where mechanical pressure is applied on the laminate during its preparation. The setup of vaccum bagging process is shown in Figure 2.4. At first, sealing tape was put around the base and then wax followed by resin is applied on the base. Wax was applied to make sure that the resin does not stick to the base and to therefore facilitate easy removal of the finally prepared specimen from base, thereby acting as a release agent. After this, the first fiber was placed in the desired orientation. Then the matrix material was applied throughout the fiber as shown in Figure 2.3(b) and then another fiber of the desired orientation was placed on top of the previous fiber as shown in Figure 2.3(c) . In the same way, remaining fibers were stacked on top of one other in the desired stacking sequence. After stacking of fibers, the distribution of matrix material in between the fibers will not be uniform throughout the fiber. For this purpose, peel ply was placed on top of the laminate
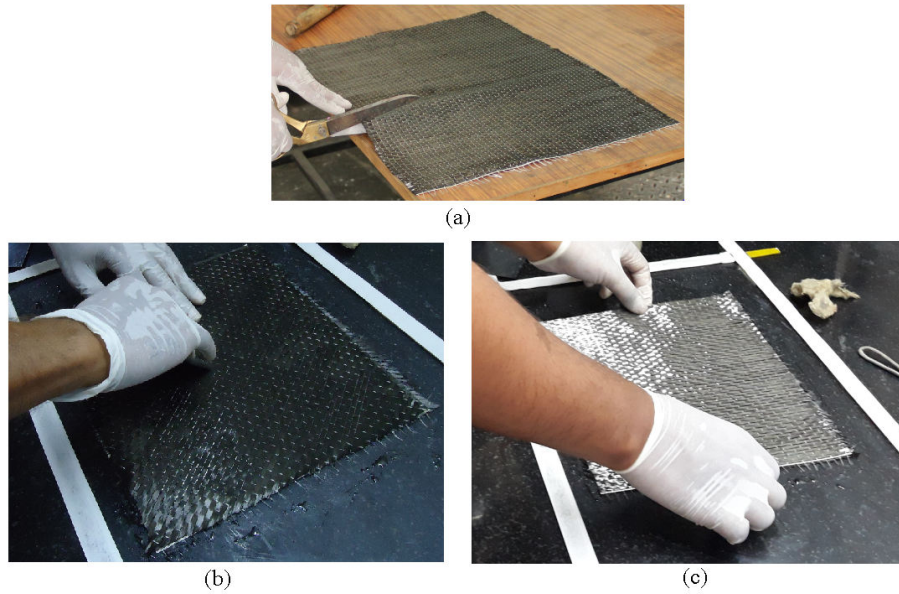
Figure 2.3: a) Cutting of carbon fibers of GSM 200 b) applying of matrix on fiber c) stacking of one fiber over another in vaccum bagging process

so that it applies uniform pressure on the laminate and thereby ensures equal distribution of matrix throughout the fiber. There will be excess matrix material present in between the fibers and they need to be taken out and absorbed, for this purpose breather material was put on top of the laminate. But to avoid absorbing of matrix more than the required limit by the breather, perforated sheet which contains small holes in it was placed beneath the breather so that only the required amount of excess matrix comes out through these holes and was absorbed by the breather. There is also another important use of peel ply. Let us say peel ply was not put on top of laminate and only perforated sheet and breather were placed. In this case, after the final preparation of laminate, it will be very difficult to remove the perforated sheet and breather from laminate. Therefore a peel ply was put beneath them so as to facilitate easy removal of perforated sheet and breather from laminate. The breather contained waviness and when pressure was applied on the laminate, the impression of these waviness also would be transferred to the laminate and thereby after the preparation of laminate, waviness would also be seen in the laminate. To avoid this, an aluminum caul plate, whose size is same as the size of fibers which were stacked, was placed on top on the breather so that when pressure was applied on the laminate, it compressed the breather thereby decreasing its waviness to a considerable extent. Next, the cover was placed on top of this whole setup and is stuck tightly by the sealing tape so as to avoid leakage of air. Finally, curing process took place for around 24 hours, where pressure was applied on the setup by removal of air from it and thereby preparation of the final laminate took place.

After the final preparation of laminate, it was then cut into different specimens of required sizes with the help of saw machine as shown in Figure 2.5(a). In the saw machine, there was a high speed rotating disk, which when given the required feed cuts the laminate. After cutting of the laminate into different specimens, there would be delaminations present at the faces which were cut. To remove those delaminations, end milling of the specimens were done as shown in Figure

16
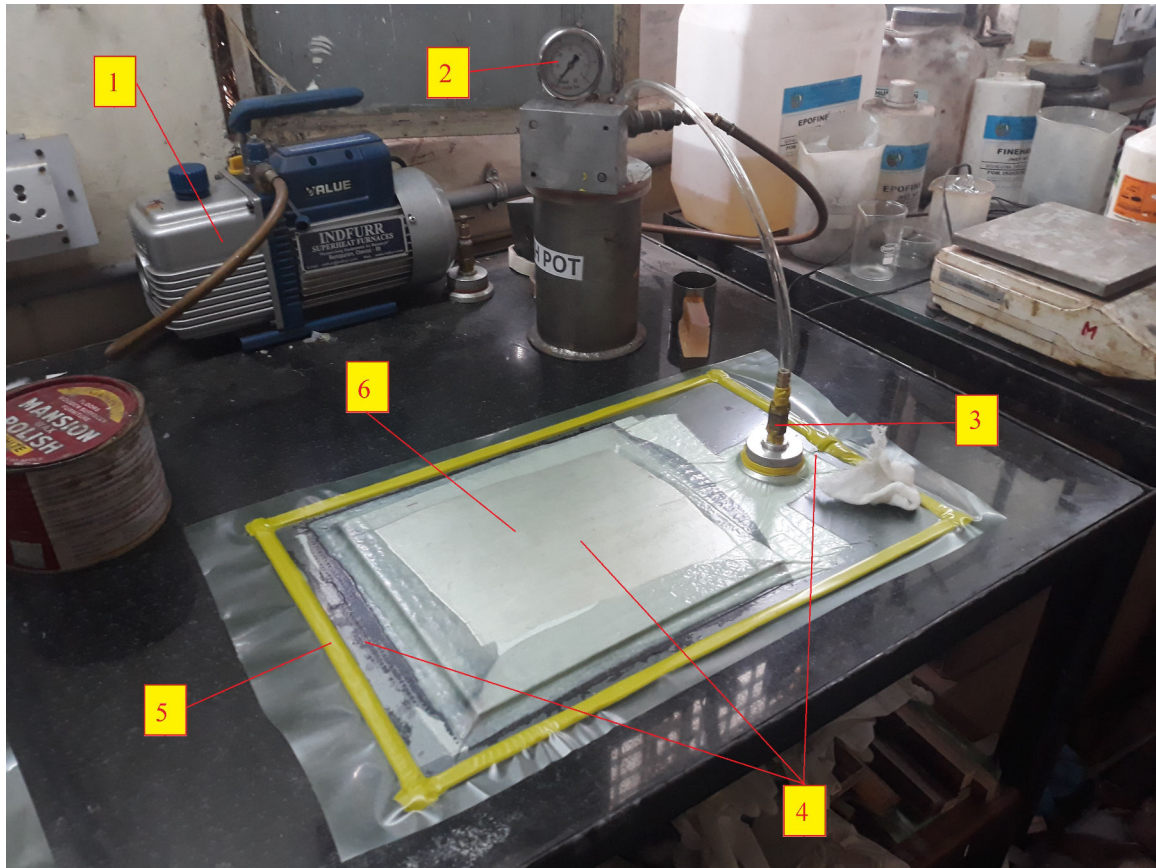
1: Vaccum pump     2: Vaccum gauge     3: Valve
4: Clamping setup     5: Sealing tape     6: Aluminium Cawl plate

Figure 2.4: Setup of vaccum bagging process

2.5(b), where the faces of specimen containing its thickness were fed into a carbide end mill of 12mm diameter and six flutes rotating at 700 rpm. When end milling was performed, some amount of material was removed from specimen and therefore the width of the specimen would reduce. Therefore during the cutting process, the specimens were cut to a width slightly more than the actual width of the specimen, so that after the end milling process, the width of the specimens were reduced to its actual value. Also during the end milling process, wooden plates were placed on the top and bottom faces of the specimen so that the milling of those faces did not occur by mistake, thereby preventing damage to those faces. For CFRP specimens having cutouts, it was necessary to drill holes of diameter 10mm at the required locations. For this marking was done on the specimen at the center of hole to be drilled and then the specimen was fixed to the benchwise with a wooden block placed at the bottom of the specimen so as to prevent any form of damage to the specimen. Then the carbide drill bit of diameter 10mm was brought just above the marking and then it rotated at 700rpm and went through the specimen thereby drilling the hole as shown in Figure 2.5(c).

After the above processes were performed on the specimen, the faces of the specimen containing its thickness would be rough. Two dimensional digital image correlation(DIC) technique was used for measuring the in-plane displacements and strains along these faces of the specimen. For the purpose
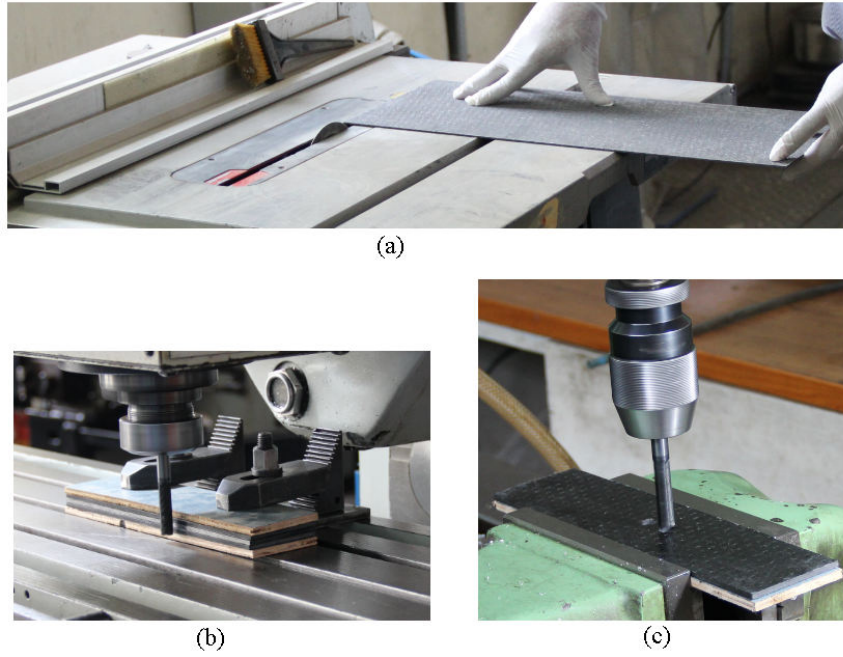
Figure 2.5: a) Cutting of laminate into specimens using saw machine b) end milling of thickness face of specimen c) hole drilling of specimens
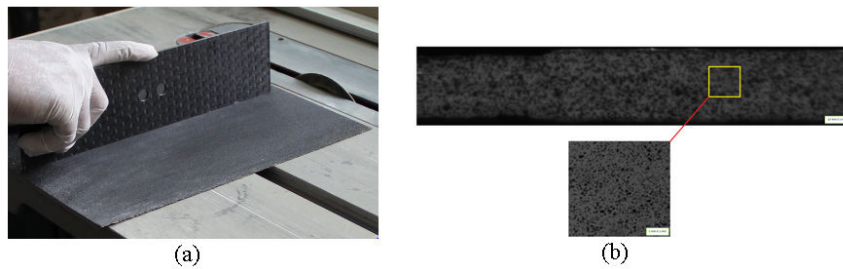


Figure 2.6: a) Rubbing of thickness face of specimen on emery b) Speckle pattern performed on thickness face

of this technique, it was required that these faces must be smooth. For smoothening the faces, these faces were rubbed over a emery paper of grid size 2000 as shown in Figure 2.6(a). After smoothening of surfaces, it was required to perform speckle pattern over those faces of the specimen again for the purpose of DIC technique which will be explained later in this chapter. It was performed by first applying spray paint of white color and then allowing it to dry for some time. Then speckles were generated through the thickness face of specimen with acrylic paint of carbon black color by an airbrush as shown in Figure 2.6(b). Now the specimens are completely prepared and are ready for experimental testing. Four CFRP specimens without and with hole for Unidirectional $[0]_{16}$ layup, three CFRP specimens without and with hole for Quasi $[45/0/-45/90]_{2s}$ layup, and two CFRP specimens with multiple holes for each configuration(2HL,2HT and 2HD) each for both lay-ups were fabricated. Images of finally fabricated CFRP specimens without hole, with single and multiple holes are shown in Figure 2.7.
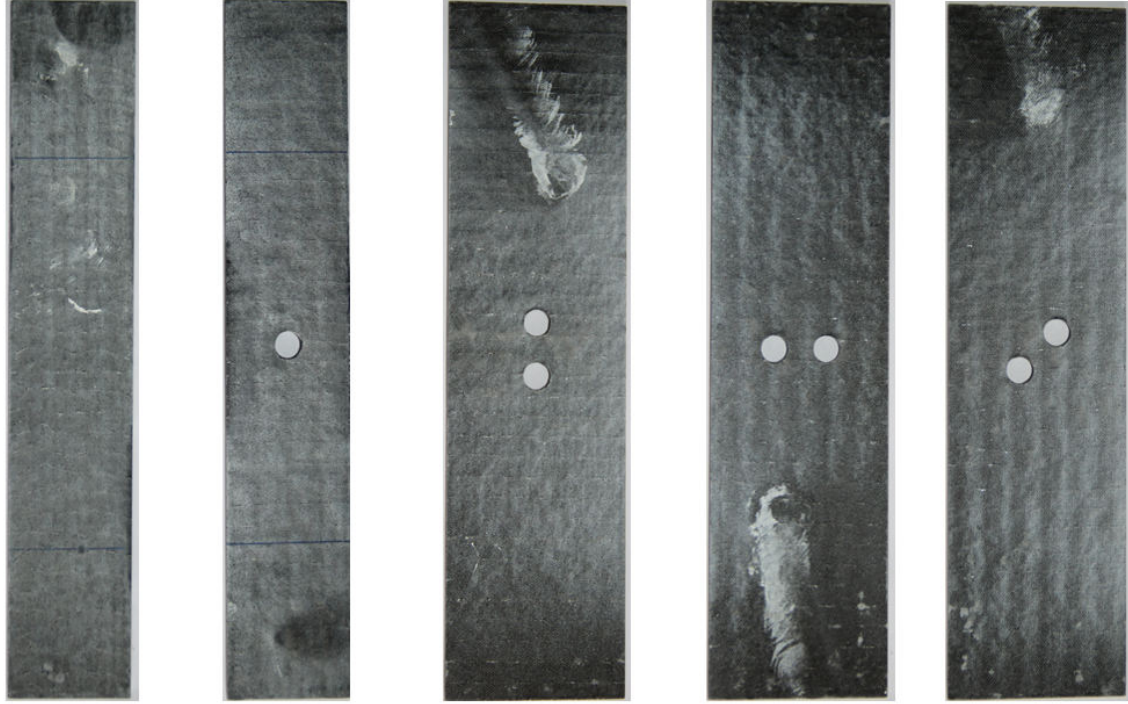
Figure 2.7: Finally fabricated CFRP specimens for multiple hole specimens a) Two hole longitudinal(2HL) b) Two hole transverse(2HT) c) Two hole diagonal(2HD)

## 2.4   Experimental Testing Setup

The experimental testing setup used for four-point bending test for all the types CFRP specimens is shown in Figure 2.8. The numbers mentioned subsequently in the explanation for testing setup is with respect to this figure. The four-point bending test was carried out through computer controlled MTS Landmark servo-hydraulic cyclic test machine(1) having load capacity of 100KN. The MTS fixture consisted of two scales, one at the top and other at bottom of the fixture, which were used for adjusting the support and load rollers to the correct position. The support rollers(10) which were of radius 25mm were fixed to the scale on the top by sliding along it to the correct position. The loading rollers(11) which were also of radius 25mm were fixed to the bottom scale in the same way as the support rollers. Then the CFRP specimen(12) was just placed in between the loading and support rollers at the correct position. The support rollers have been fixed symmetrically with respect to the specimen and the distance between them is 70mm. The loading rollers have also been fixed symmetrically with respect to the specimen and distance between them is 140mm. The four-point bending experiment was performed under displacement control mode with the displacement rate being 1mm/min.This means the actuator(9) in the MTS machine moved up vertically at the rate of 1mm/min thereby moving the loading rollers at the same rate and in this way, flexural loading was being applied to the specimen. The computer which controls the MTS machine(3) displayed the variation of load experienced by the actuator with the displacement of the actuator over time. Two-dimensional Digital image correlation technique(DIC) was employed for capturing the in-plane displacements and strain across the thickness of the specimen. The 2-D DIC system consisted of
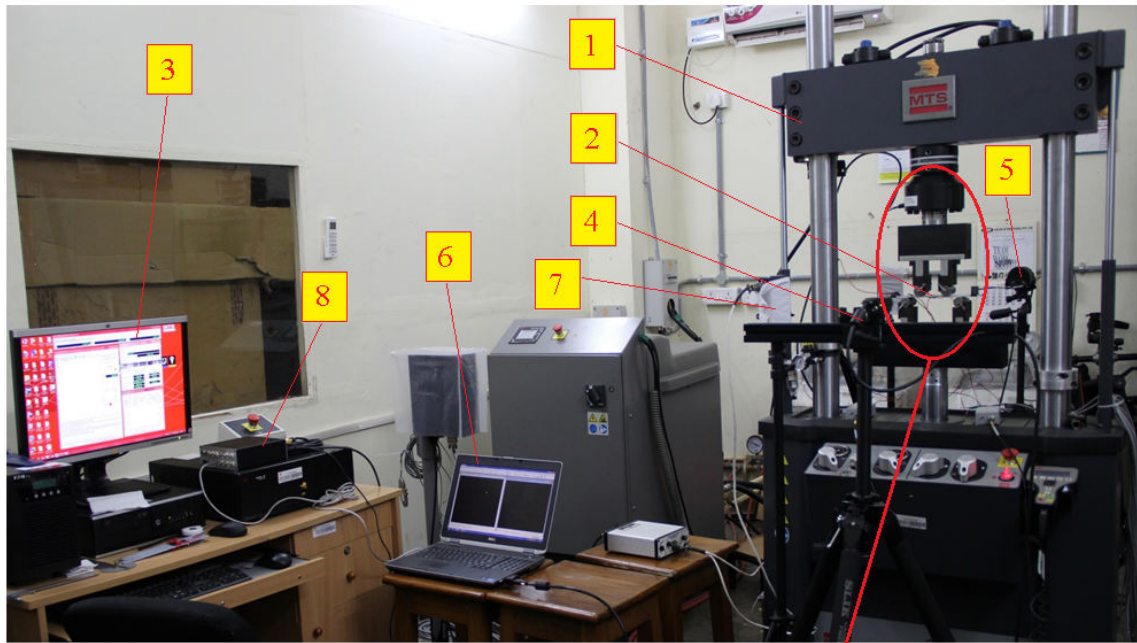
1: MTS Machine
2: Four-point bending fixture
3: MTS controller PC
4: DIC Front camera
5: DIC Rear camera
6: DIC Image grabbing PC
7: LED light source
8: Data Acquisition card(DAQ)
9: Actuator
10: Support rollers
11: Load rollers
12: CFRP specimen
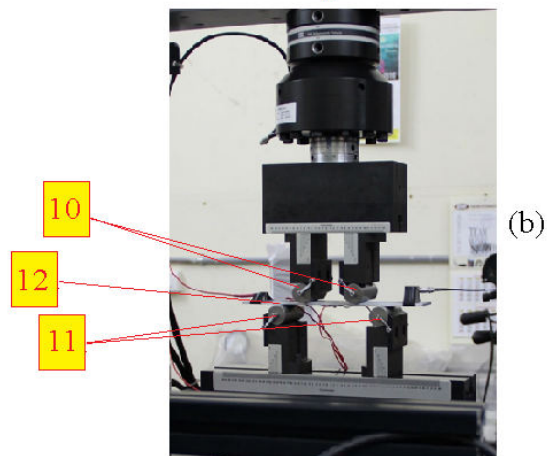
Figure 2.8: a) Setup for four-point bending experimental testing b) Detailed view of four-point bending fixture

Grasshopper CCD camera(POINTGREY-GRAS50s5M-C) which was placed at the front of specimen(4) by mounting it on a tripod stand. This camera had resolution of 2448x2448 pixels and was coupled with Schneider kreuznach lens of focal length 50mm. It also consisted of camera placed at the rear of the specimen(5) whose specifications were same as that of front camera. Horizontal level of both the cameras were ensured by adjusting the spirit level accordingly. The cameras were properly aligned with the specimen so that it can capture the images of face of specimen along thickness without any inclination. The aperture of the cameras, which is a opening or hole in the camera where the light passes through, was tuned at the correct level so the brightness of the images of specimen which were captured was at a optimum level.Two LED sources of power 30W(7) were also placed, one near the front camera and other near the rear one, so as to ensure proper illumination

of specimen face along thickness for capturing the images. Both the cameras captured images of faces of the specimen along thickness at the rate of 2 images per second or in other words 2HZ. The images captured by these cameras were grabbed by a computer(6) through the Vic-snap 2009 software(from correlated solutions Inc.) which was pre-installed in it. A data acquisition card(DAC)(8) (from National Instruments) was connected to the this computer and also to the computer which controls MTS machine for correlating the load-displacement data obtained from MTS system to the images grabbed this computer over time. 2-D DIC postprocessing was performed by feeding these grabbed images into Vic-2D software(from correlated solutions Inc.) and the in-plane displacements and strains for the specimen face at each image were calculated by the software. The first image taken by both the cameras was at zero displacement and load and was taken to be the reference image. All the calculations for in-plane displacements and strain for the remaining images were performed with respect to the reference image.

## 2.5 Digital Image correlation technique and its Principle

Digital Image correlation technique(DIC) is a optical, non-contact and full-field computer assisted experimental technique for displacement and strain measurement. It belongs to a class of non-interferometric optical technique, that is, it is a technique that does not involve superposition of two light waves. Both two-dimensional and three-dimensional DIC techniques exist. The setup of DIC technique is shown in Figure 2.9(a).
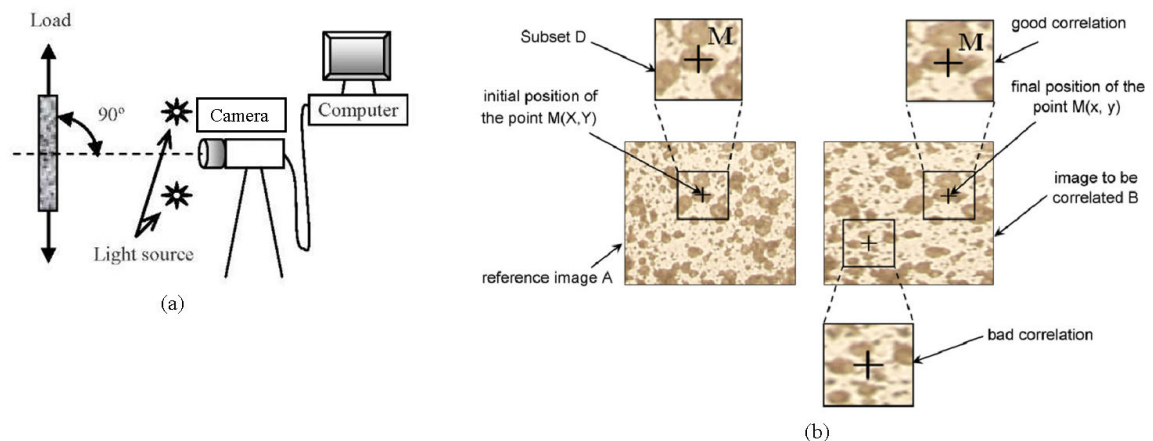


Figure 2.9: Setup of Digital Image Correlation technique
Courtesy: google images

The setup consists of a camera which continuously captures images of the specimen which is being experimentally tested. The computer which is connected to the camera contains a pre-installed software which is used for grabbing these images. These images are then fed into a another software which calculates the displacements and strains for the specimen at each of the images with respect to some reference image captured. Principle of DIC technique is explained as follows. The captured image of specimen whose displacements and strains is to be computed is divided into large number of pixels. As mentioned in previous section, speckle pattern has been performed on the face of specimen where the displacements and strains has to be calculated. The image consisting of speckle pattern

21

will consist of series of gray and white pixels. For calculating the displacements, this image is divided into a number of subsets, where each subset contains a certain number and pattern of the gray and white pixels. This pattern of gray and white pixels carries information for the subset and gives a unique identity for the subset, and this information is known as the gray value information for the subset. When this subset deforms under loading, a function known as correlation function is used to match the similarity between subsets in the original and deformed image as shown in Figure 2.5(b). The displacement of subset is calculated by calculating the displacement of the center of subset through solving of non-linear equations that involves the correlation function. The same procedure can be employed in calculated the displacement for other subsets in the image of deformed specimen and thereby the complete displacement variation throughout the region of interest of specimen is computed. Once the variation of displacement is calculated, strains in the region of interest of specimen can be computed by taking appropriate partial derivatives of displacement. The accuracy of correlation depends on how random the gray and white pixels are distributed in the image of specimen, and this randomness depends on how well the speckle pattern is performed on the face of specimen. If the speckle pattern is performed more accurately, the randomness in the gray and white pixels will be more, therefore the uniqueness of the gray value information of each subset will be more and this leads to a better correlation between subsets. Also there is one more terminology involved in this principle which is known as step size. Step size is a parameter that controls the spacing between the subsets for which displacements are to be calculated. For example, step size of two implies correlation of subsets will occur for every other subset in the image of specimen. It can easily be concluded that more the step size, less accurate is the solution for displacement and therefore for strain. Since in this technique, the speckles which have been introduced in the specimen act as information carriers, DIC technique is also known as White light speckle correlation technique. This technique can also handle large specimen sizes and used successfully for large deformation measurements in the specimen. Still the accuracy of the technique is not high, but it can come handy in certain situations for extracting information of displacements and strains where conventional techniques fail such as in a situation when the specimen is exposed to a very high temperature.

## 2.6 Results and discussion

In this section, the variation of load versus displacement for CFRP specimen without hole, with single hole(1H) and with multiple holes of three different configurations(2HL,2HT,2HD) will be discussed. Also, the damage behavior for each of the previously mentioned specimens will discussed in detail.

### 2.6.1 Load-Displacement plots

The plot of load versus displacement for all Unidirectional CFRP specimens is shown in Figure 2.10. It can seen in each of the specimens that initially, load varies linearly with applied displacement. Then at a particular point the load ceases to increase linearly with displacement and this is the point at which final or ultimate failure occurs. From this point onwards, the load decreases very sharply with displacement. Then from a particular point onwards, the variation of load with displacement becomes

**Unidirectional [0]$_{16}$**
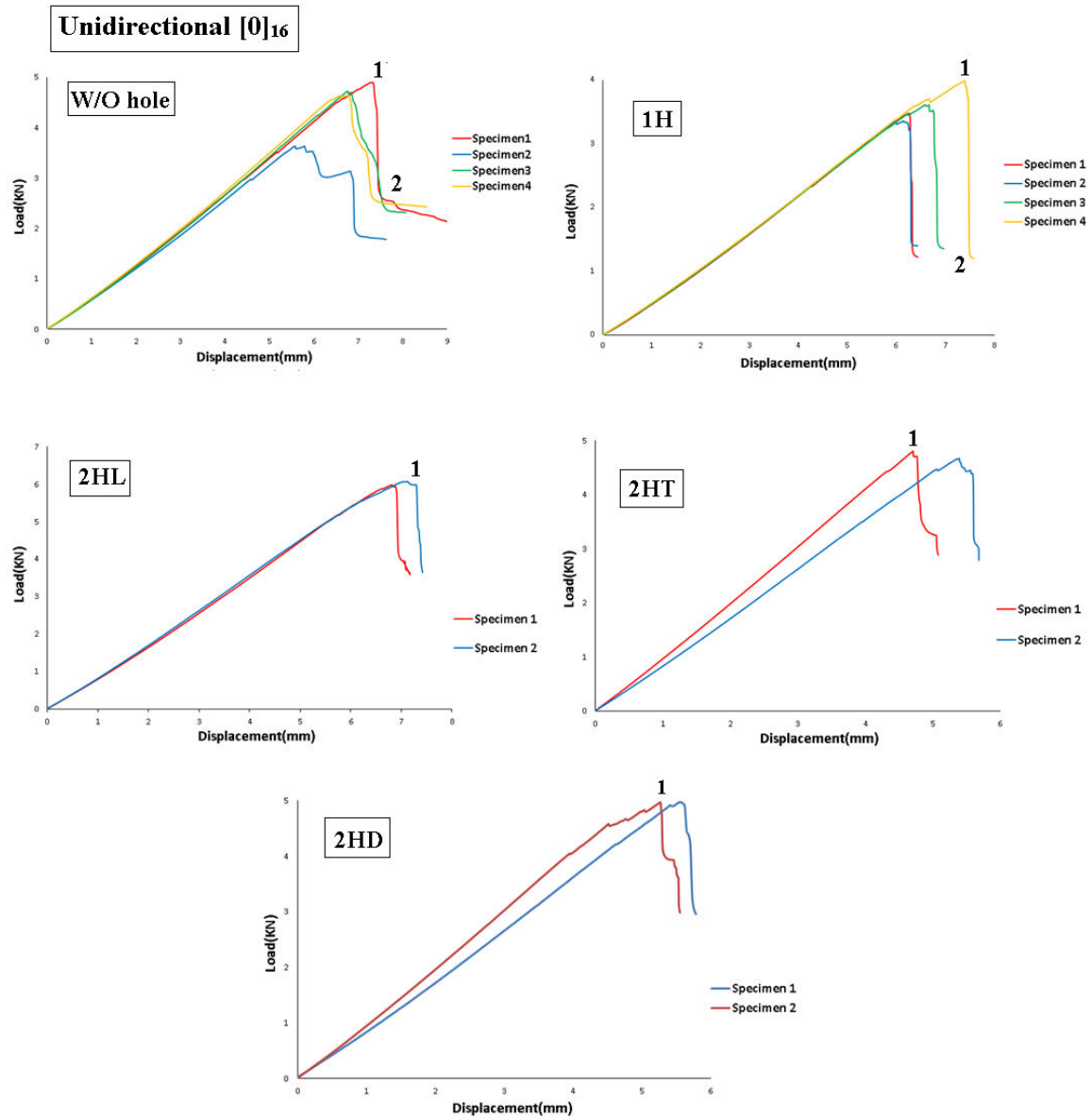
At 1: Final or ultimate failure
From 2 onwards: Delamination

Figure 2.10: Load-displacement plots for Unidirectional CFRP specimens

almost constant and this is the region where delamination occurs. It can also be observed that among the CFRP specimens having multiple holes, the one having two hole longitudinal(2HL) configuration has the highest load carrying capacity.

The plot of load versus displacement for Quasi-isotropic CFRP specimens is shown in Figure 2.11. In this case also, it can be seen that initially the load varies linearly with the applied displacement. Then at a particular point the load ceases to increase linearly with displacement and becomes almost constant with displacement. This is the region where delamination occurs. Then from a particular point, the load decreases sharply with displacement where final or ultimate failure occurs. It is seen

**Quasi-Isotropic [45/0/-45/90]₂ₛ**
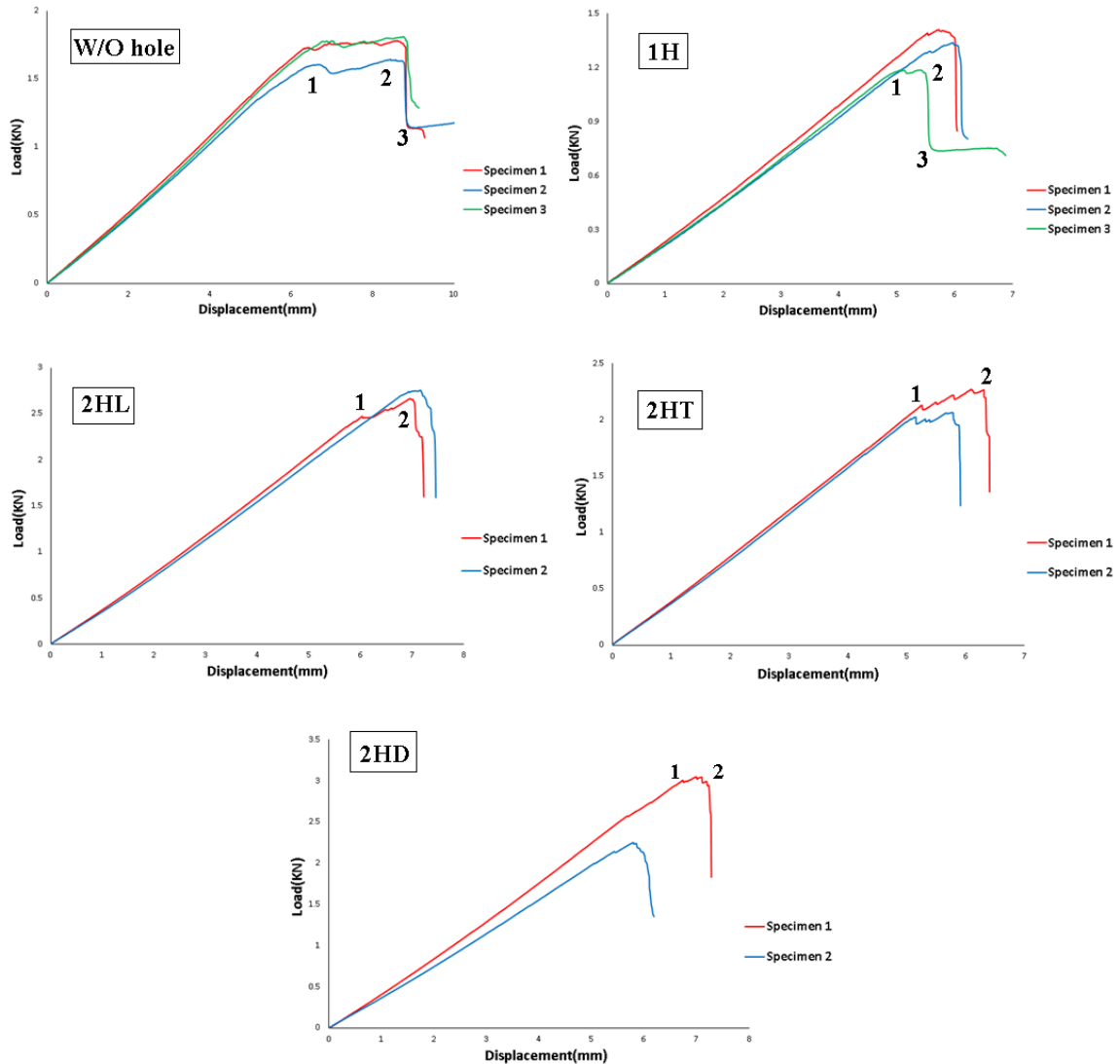
From 1 to 2: Delamination
At 2: Final or ultimate failure

Figure 2.11: Load-displacement plots for Quasi-isotropic CFRP specimens

that the value of final failure load obtained for specimen without hole is around 70 percent of value obtained for that with single hole both in Unidirectional and Quasi-isotropic specimens. It can be seen that in quasi-isotropic specimens, delamination begins to occur before final failure of specimen in contrary to unidirectional specimens where it happens after the final failure of specimen. Therefore delamination has a post-failure effect in unidirectional specimens and pre-failure effect in quasi-isotropic specimens. It can be seen that the slope of plot between load versus displacement is higher in unidirectional specimens than quasi-isotropic specimens. Also the load-carrying capacity of quasi-isotropic specimens is lesser than that of unidirectional specimens. This is due to the fact that when the specimen is loaded by four point bending in this case, the bending stresses will be

24

in the longitudinal direction and therefore it is required to have high stiffness and strength in this direction. In unidirectional specimens, all the fibers are in longitudinal direction which is not the case in quasi-isotropic panels.Since the stiffness and strength is highest in the direction of fibers, unidirectional specimens are more stronger and stiffer than quasi-isotropic specimens in this case.

## 2.6.2 Damage behavior

The damaged unidirectional CFRP specimens on compressive, tensile and thickness side is shown in Figure 2.12. It can be observed that in specimens without hole, first ply failure or failure initiation occurs in the top most ply on compressive side and it occurs in the region of specimen which are in contact with the support rollers as the compressive strength of CFRP composite is lesser than its tensile strength and the compressive stresses and strains are maximum in this region under flexural loading. Then the failure propagates in the transverse direction or the direction along
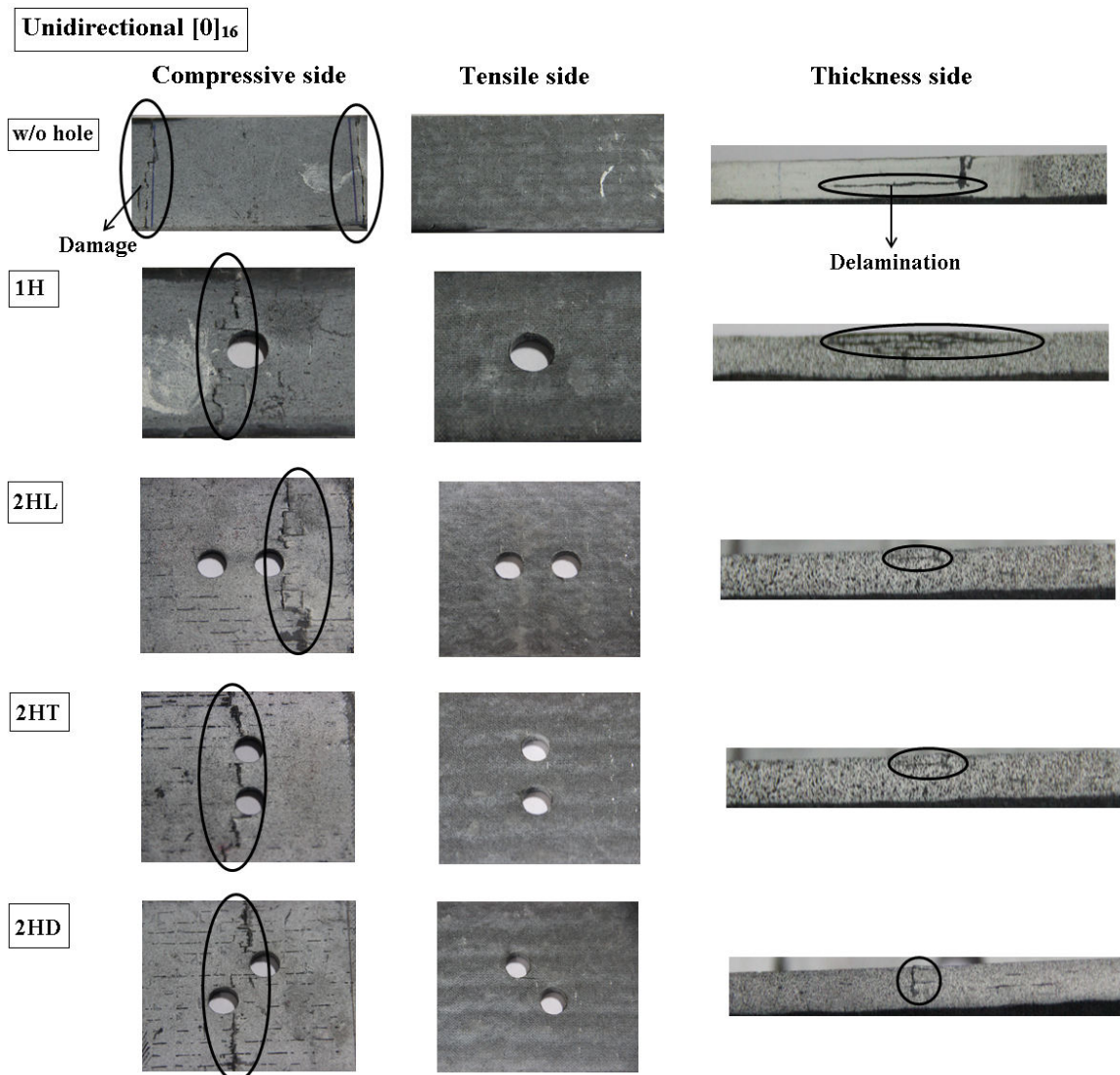


Figure 2.12: Damaged CFRP Unidirectional specimens

width of the specimen. No damage has been observed in the bottom most layer on the tensile side of the specimen. In case of specimens having single and multiple cutouts, first ply failure also occurs in the top most layer on compressive side and it occurs in the region near hole as the hole acts as a stress riser and therefore there will be stress concentration in this region. Then the failure propagates in the transverse direction. Even in these specimens, there was no failure observed on the tensile side. It can also be observed that in specimens having multiple holes having 2HT and 2HD configuration, failure also occurs in the region in-between the holes which implies there is interaction between holes. For Unidirectional CFRP specimens, delamination was observed to occur on the
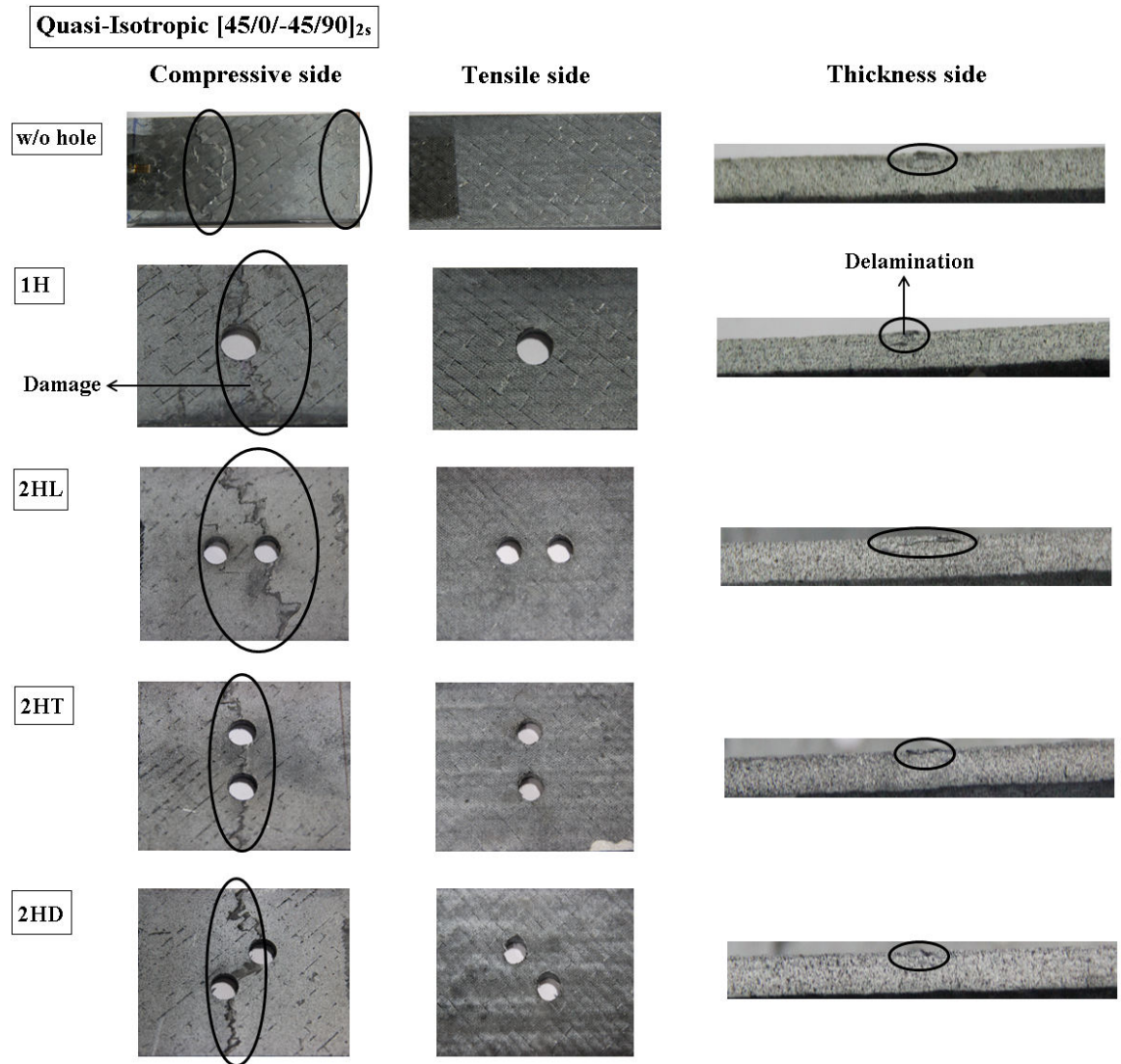


Figure 2.13: Damaged CFRP Quasi-isotropic specimens

compressive side and in case of holes, it was closer to the top most ply.The damaged Quasi-isotropic CFRP specimens on compressive ,tensile and thickness side is shown in Figure 2.13. For all the specimens, the damage behavior was found to be similar to that of unidirectional specimens. Also in this case, there was no failure observed on the bottom most layer on tensile side and delamination in all the specimens occurred on the compressive side.

## 2.7   Closure

The damage behavior CFRP specimens without hole, with single hole(1H) and with multiple holes having three different configurations(2HL, 2HT and 2HD) was studied experimentally. First of all, the CFRP laminate was fabricated through vaccum bagging process. Then the laminate was cut into different specimens through saw machine and end milling on the thickness face and drilling of holes on the specimen were performed. Then the specimens were rubbed against emery paper and speckle pattern was performed along the thickness face of the specimen for the purpose of Digital image correlation(DIC) technique . Once the specimens were completely prepared for experimental testing, they were tested by four point bending test in the MTS machine. Digital image correlation(DIC) technique was employed to measure the in-plane displacements and strains along the thickness face of specimen. It was observed that in both unidirectional and quasi specimens without hole, failure initiation or first-ply failure occurred at the top most region on compressive side and in the region in contact with support rollers. Then the failure propagated through the transverse direction or the direction along the width of the specimen. In case of specimens having single and multiple cutouts, failure initiation occurred near the hole and propagated in the transverse direction. No failure was observed in the bottom most layer on the tensile side of every specimen. Delamination was observed to occur on the compressive side and in case of specimen having single and multiple holes, it was observed to occur close to the top most ply in compression. Also the variation of load versus displacement for each of the specimens was studied. It was found that in Unidirectional specimens, the load varied linearly with displacement until final failure and, the load decreased sharply with displacement and then delamination occured where the load remains almost constant with displacement. In case of quasi isotropic specimens, everything remains the same except that delamination occured before final failure of specimen. Therefore, delamination has a post-failure effect in unidirectional specimens and pre-failure effect in case of quasi-isotropic specimens. In this case, the slope of plot between load and displacement before final failure was higher in unidirectional specimens than in quasi-isotropic specimens. Also the load carrying capacity of unidirectional specimens was higher than that of quasi-isotropic specimens in this case. Therefore unidirectional specimens are stronger and stiffer than quasi-isotropic specimens in this case.

# Chapter 3

# Numerical simulations and comparisons

## 3.1 Introduction

As discussed in the previous chapter, one of the main objectives of this thesis includes performing experimental study of damage behavior of CFRP specimens. Similarly, another main objective includes numerically performing progressive damage analysis and validating the experimental results with the results obtained from this analysis. The numerically study was performed by implementing a three dimensional progressive damage model into a three dimensional finite element simulation. Finite element method(FEM) is a more efficient and quicker way for performing numerical analysis of a structure subjected to a particular loading.Just like in experimental study, numerical study of CFRP specimen without cutout has also been performed for more sequential study better understanding of the problem. This chapter focuses on modeling of CFRP specimens without hole, with single hole(1H) and with multiple cutouts having three different configuration(2HL,2HT,2HD) in the finite-element package. Modeling of CFRP specimen includes creation of the models of previously mentioned configuration, performing meshing and application of boundary conditions on the model,defining material properties and strength parameters of model, description and flowchart of progressive damage model(PDM). PDM includes Hashin failure criteria for predicting failure initiation in model, Material property degradation model(MPDM) for predicting failure propagation in model and cohesive zone model for predicting delamination between layers in the model. Finally the experimental results are compared with the results obtained from numerical study and discussion of these results are done.

## 3.2 Creation of model

Three dimensional FEM models were created in ANSYS 18 Mechanical APDL commercial finite element package for CFRP specimen without cutout, with single hole(1H) and with multiple holes having three different configurations which are two hole longitudinal(2HL), two hole transverse(2HT) and two hole diagonal(2HD) as shown in Figure 3.1. The dimensions given to every model is similar to that of the specimens that were experimentally tested. For models of CFRP specimens without
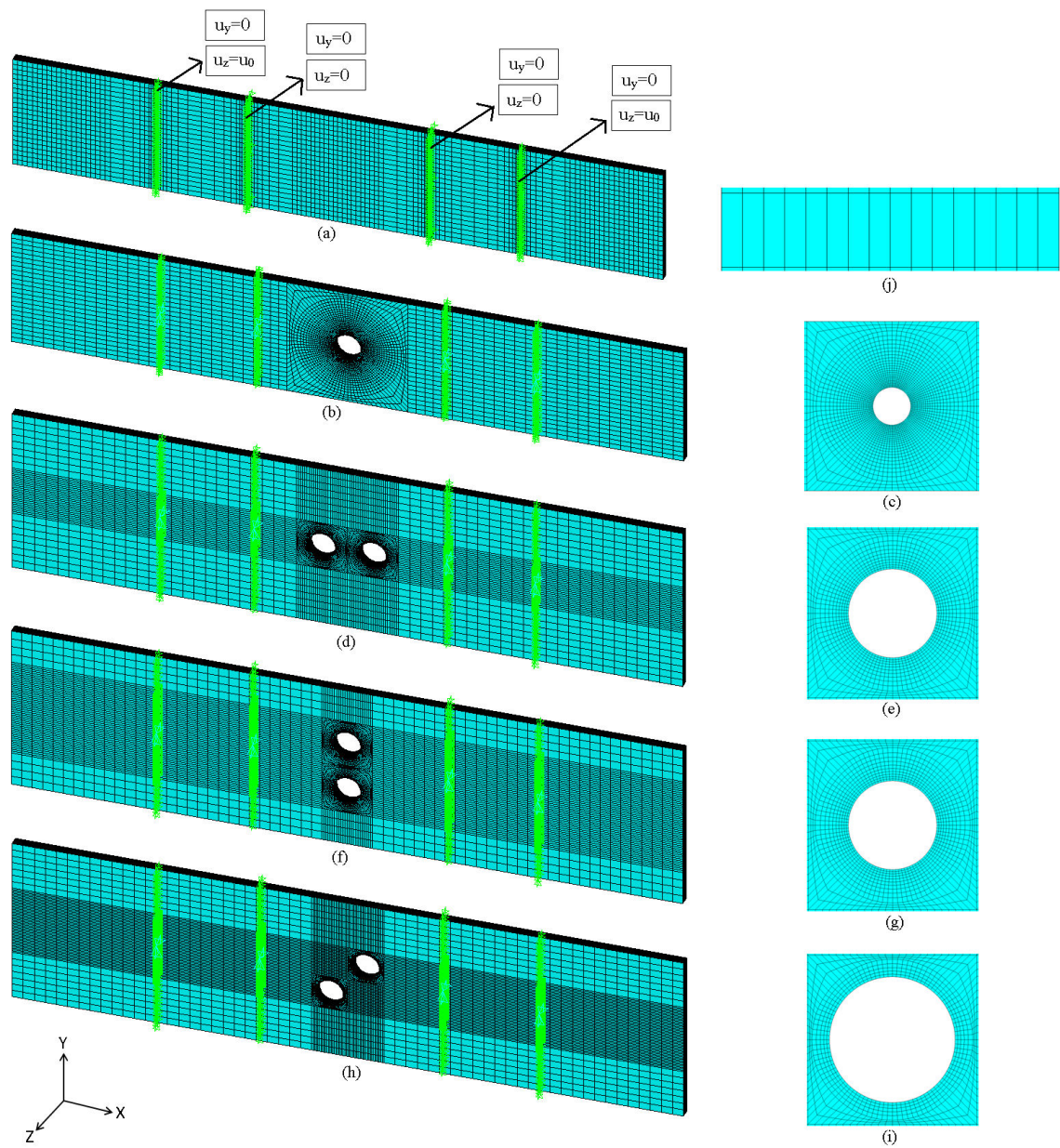
Figure 3.1: 3D Meshed FEA Model along with boundary conditions of CFRP specimen a) without cutout b) single cutout d) 2HL cutouts f) 2HT cutouts h) 2HD cutouts Enlarged view of mesh around hole for CFRP specimen c) single cutout e) 2HL cutouts g) 2HT cutouts i) 2HD cutouts j) Enlarged view of mesh along thickness

29

and with cutout, dimensions include 250mm along length, 45mm along width and 3.6mm along thickness. There was a circular cutout of 10mm diameter created centrally to the model of CFRP specimen with cutout. Dimensions of models of CFRP specimen having multiple cutouts include 250mm along length, 64mm along width and 3.6mm along thickness. Two circular cutouts of diameter 10mm each and their centers separated by 19mm were created for each of the configurations of multiple hole CFRP specimens. As seen in Figure 3.1, each of the models are symmetric and it can be asked that why only a certain portion of the specimen can be modeled so as to save computational time. But the answer is when failure starts initiating and propagating in the specimen, the model loses its symmetricity and therefore whole specimen is modeled for every specimen.

## 3.3    Meshing of model

Each of the models of CFRP specimens were meshed through SOLID 186 brick element. This element has 20 nodes, 8 of which are located at its vertices and the remaining 12 nodes are located at the center of its edges. Three dimensional FEM meshed models for all types of CFRP specimen are shown in Figure 3.1. For CFRP specimen without cutout, mesh size was kept finer close to the regions where the support rollers are placed to get more accurate solutions(Figure 3.1(a)) in those regions. For CFRP specimen having single and multiple cutouts, the mesh was kept finer in region near hole as the stress concentration in this region is very high and it is required to get more accurate solutions in this region. The size of mesh was chosen according to the specifications of [35]. For model with single cutout, circular mesh of radius 20mm was created around the cutout in a square region of dimensions 45x45mm which is equal to the width of the model(Figure 3.1(c)). 96 elements were created in the circumferential direction of cutout and 24 elements were created in the radial direction. For models having multiple cutouts with 2HL and 2HT configuration, circular mesh was created in a square region having dimensions equal to the center of center distance of the cutouts in the model which is 19mmx19mm (Figure 3.1(g)). In model with single cutout, there was circular mesh of radius 20mm in square of length 45mm, so in this case of square having length 19mm, the radius of the circular mesh was proportionally determined and it turned out be 8.75mm. The number of elements in circumferential direction remain same as that of model with cutout because the diameter of cutout remains same and is equal to 96, but since the radius of the circular mesh was decreased in this case, the number of elements along the radial direction also got decreased accordingly and it was reduced to 10. In model having 2HD configuration, the length of diagonal of the square region in which the circular mesh was created equals the center to center distance of the cutouts which is 19mm(Figure 3.1). From this information, the dimensions of square could be calculated and it turned out to be 13.86mmx13.86mm. Similar to previous case of models with 2HL and 2HT cutouts, the radius of the circular mesh in this region was to be reduced proportionally and in this case it becomes 6.4mm. Since the radius of circular mesh became smaller in this case, the number of elements along the radial direction also reduced and it became 5, whereas the number of elements along circumferential direction remains the same which is 96 as the diameter of cutout did not change. For each of the models, the number of elements along the thickness direction is equal to the number of layers in the CFRP laminate which is 16 so that each element corresponds to one layer.

## 3.4    Boundary conditions on model

The boundary conditions for every model were applied according to the boundary conditions of four-point flexural configuration as shown in Figure 3.1(a). In the specified four-point flexural configuration, the specimen was supported and loaded by a set of rollers. The support and load rollers were placed symmetric with respect to specimen and support rollers are separated by 70mm and the load rollers are separated by 140mm. Each support and load roller was in contact with a line of the specimen. With respect to model, X, Y and Z direction represents direction along length, width and thickness respectively. Since the model was supported by rollers, the two lines which were in contact with the support rollers were given roller boundary conditions which means the Z and Y displacement of each of the nodes along these lines is zero. Since the load roller applied load on the model by moving along the z-direction, the nodes along the two lines of the model which were in contact with the two load rollers were given displacement conditions such that the Z component of displacement of the nodes along each of these lines is equal to the maximum value of displacement and the Y component of displacement are zero.

## 3.5    Material properties

The material properties which include elastic constants and strength parameters of CFRP specimen are shown in Table 3.1 and Table 3.2 respectively. These elastic constants and strength parameters were obtained from [36]. The reinforcement for each of the CFRP specimens is carbon fiber of 200 grams per square meter(GSM) and the matrix material includes mixture of resin which is Araldite CY-930 and hardener which is Araldite HY-951 in the ratio of 10:1 by weight. Composite are orthotropic material and therefore there will be 9 independent material constants as shown in Table 3.1. It can be seen from the table 3.1 that the value of Longitudinal modulus, which is the value of Young's modulus along the fiber is very much more than the value of Transverse modulus, which is the value of Young's modulus transverse to the fiber. This information implies that the CFRP composite specimen is much stiffer in the direction along the fiber than in the direction transverse to the fibers. It can also be seen from table 3.1 that the value of Longitudinal compressive strength is lesser and around 50 percent of the value of Longitudinal tensile strength. This detail implies that CFRP composite specimen has weaker strength in compression than in tension along the direction of fiber.

| Material Property | Notation | Value |
|---|---|---|
| Longitudinal modulus | $E_{11}$ | 105.68 Gpa |
| Transverse modulus | $E_{22}$ | 4.64 Gpa |
| Transverse modulus | $E_{33}$ | 4.64 Gpa |
| In-plane shear modulus | $G_{12}$, $G_{13}$ | 3.34 Gpa |
| Out-of plane shear modulus | $G_{23}$ | 1.55 Gpa |
| In-plane poisson ratio | $v_{12}$, $v_{13}$ | 0.36 |
| Out-of plane poisson ratio | $v_{23}$ | 0.49 |

Table 3.1: Elastic constants of CFRP specimen

| Strength Parameter | Notation | Value |
|---|---|---|
| Longitudinal tensile strength | $X_T$ | 1201 MPa |
| Longnitudnal compressive strength | $X_C$ | 600 MPa |
| Transverse tensile strength | $Y_T$ | 15.56 MPa |
| Transverse compressive strength | $Y_C$ | 3.34 MPa |
| Transverse tensile strength | $Z_T$ | 1.55 MPa |
| Transverse compressive strength | $Z_C$ | 0.36 MPa |
| In-plane shear strength | $S_{12}$ | 26.5 MPa |
| In-plane shear strength | $S_{13}$ | 26.5 MPa |
| Out of plane shear strength | $S_{12}$ | 25.13 Mpa |

Table 3.2: Strength parameters of CFRP specimen

## 3.6 Progressive Damage Model

A three dimensional progressive damage model(PDM) has been implemented in the ANSYS Mechanical APDL 18 finite element package to study the damage behavior of CFRP models without hole, with hole(1H) and having multiple holes of three different configuration(2HL,2HT,2HD). This PDM includes prediction of failure initiation which was done through Hashin failure criteria, prediction of failure propagation which was performed through Material property degradation model(MPDM) and prediction of delamination between layers of the model which was done through Cohesive zone model(CZM). In the subsequent subsections, detailed description of each of the previously mentioned models will be given and finally the flowchart of the Progressive damage model will be discussed in detail.

### 3.6.1 Hashin failure criteria

Prediction of failure initiation in the model was done by implementing Hashin failure criteria [37] in the progressive damage model. This failure criteria was initially proposed for Unidirectional polymeric composites as these composites can be treated as transversely isotropic material. It is known that Transversely isotropic materials have one plane of rotational symmetry and it also follows from transverse isotropy that failure criterion must be invariant under rotation of axis on this plane. Since it is also known that the stress invariants are independent of reference axis, the failure criteria can be expressed in terms of these stress invariants. Hashin found out that this equation of failure criteria containing invariants is in such a way that it contains stresses of quadratic nature. An equation of failure criteria containing liner stresses was found to underestimate the failure prediction in the model and on the other hand equation containing cubic and higher order polynomial stresses was too complicated to deal with. The equation of failure criteria containing quadratic stresses was reduced to separate equations for fiber tensile and compressive failure and matrix tensile and compressive failure based on the appropriate conditions for each failure mode. Since this criterion was initially proposed for Unidirectional fiber composites, applications to other types of composites hold significant approximations. The equations of Hashin's failure criteria for fiber tensile failure, fiber

compressive failure, matrix tensile failure and matrix compressive failure are given from Equation 3.1 to 3.6. In these equations,$\sigma_{ij}$, i,j=1,2,3 denotes the stress components, $X_T$ and $X_C$ represents longitudinal tensile and compressive strengths respectively, $Y_T$ and $Y_C$ represents transverse tensile and compressive strengths respectively, $S_{12}$ and $S_{13}$ represents the in-plane shear strengths and $S_{23}$ represents the out-of plane shear strength. In ANSYS 18 Mechanical APDL, Hashin failure criteria was incorporated through APDL macros, which is through user written code.

1. Fiber tensile failure

$$\left(\frac{\sigma_{11}}{X_T}\right)^2 + \frac{\sigma_{12}^2 + \sigma_{13}^2}{S_{12}^2} = \begin{cases} > 1, & \text{failure} \\ < 1, & \text{no failure} \end{cases} \tag{3.1}$$

2. Fiber compressive failure

$$\left(\frac{\sigma_{11}}{X_C}\right)^2 = \begin{cases} > 1, & \text{failure} \\ < 1, & \text{no failure} \end{cases} \tag{3.2}$$

3. Matrix tensile failure

$$\left(\frac{\sigma_{22} + \sigma_{33}}{Y_T}\right)^2 + \frac{\sigma_{23}^2 - \sigma_{22}\sigma_{33}}{S_{23}^2} + \frac{\sigma_{12}^2 + \sigma_{13}^2}{S_{12}^2} = \begin{cases} > 1, & \text{failure} \\ < 1, & \text{no failure} \end{cases} \tag{3.3}$$

4. Matrix compressive failure

$$\left[\frac{Y_C}{2S_{23}} - 1\right]\left(\frac{\sigma_{22} + \sigma_{33}}{Y_C}\right) + \frac{\sigma_{23}^2 - \sigma_{22}\sigma_{33}}{S_{23}^2} + \frac{\sigma_{12}^2 + \sigma_{13}^2}{S_{12}^2} = \begin{cases} > 1, & \text{failure} \\ < 1, & \text{no failure} \end{cases} \tag{3.4}$$

5. Fiber matrix shear failure in tension

$$\left(\frac{\sigma_{11}}{X_T}\right)^2 + \left(\frac{\sigma_{12}}{S_{12}}\right)^2 + \left(\frac{\sigma_{13}}{S_{13}}\right)^2 = \begin{cases} > 1, & \text{failure} \\ < 1, & \text{no failure} \end{cases} \tag{3.5}$$

6. Fiber matrix shear failure in compression

$$\left(\frac{\sigma_{11}}{X_C}\right)^2 + \left(\frac{\sigma_{12}}{S_{12}}\right)^2 + \left(\frac{\sigma_{13}}{S_{13}}\right)^2 = \begin{cases} > 1, & \text{failure} \\ < 1, & \text{no failure} \end{cases} \tag{3.6}$$

### 3.6.2 Material Property Degradation Model

Once initiation of failure has occurred in an element of the model, damage modeling has to be done which accounts for the reduction of stiffness and load carrying capacity of the model. This can be performed through various damage evolution or propagation models such as Material property degradation model(MPDM) in which the selective elastic material properties of the element which has failed is reduced instantaneously depending on the damage mode occurred, Continuum damage model(CDM) where the stiffness of the element which has failed is reduced gradually. In our study, Material property degradation model(MPDM) was implemented for prediction of failure propagation in the model. In this model, if the selective elastic properties of the element were reduced

instantaneously to zero, then the inverse of stiffness matrix becomes undefined which is not possible. Therefore these properties of element were reduced by a factor close to one so that inverse of stiffness matrix does not become undefined. Depending on the damage mode occurred, the selective elastic properties of element were reduced to five percent of its original value as shown in Table 3.3 according to the degradation rule followed in [38]. Similar to Hashin's failure criteria for failure initiation, this model was incorporated in ANSYS 18 Mechanical APDL through macros.

| Damage mode | Elastic properties reduced | Stiffness reduction factor |
|---|---|---|
| Tensile fiber damage | $E_{11}$, $v_{12}$, $v_{13}$, $G_{12}$, $G_{13}$ | 0.95 |
| Compressive fiber damage | $E_{11}$, $v_{12}$, $v_{13}$, $G_{12}$, $G_{23}$, $G_{13}$ | 0.95 |
| Tensile matrix damage | $E_{22}$, $E_{33}$, $v_{23}$, $G_{23}$ | 0.95 |
| Compressive matrix damage | $E_{22}$, $E_{33}$, $v_{23}$, $G_{23}$ | 0.95 |
| Fiber matrix shear damage in tension | $v_{12}$, $G_{12}$ | 0.95 |
| Fiber matrix shear damage in compression | $v_{12}$, $G_{12}$ | 0.95 |

Table 3.3: Properties for MPDM

### 3.6.3 Cohesive zone model

Prediction of delamination between layers of model was done by employing Cohesive zone model(CZM) in the progressive damage model. The cohesive zone model (CZM) is a model in fracture mechanics in which fracture propagation is regarded as a gradual separation of the surfaces in the region ahead of the crack tip. In this model, a narrow-band of vanishing thickness ahead of crack tip is termed the cohesive zone is assumed to exist ahead of a crack tip to represent the fracture process zone as shown in Figure 3.5 (a). The cohesive zone is divided into a number of cohesive elements. The upper and lower surfaces of the cohesive element are termed as the cohesive surfaces. These cohesive surfaces separate on increasing load and are acted by so called cohesive traction as shown in Figure 3.5 (b). There is a cohesive constitutive law that relates these cohesive tractions to the separation displacement between two cohesive surfaces. Many cohesive constitutive laws were suggested by
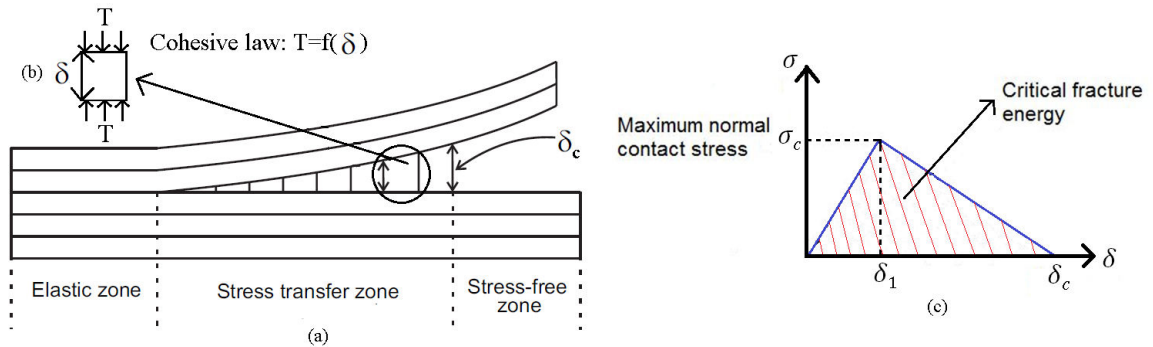


Figure 3.2: a) cohesive zone in front of crack tip divided into cohesive elements b) Traction acting on separated cohesive surfaces c) Bilinear cohesive law
    Courtesy of image (a): Finite element analysis of composite materials by by J.Barbero

34

various researchers who include Dugdale [39], Barenblatt [40], Hillerborg [41], Tvergaard [42], Xu and Needleman [43] etc. Various constitutive laws include bilinear law, polynomial law, trapezoidal law by Tvergaard and exponential law by Xu and Needleman. The cohesive constitutive law which will be implemented here is the bilinear law which is shown in Figure 3.5 (c). From the figure, it can be seen that the stress or traction on the cohesive surfaces increases linearly with the separation distance until a particular value of separation distance. From this value of separation distance, the stress starts to decrease linearly until it vanishes at a critical value of separation distance. The area under the curve of bilinear law is known as critical fracture energy density, which is the energy required per unit area to form two separate surfaces through fracture. Crack growth occurs when the separation of the tail of the cohesive zone, which is the physical crack tip reaches this critical value. Therefore, it can be implied from Cohesive zone model that when initiation of damage occurs, the stress carrying capacity of the two separating faces is not lost completely at that time itself but rather is a progressive event governed by progressive stiffness reduction of the interface between the two separating faces. Cohesive zone model has few advantages over other conventional fracture modeling techniques. One of them is where this approach does not involve crack tip stress singularities as in classical fracture mechanics. Also in this case, material failure is controlled by quantities such as displacements and stresses, which are consistent with the usual strength of materials theory. In ANSYS 18 Mechanical APDL, the cohesive zone modeling was done by introducing contact elements as cohesive elements. For this purpose, firstly three dimensional target elements whose element type is TARGE170 were inserted between the layers of the model. Then three dimensional 8-node surface to surface contact elements whose element type is CONTA174 were inserted in between the layers of model so that they are in complete contact with the target segments. When delamination occurs in the model, the contact elements separate from the target segments. The separation distance between the target element and contact element is known as the contact gap and the tractions which act on the faces of these two elements which are being separated is known as the contact stresses. Bilinear cohesive constitutive law was implemented in this case and it was already inbuilt in Mechanical APDL package. The cohesive zone parameters for the bilinear cohesive law that were fed into the package include the maximum normal contact stress, critical fracture energy density for normal speration, maximum tangential contact stress and critical fracture energy density for tangential slip and artificial damping coefficient as shown in Table 3.6. These parameters have been obtained from [44].

| Property | Value |
|---|---|
| Maximum normal contact stress | 3.25 MPa |
| Critical fracture energy density (energy/area) for normal separation | 0.35 N/mm |
| Maximum tangential contact stress | 6.4 Mpa |
| Critical fracture energy density (energy/area) for tangential slip | 0.68 N/mm |
| Artificial damping coefficient | 0.8 |

Table 3.4: Properties for cohesive zone modeling

### 3.6.4 Flow chart for implementing PDM
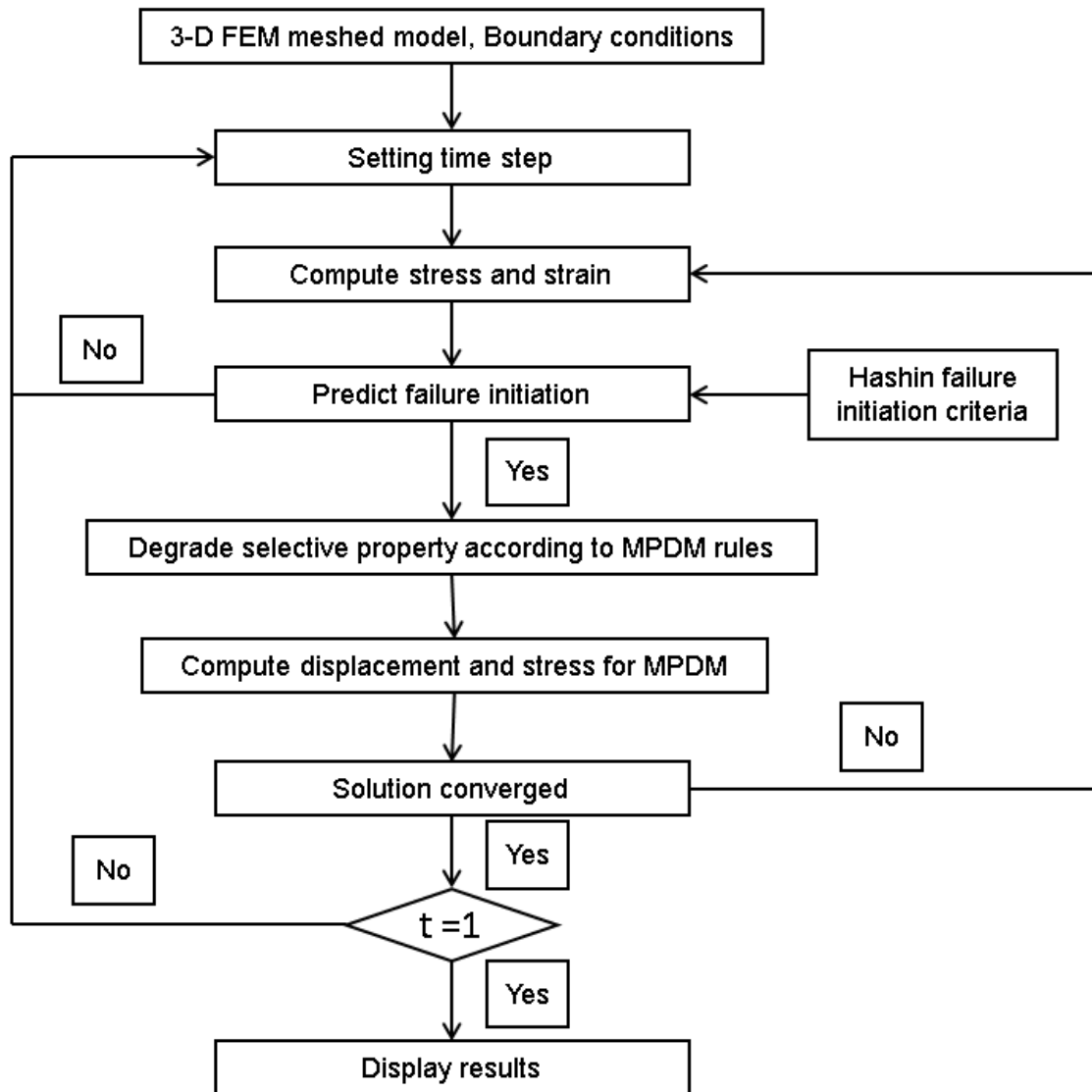


Figure 3.3: Flowchart for implementing PDM

The flowchart for implementation of the three dimensional progressive damage model is shown in Figure 3.3. Once the meshed three dimensional FEM model is created and the required boundary conditions are applied, the number of time steps for the computation of solution was set and then the simulation was being run. During the computation process, first the stress and strain for each element in the model were computed through Finite element method. Once they are computed, failure initiation in the element was checked through Hashin failure criteria. If this failure criteria is satisfied, then the selective elastic properties of the element were reduced according to the rules Material Property Degradation Model(MPDM) and then the displacement and stress for MPDM were calculated. After that it was checked whether the solution is converged.To explain the concept of convergence, the calculation displacement of any node in the model during the failure propagation

phase required solving of non-linear equations. These non-linear equations were solved through a method known as Newton-Raphson method where a particular procedure for finding displacement of node at a particular time step was iterated or repeated certain number of times until the solution is converged. If the solution is converged, then the same procedure for PDM as described before was implemented for the next time step. But if the solution is not converged, then the same procedure starting from computing stress and strain till convergence of solution was performed once more. When the time step reached one, the solution was completely finished and the results which is required by the user can be displayed.

## 3.7 Results and discussion

In this section, firstly the variation of load vs displacement of CFRP specimen without hole, with single hole(1H) and with multiple holes of three different configurations(2HL,2HT,2HD) obtained from this numerical study will be compared with that of experiment and discussed. Then the longitudinal strain contours and plots obtained from FEA will be compared with that of DIC and further discussed.Finally, the progressive damage illustration with increasing load for each of the specimens on compressive and tensile side will be discussed in detail.

### 3.7.1 Load-Displacement plots

The plot of load versus displacement for Unidirectional CFRP specimens are shown in Figure 3.4. The plots obtained from FEA are in decent agreement with that obtained from experiment. From the plots, it can be observed that for CFRP specimen without hole, Hashin's failure criteria used in PDM predicts the final failure load closer to the experimental one but overpredicts the corresponding displacement. For CFRP specimen with single and multiple holes, the failure criteria overpredicts the displacement and underpredicts the final failure load.

The plot of load versus displacement for Quasi-isotropic CFRP specimens are shown in Figure 3.5. In CFRP specimens without,with single hole and multiple holes of 2HT configuration, Hashin's failure criteria predicts both final failure load close to the experimental one but in specimen without hole and 2HT configuration, it underpredicts the final displacement and in specimen with single hole, it overpredicts the corresponding displacement. In 2HL and 2HD configuration, the failure criteria underpredicts the final failure load but predicts the corresponding displacement close to the experimental one. The values of final failure load and corresponding displacement obtained from experiment and PDM are shown in Table 3.5 and Table 3.6 respectively. The deviation of PDM from experiment occurs due to the choice of failure theory. Several composite failure theories perform well in some cases and does not perform well in some cases. Even the prediction of damage behavior by PDM is dependent on the choice of model for predicting damage evolution, which in our case is Material property degradation model(MPDM). Since in this model, selective material properties were degraded instantaneously to five percent rather than gradually, the damage behavior could not be studied properly.
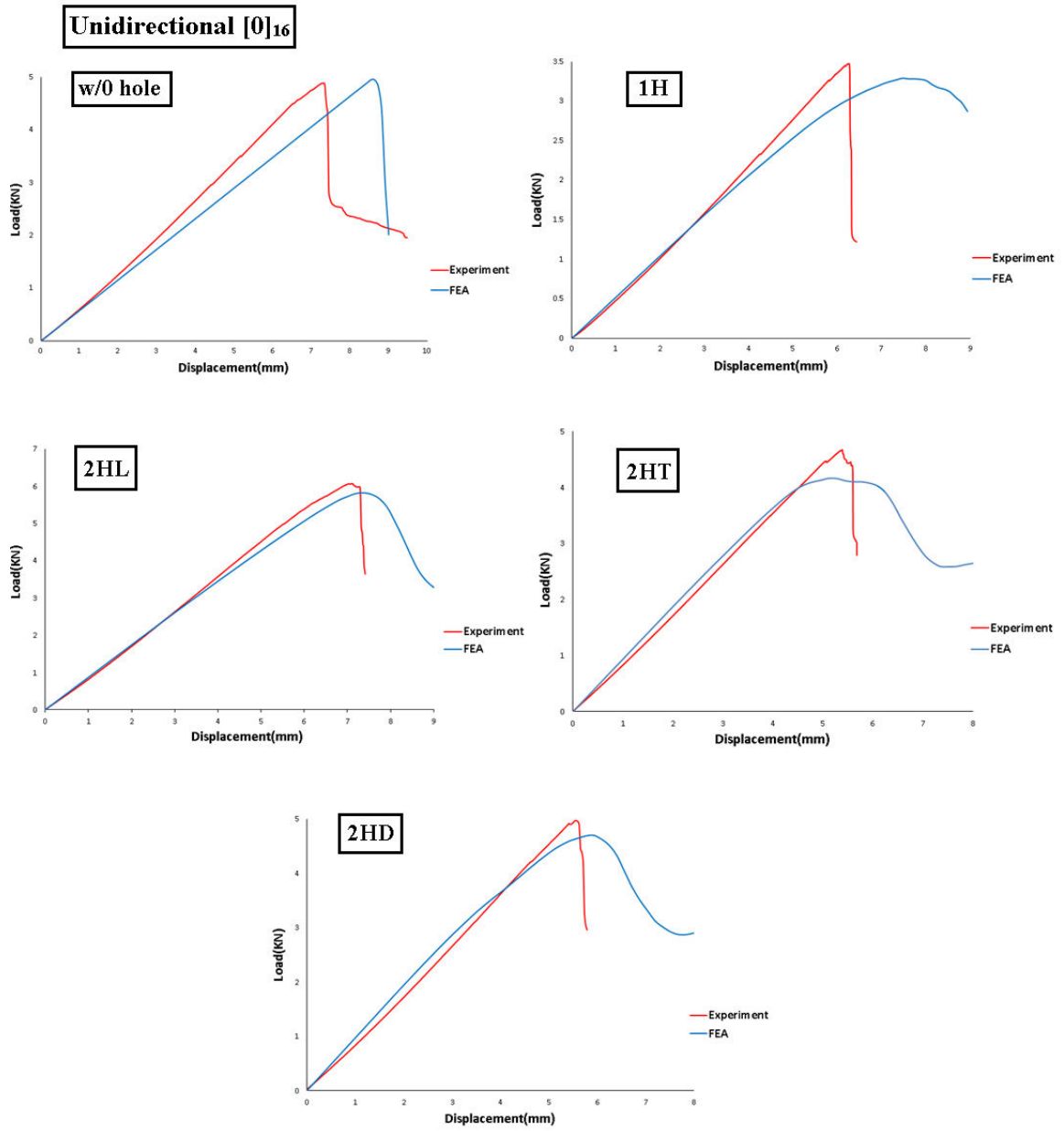
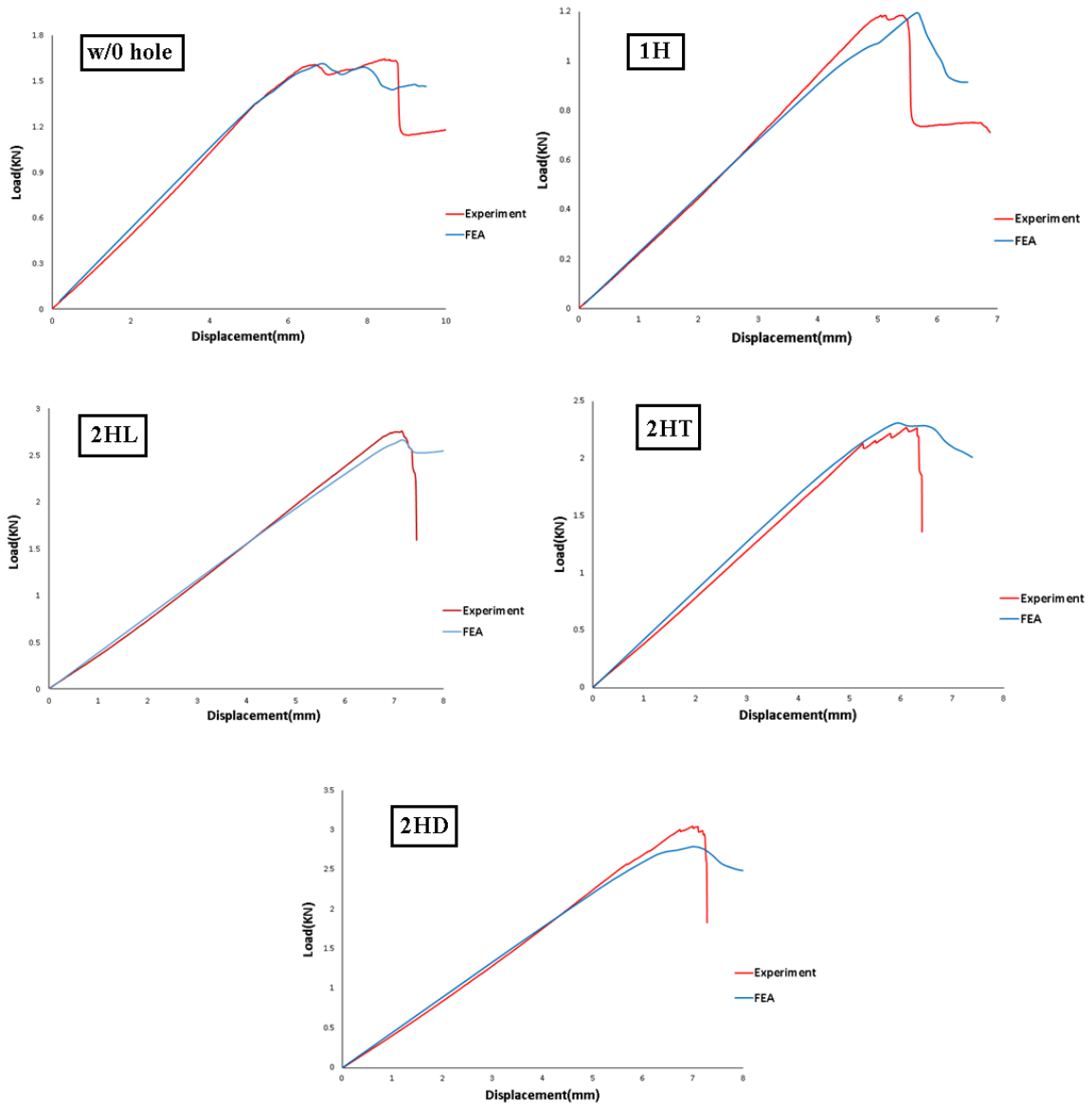Figure 3.4: Load-displacement plots for Unidirectional specimens

Figure 3.5: Load-displacement plots for Quasi-Isotropic specimens

| Configuration | Experiment | | PDM | |
|---|---|---|---|---|
| | Ultimate load(KN) | Disp(mm) | Ultimate load(KN) | Disp(mm) |
| Without hole | 4.892 | 7.284 | 4.95 | 8.55 |
| Single hole(1H) | 3.477 | 6.266 | 3.286 | 7.283 |
| Two hole Longitudinal(2HL) | 5.978 | 6.425 | 5.82 | 7.38 |
| Two hole transverse(2HT) | 4.672 | 5.248 | 4.03 | 6.08 |
| Two hole diagonal(2HD) | 4.9 | 5.412 | 4.7 | 5.92 |

Table 3.5: Final failure load and displacement for Unidirectional specimens

| Configuration | Experiment | | PDM | |
|---|---|---|---|---|
| | Ultimate load(KN) | Disp(mm) | Ultimate load(KN) | Disp(mm) |
| Without hole | 1.634 | 8.72 | 1.59 | 7.89 |
| Single hole(1H) | 1.186 | 5.414 | 1.19 | 5.63 |
| Two hole Longitudinal(2HL) | 2.77 | 6.877 | 2.66 | 7.2 |
| Two hole transverse(2HT) | 2.266 | 6.198 | 2.29 | 6.48 |
| Two hole diagonal(2HD) | 2.947 | 6.866 | 2.79 | 7.02 |

Table 3.6: Final failure load and displacement for Quasi-isotropic specimens

### 3.7.2   Strain plots

The longitudinal strain contours for Unidirectional and Quasi-isotropic CFRP specimens without and with single hole are shown in Figure 3.6 for CFRP specimens with multiple holes are shown in Figure 3.7 and Figure 3.8. It can be seen that the contours obtained from DIC agree well with that obtained from FEA. It can also be seen from these contours that the strain increases gradually from one particular negative value at the top most layer in compression to around positive of that same value at the bottom most layer in tension. The plot of longitudinal strain versus specimen thickness for Unidirectional and Quasi-isotropic CFRP specimens are shown in Figure 3.9 and Figure 3.10 respectively. All the contours and plots were taken at 80 percent of final failure load. From the plots, it can be seen that the results obtained from DIC agree well with that of FEA. It can also be seen that there is a linear variation of longitudinal strain along the specimen thickness from one negative value to around the positive of that same value. It can also be seen at zero location where the neutral axis is present, the longitudinal strain is close to zero. The deviation of DIC results from FEA can mainly be due to speckle pattern which was performed manually because of which to which few pixels may not have a unique identity or grey value information and because of this wrong correlation from one subset from deformed image to original image might occur. The accuracy of DIC results also depends on the pixel size in the images taken and number of subsets.
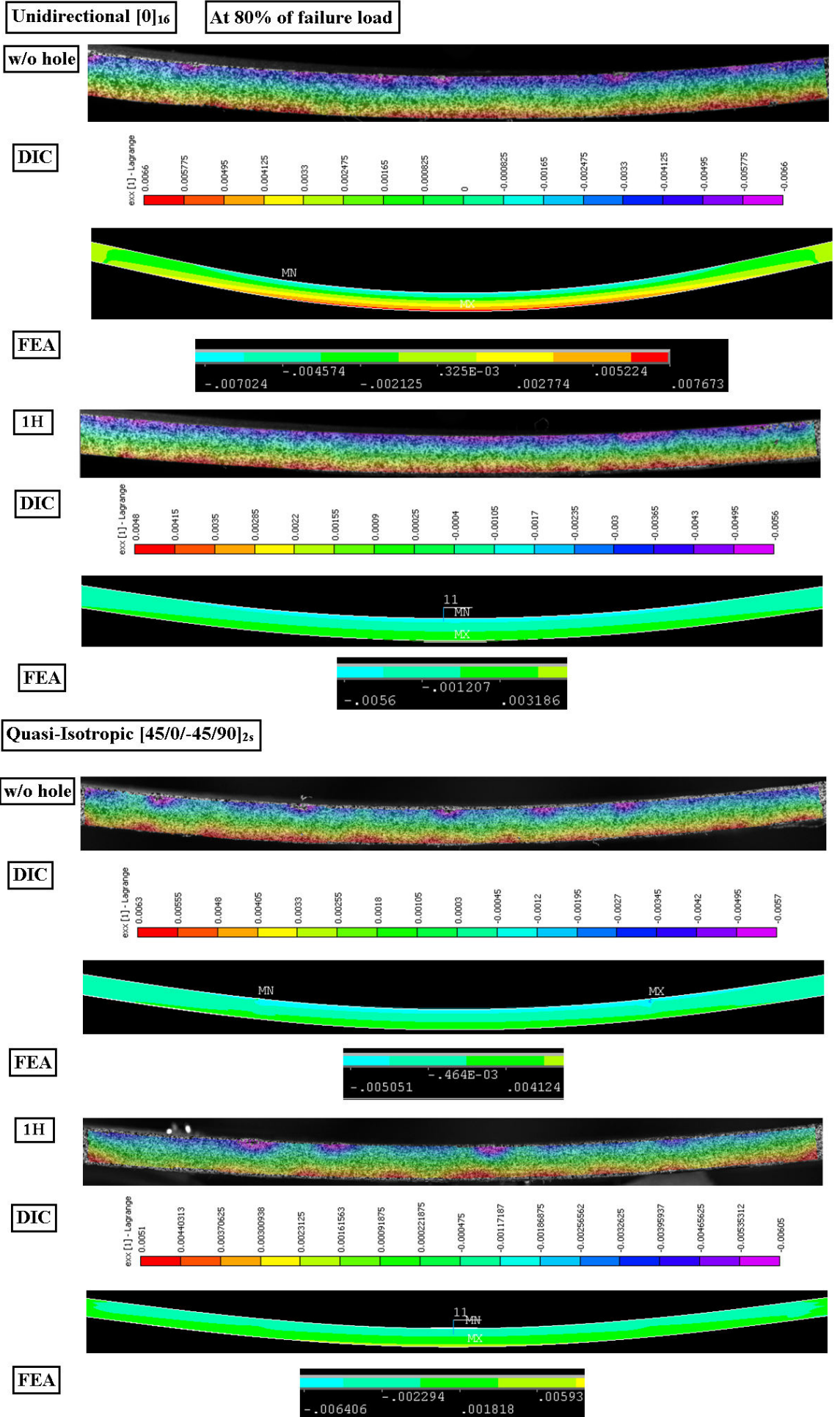
Figure 3.6: Longitudinal strain contours for Unidirectional and Quasi-isotropic specimens without and with single hole
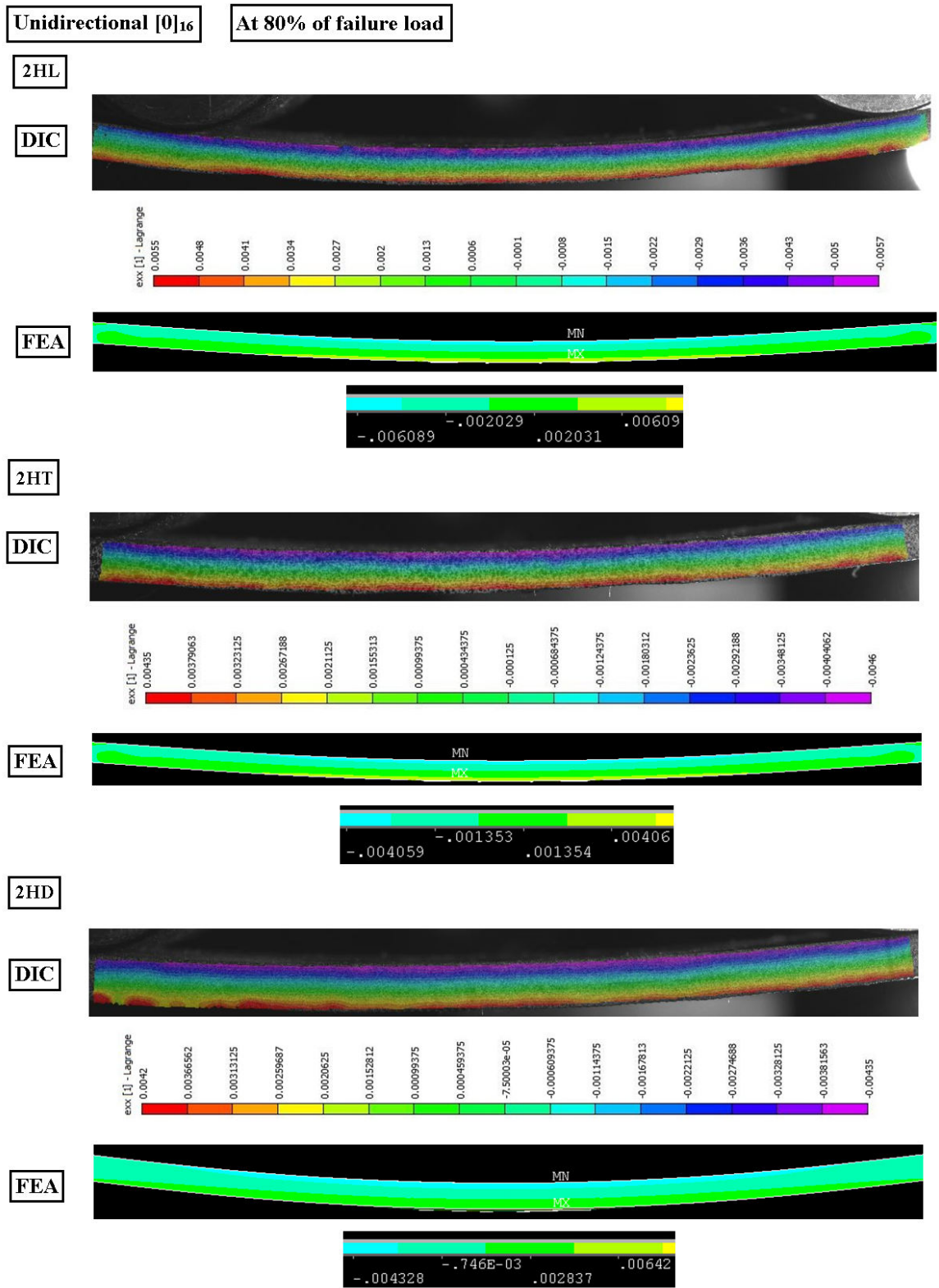
Figure 3.7: Longitudinal strain plots for Unidirectional specimens with multiple holes
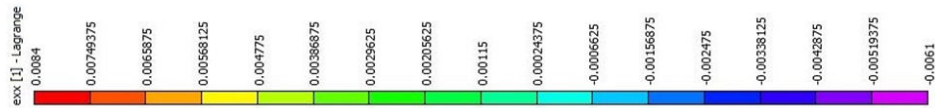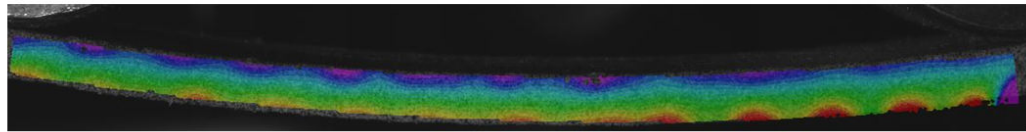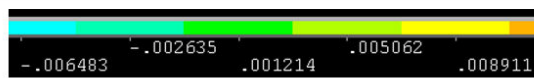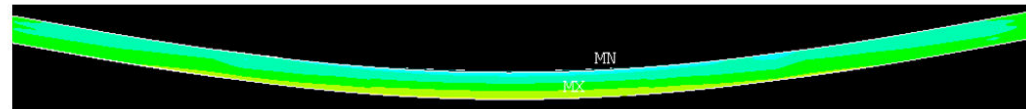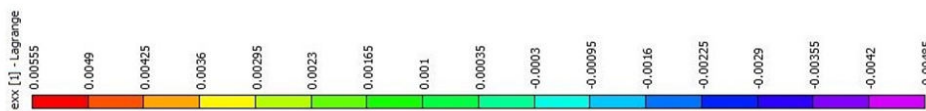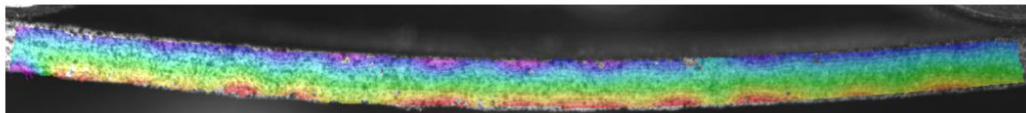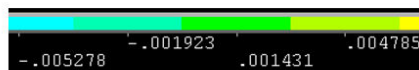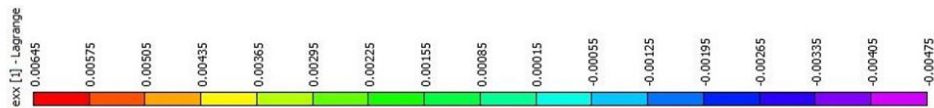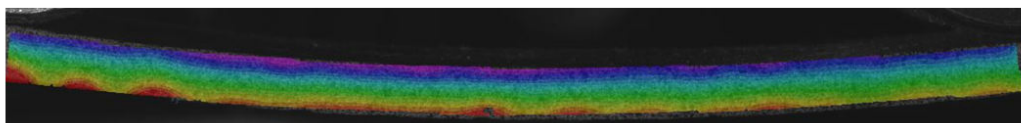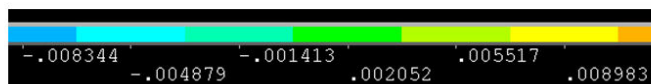
Figure 3.8: Longitudinal strain contours for Quasi-Isotropic specimens with multiple holes
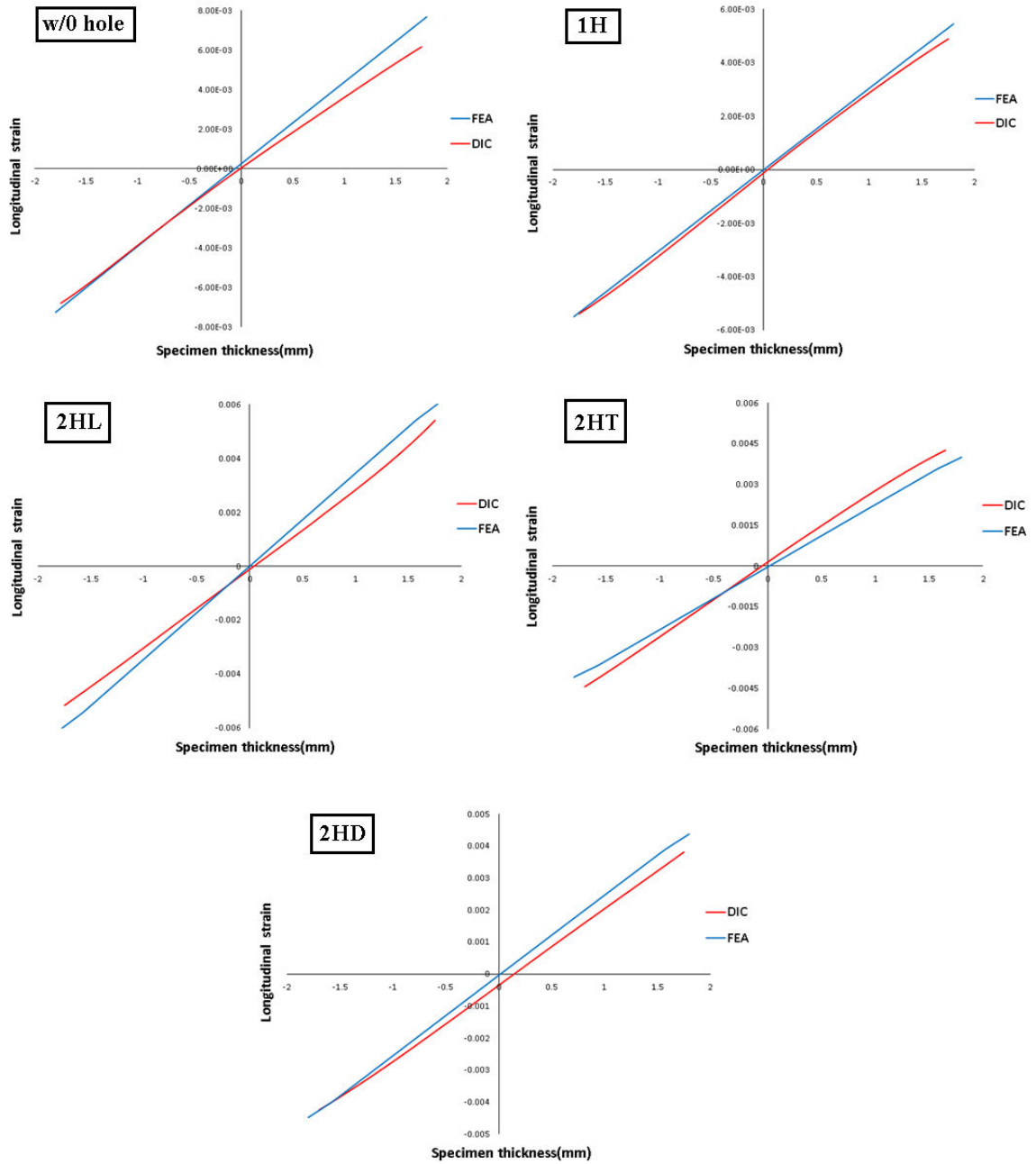
Figure 3.9: Longitudinal strain plots for Unidirectional specimens
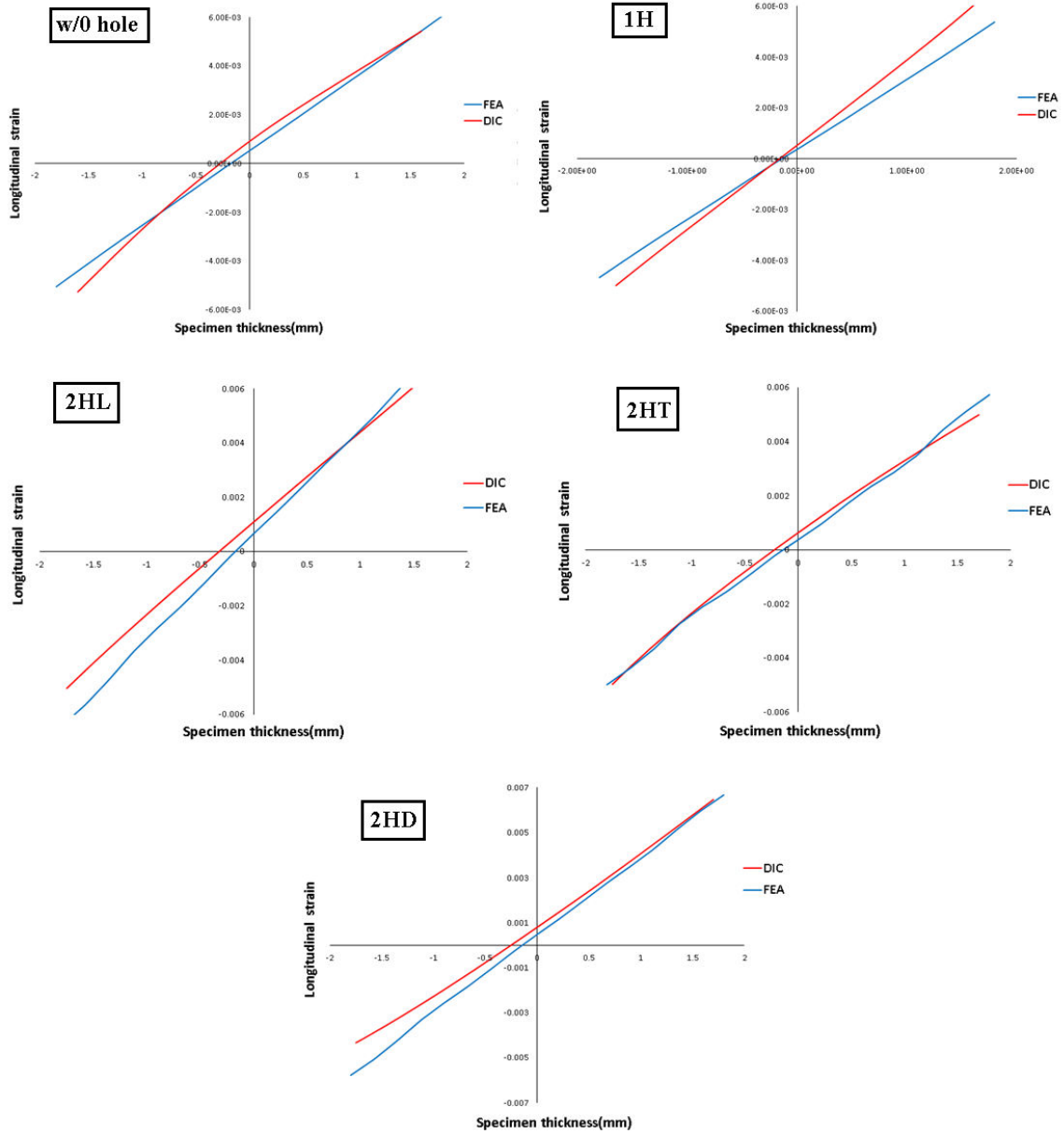
Figure 3.10: Longitudinal strain plots for Quasi-Isotropic specimens

### 3.7.3 Progressive damage illustration

**Unidirectional CFRP Specimens**

The illustration of damage propagation predicted by PDM for Unidirectional specimen are shown from Figure 3.11 to Figure 3.15. For CFRP specimen without hole, damage initiates at the top most layer on the compressive side at the location of support rollers. Damage initiates in the form of fiber matrix shear failure. With increase in load, fiber matrix shear failure increases and also more than one mode of failure occurs near the location of support rollers. On the tensile side, damage initiates in the form of matrix failure at the location of support rollers and with increase in load, matrix failure increases and more than one mode of failure happens near the support rollers. For CFRP specimen having single and multiple holes, damage initiates at the top most layer on the compressive side near hole in the form of fiber matrix shear failure. As the load increases, fiber matrix shear failure propagates in the transverse direction and slightly in the longitudinal direction. Also more than one mode of failure begins to occur and propagates in the transverse direction. On the tensile side, damage initiates in the form of matrix cracking with increase in load, this mode of failure propagates in the longitudinal direction and more than one mode of failure also occurs.Also it can be seen that there is damage in-between holes for 2HT and 2HD specimen which implies there is interaction between holes in these cases. The comparison of finally failed specimen from experiment and that from PDM on compressive and tensile side are shown in Figure 3.16 and Figure 3.17 respectively. It can be seen that on the compressive side, the path of damage progression obtained from PDM agrees well with that from experiment. On the tensile side, no fiber failure is observed from experiment but more than one mode of failure is observed from PDM. This implies the modes of damage occuring on tensile side in PDM are matrix failure and fiber matrix shear failure.



Figure 3.11: Illustration of damage propagation predicted by PDM with increasing load for Unidirectional specimen without hole
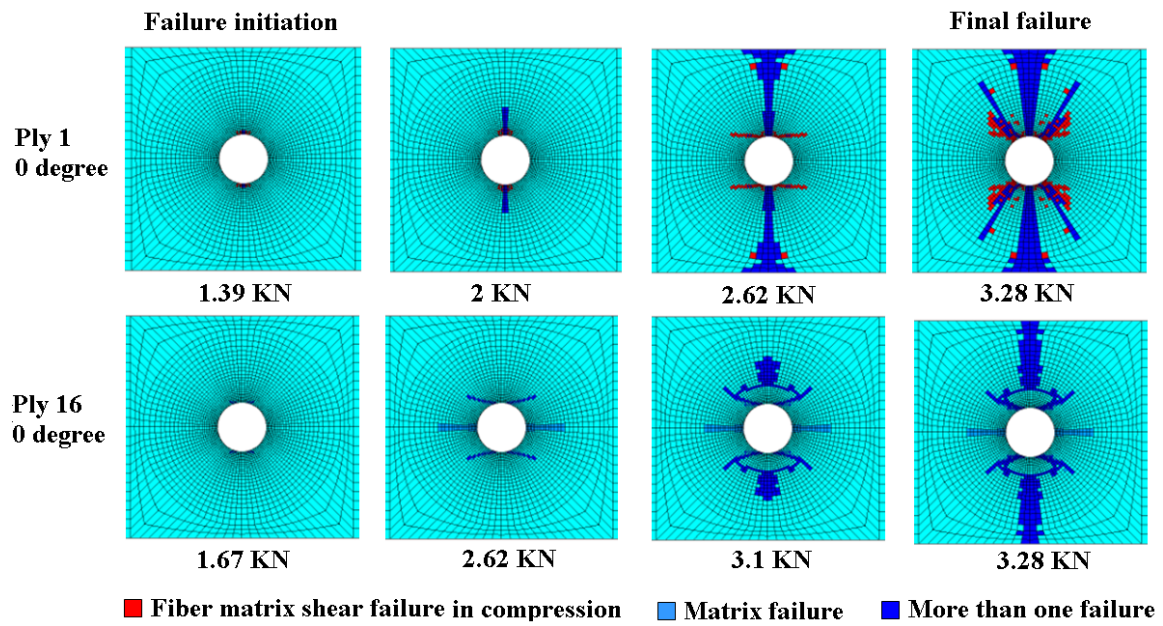
Figure 3.12: Illustration of damage propagation predicted by PDM with increasing load for Unidirectional specimen with single hole(1H)
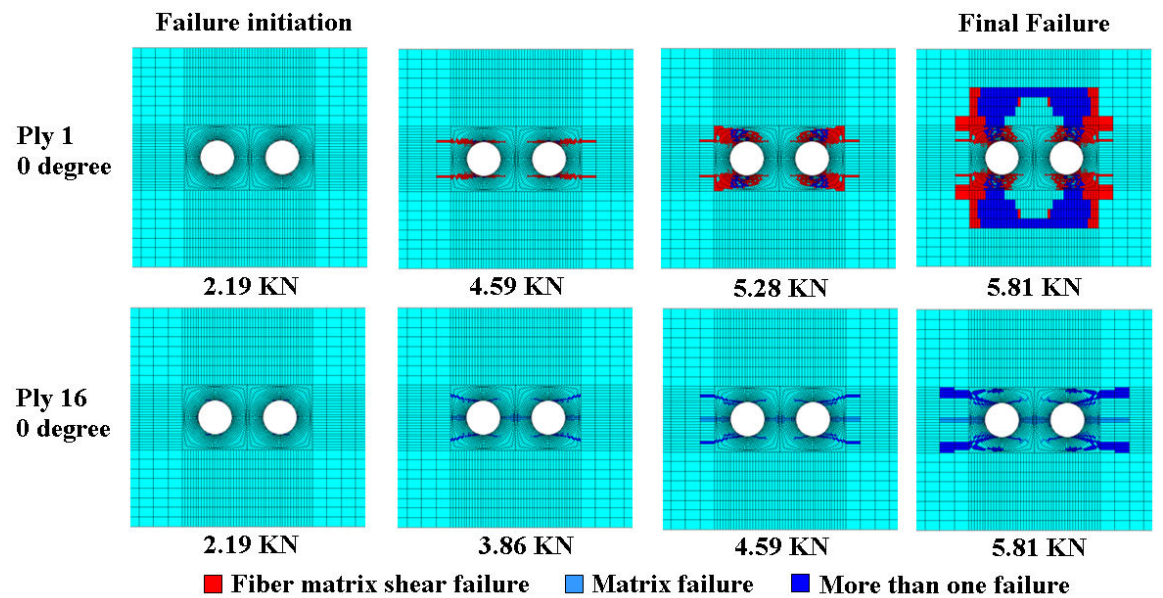


Figure 3.13: Illustration of damage propagation predicted by PDM with increasing load for Unidirectional specimen having 2HL configuration

**Failure initiation**  **Final Failure**

| | | | |
|---|---|---|---|
| Ply 1 0 degree | 1.95 KN | 3.63 KN | 4.1 KN | 4.03 KN |

| | | | |
|---|---|---|---|
| Ply 16 0 degree | 1.95 KN | 3.63 KN | 4.1 KN | 4.03 KN |

■ **Fiber matrix shear failure**  ■ **Matrix failure**  ■ **More than one failure**
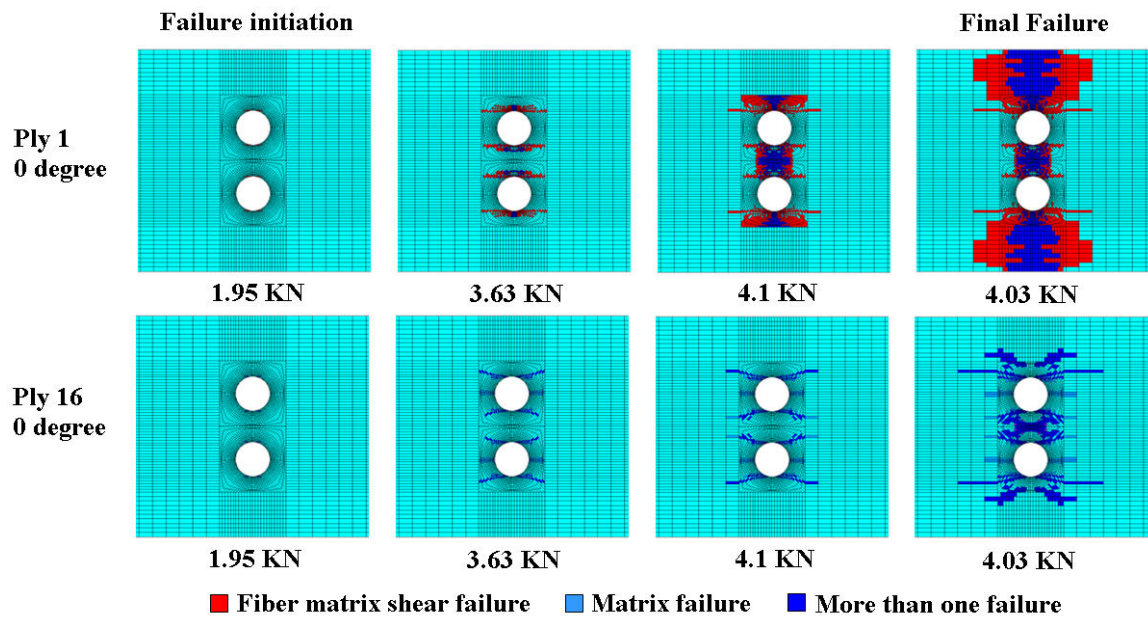
Figure 3.14: Illustration of damage propagation predicted by PDM with increasing load for Unidirectional specimen having 2HT configuration



**Failure initiation**  **Final Failure**

| | | | |
|---|---|---|---|
| Ply 1 0 degree | 1.86 KN | 3.64 KN | 4.16 KN | 4.53 KN |

| | | | |
|---|---|---|---|
| Ply 16 0 degree | 1.86 KN | 2.76 KN | 3.88 KN | 4.53 KN |

■ **Fiber matrix shear failure**  ■ **Matrix failure**  ■ **More than one failure**
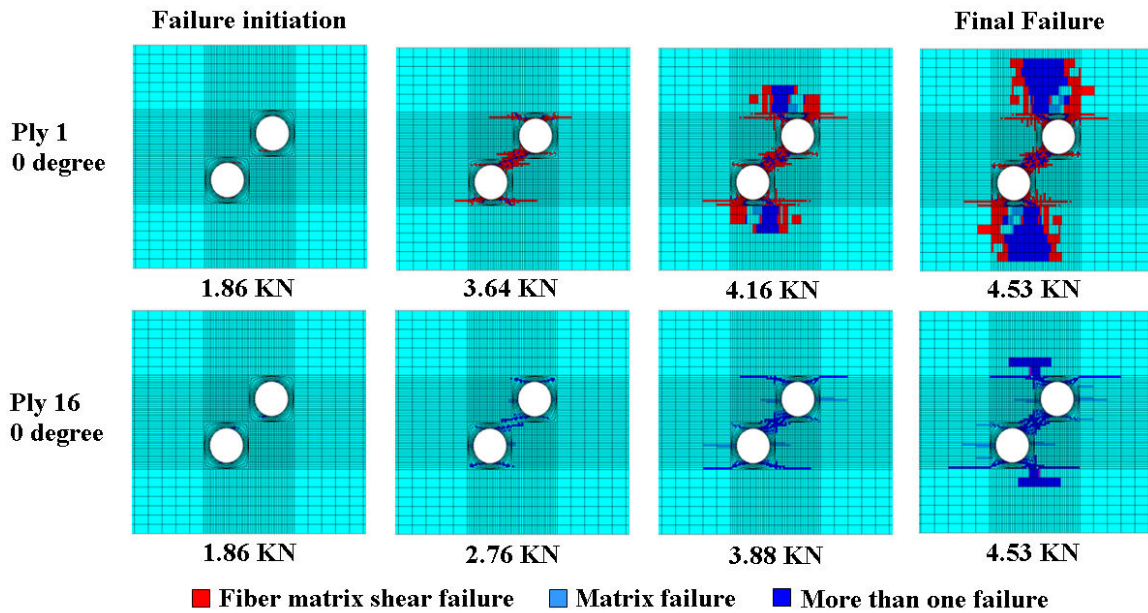
Figure 3.15: Illustration of damage propagation predicted by PDM with increasing load for Unidirectional specimen having 2HD configuration

|  | PDM | Experiment |
|---|---|---|
| w/o hole | | |
| 1H | | |
| 2HL | | |
| 2HT | | |
| 2HD | | |

■ Fiber matrix shear failure    ■ Matrix failure    ■ More than one failure
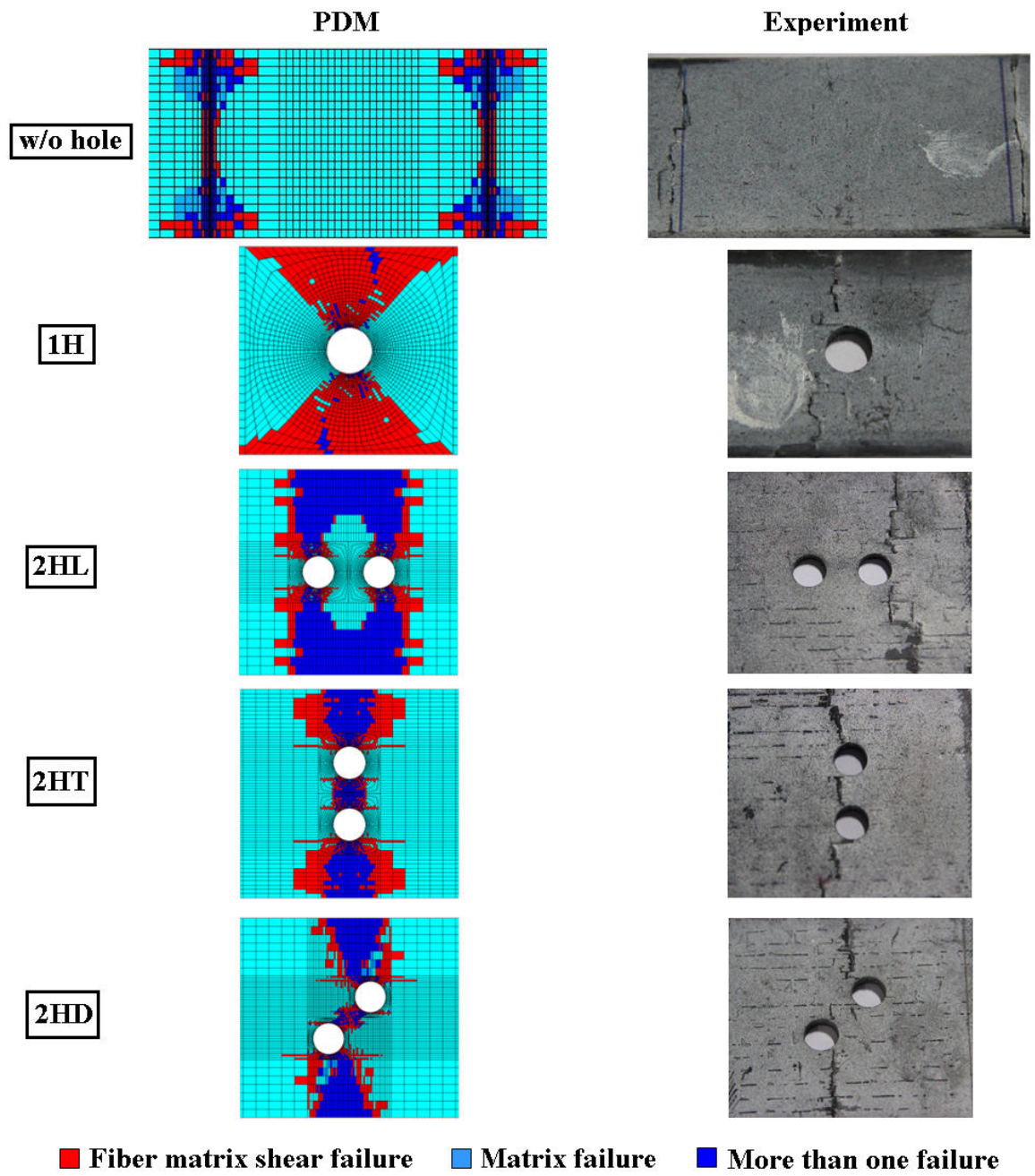
Figure 3.16: Final failure of Unidirectional specimens on compressive side

|          | PDM | Experiment |
|----------|-----|------------|
| w/o hole |     |            |
| 1H       |     |            |
| 2HL      |     |            |
| 2HT      |     |            |
| 2HD      |     |            |

■ Fiber matrix shear failure in compression    ■ Matrix failure
■ More than one failure    ■ Fiber matrix shear failure in tension

Figure 3.17: Final failure of Unidirectional specimens on tensile side

**Quasi-Isotropic CFRP Specimens**

The illustration of damage propagation predicted by PDM for Quasi-isotropic specimen on the top four plies in compression and on the bottom four plies in tension are shown from Figure 3.18 to Figure 3.26. For CFRP specimen without hole, damage initiates at the top most ply in compression whose fiber orientation is 45 degrees at the location of support rollers. On increase with load, this mode of failure begins to occur throughout the specimen in the region between support rollers and becomes the dominant mode of failure in this ply. In 0 degree ply, more than one mode of failure occurs with increasing load near the location of support rollers. In -45 degree ply, fiber matrix shear occurs with increasing load in the region near support rollers and becomes the dominant mode of failure. But the damage in this ply is lesser compared to 45 degree ply as this ply is closer to the neutral axis. The damage in 90 degree ply is very less compared to the other plies as this ply is closest to the neutral axis. On the tensile side, damage initiates at the bottom most ply whose fiber orientation is 45 degrees in the form of matrix failure and with increase in load, this mode of failure increases and occurs throughout the region of specimen in between the support rollers and on further increase in load, more than one mode of failure occurs dominantly in this region in this ply. In the zero degree ply, more than one mode of failure occurs with increasing load near the support rollers. In -45 degree ply, matrix failure occurs throughout the specimen with more than one mode of failure occurring near the support rollers. In 90 degree ply, predominantly matrix failure occurs throughout the specimen with increase in load. In CFRP specimens with single and multiple holes, the modes of damage in each ply are similar to that of CFRP specimen without hole except in -45 and 45 degree plies in tension, both matrix failure and more than one mode of failure occurs with uncertainty which mode of failure is dominant. However, the location of damage initiation and propagation is different. In this case, damage initiates near hole and propagates in the transverse direction. Also it can be seen that there is interaction between holes for 2HT and 2HD specimen. The comparison of finally failed specimen from experiment and that from PDM on compressive and tensile side are shown in Figure 3.27 and Figure 3.28 respectively. It can be seen that on the compressive side, the the path of damage progression obtained from PDM agrees well with that from experiment. On the tensile side, no fiber failure is observed from experiment but more than one mode of failure is observed from PDM. This implies the modes of damage occurring on tensile side in PDM are matrix failure and fiber matrix shear failure.
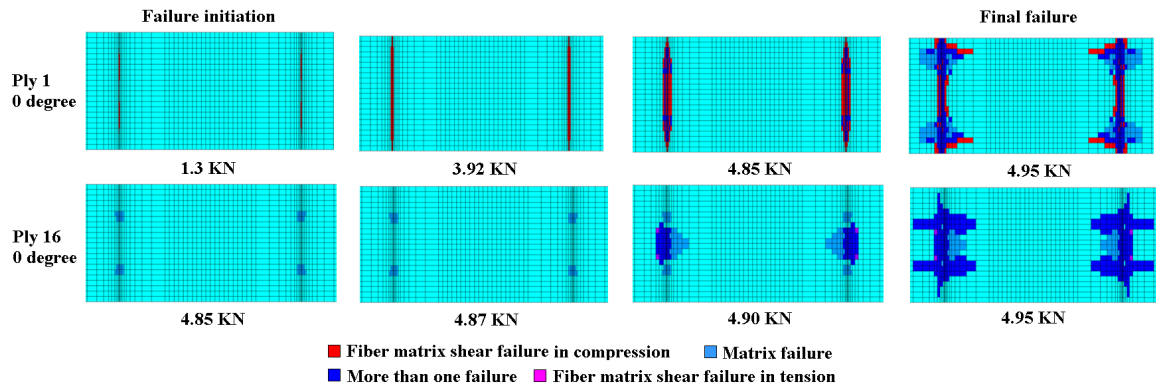
Figure 3.18: Illustration of damage propagation predicted by PDM with increasing load for Quasi-isotropic specimen without hole on compressive(top) and tensile side(bottom)
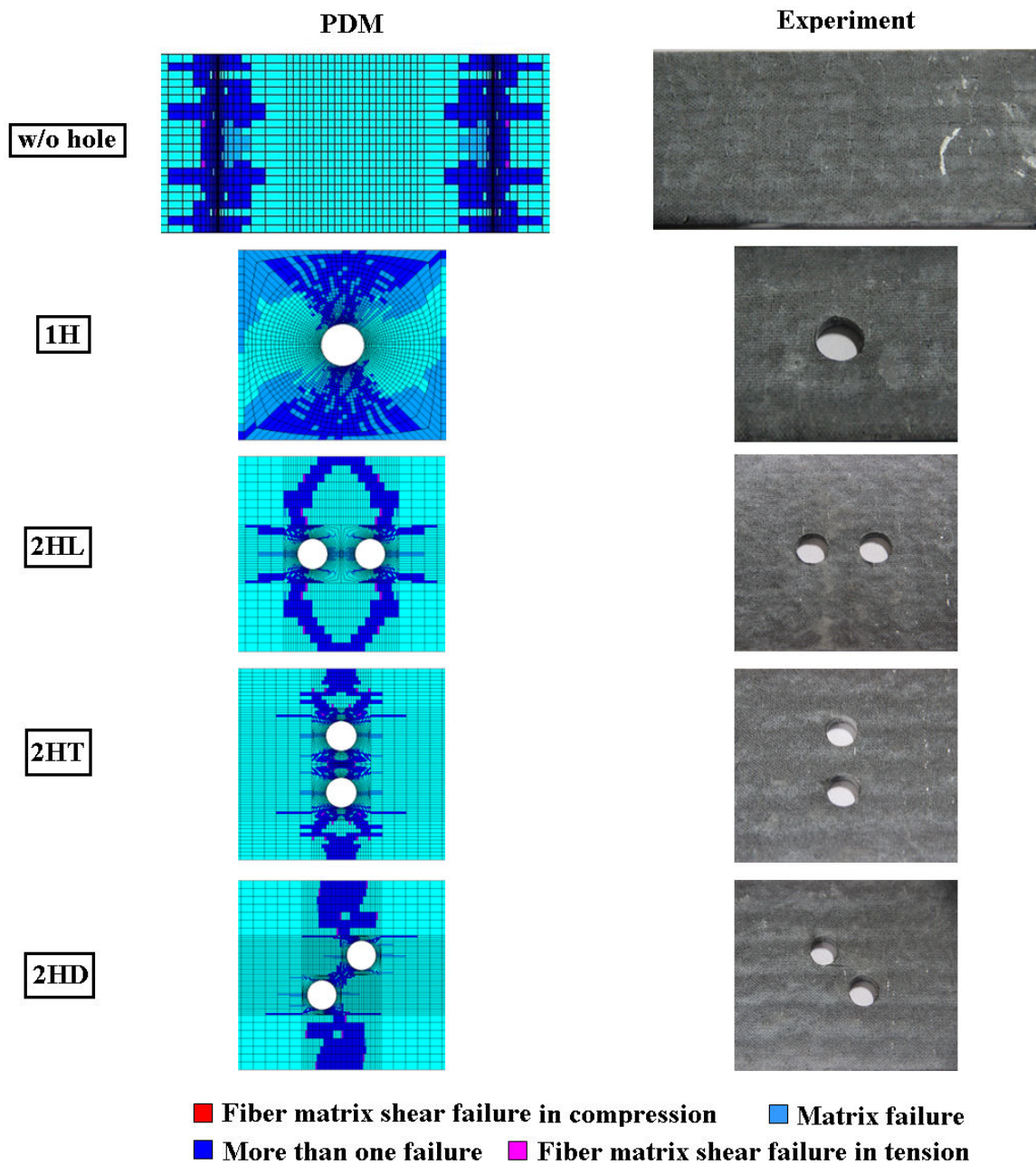
**Failure initiation**                                                  **Final failure**

**Ply 1 45 degree**

0.47 KN         0.94 KN         1.02 KN         1.19 KN

**Ply 2 0 degree**

0.59 KN         0.94 KN         1.07 KN         1.19 KN

**Ply 3 -45 degree**

0.69 KN         0.94 KN         1.07 KN         1.19 KN

**Ply 4 90 degree**

1.07 KN         1.13 KN         1.17 KN         1.19 KN

■ **Fiber matrix shear failure in compression**    ■ **Matrix failure**    ■ **More than one failure**

Figure 3.19: Illustration of damage propagation predicted by PDM with increasing load for Quasi-isotropic specimen with single hole(1H) on compressive side

Figure 3.20: Illustration of damage propagation predicted by PDM with increasing load for Quasi-isotropic specimen with single hole(1H) on tensile side

Figure 3.21: Illustration of damage propagation predicted by PDM with increasing load for Quasi-isotropic specimen having 2HL configuration on compressive side

Figure 3.22: Illustration of damage propagation predicted by PDM with increasing load for Quasi-isotropic specimen having 2HL configuration on tensile side
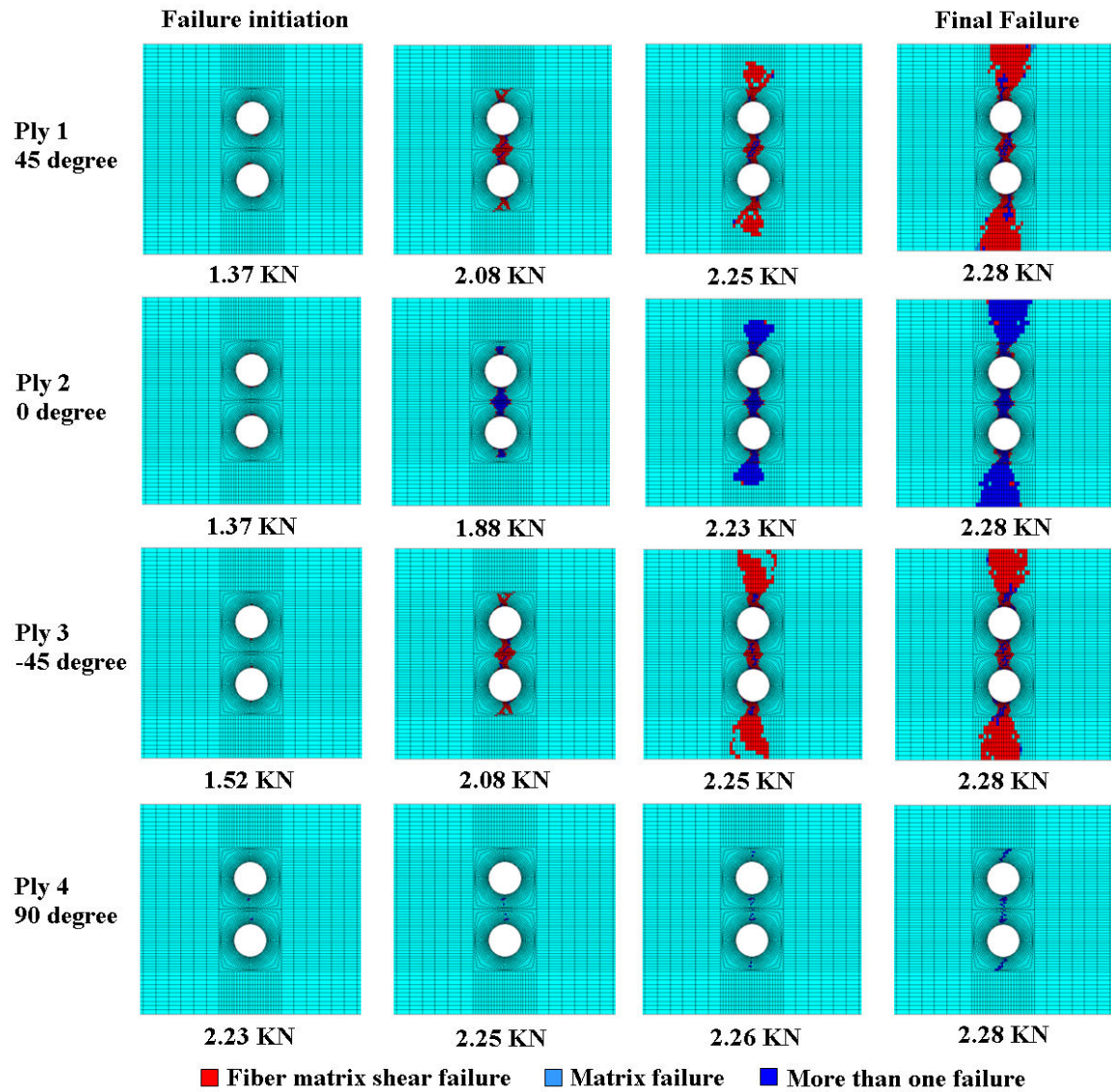
Figure 3.23: Illustration of damage propagation predicted by PDM with increasing load for Quasi-isotropic specimen having 2HT configuration on compressive side

**Failure initiation**                                                **Final Failure**

Ply 13
90 degree

1.37 KN            2.07 KN            2.26 KN            2.28 KN

Ply 14
-45 degree

1.45 KN            2.07 KN            2.26 KN            2.28 KN

Ply 15
0 degree

1.45 KN            2.07 KN            2.26 KN            2.28 KN

Ply 16
45 degree

1.33 KN            2.07 KN            2.26 KN            2.28 KN

🟥 **Fiber matrix shear failure**   🟦 **Matrix failure**   🟦 **More than one failure**
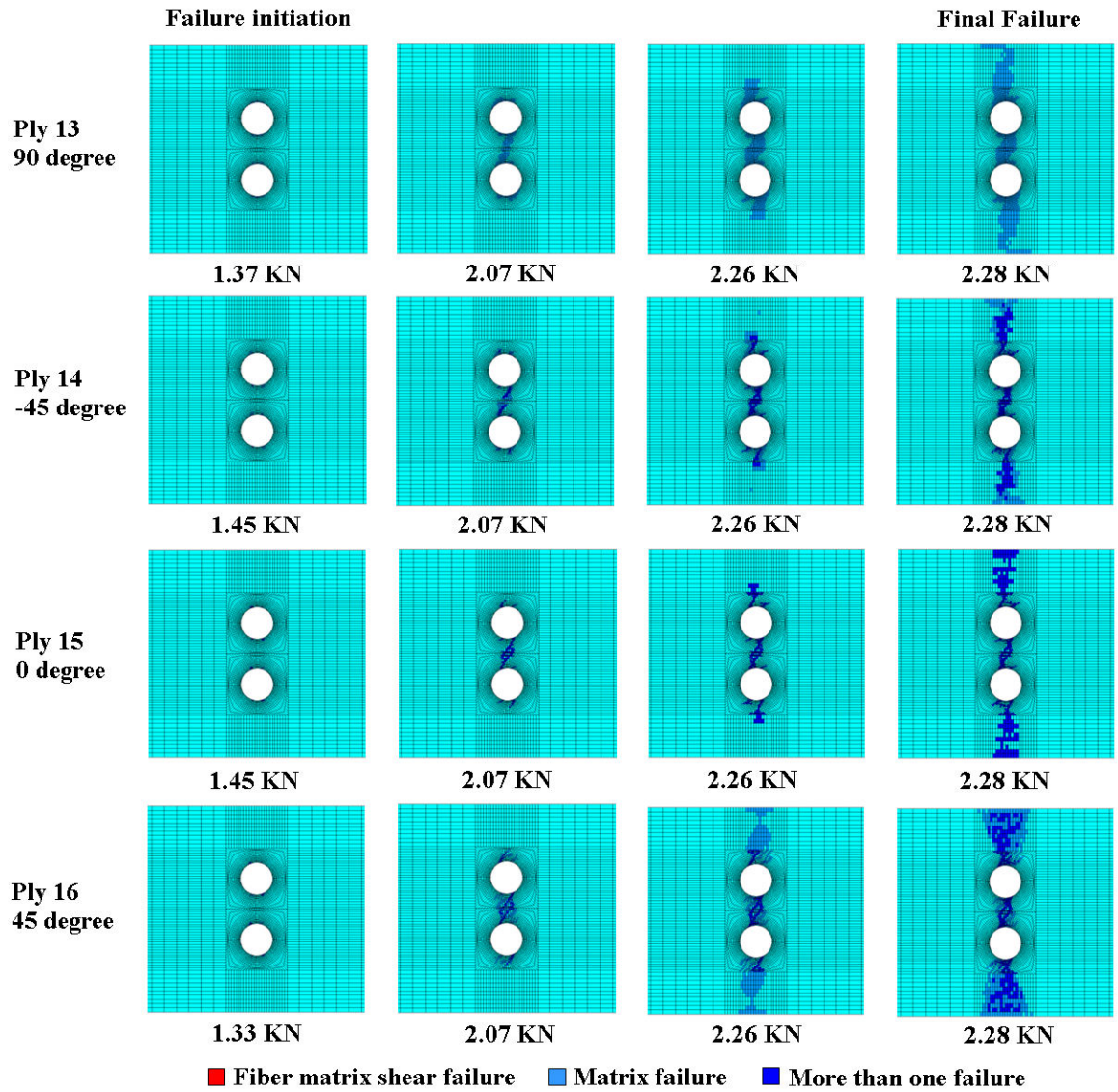
Figure 3.24: Illustration of damage propagation predicted by PDM with increasing load for Quasi-isotropic specimen having 2HT configuration on tensile side

**Failure initiation**                                                                            **Final Failure**

Ply 1
45 degree

1.52 KN            2.44 KN            2.64 KN            2.79 KN

Ply 2
0 degree

1.6 KN            2.44 KN            2.64 KN            2.79 KN

Ply 3
-45 degree

1.75 KN            2.44 KN            2.7 KN            2.79 KN

Ply 4
90 degree

2.72 KN            2.74 KN            2.77 KN            2.79 KN

■ **Fiber matrix shear failure**    ■ **Matrix failure**    ■ **More than one failure**
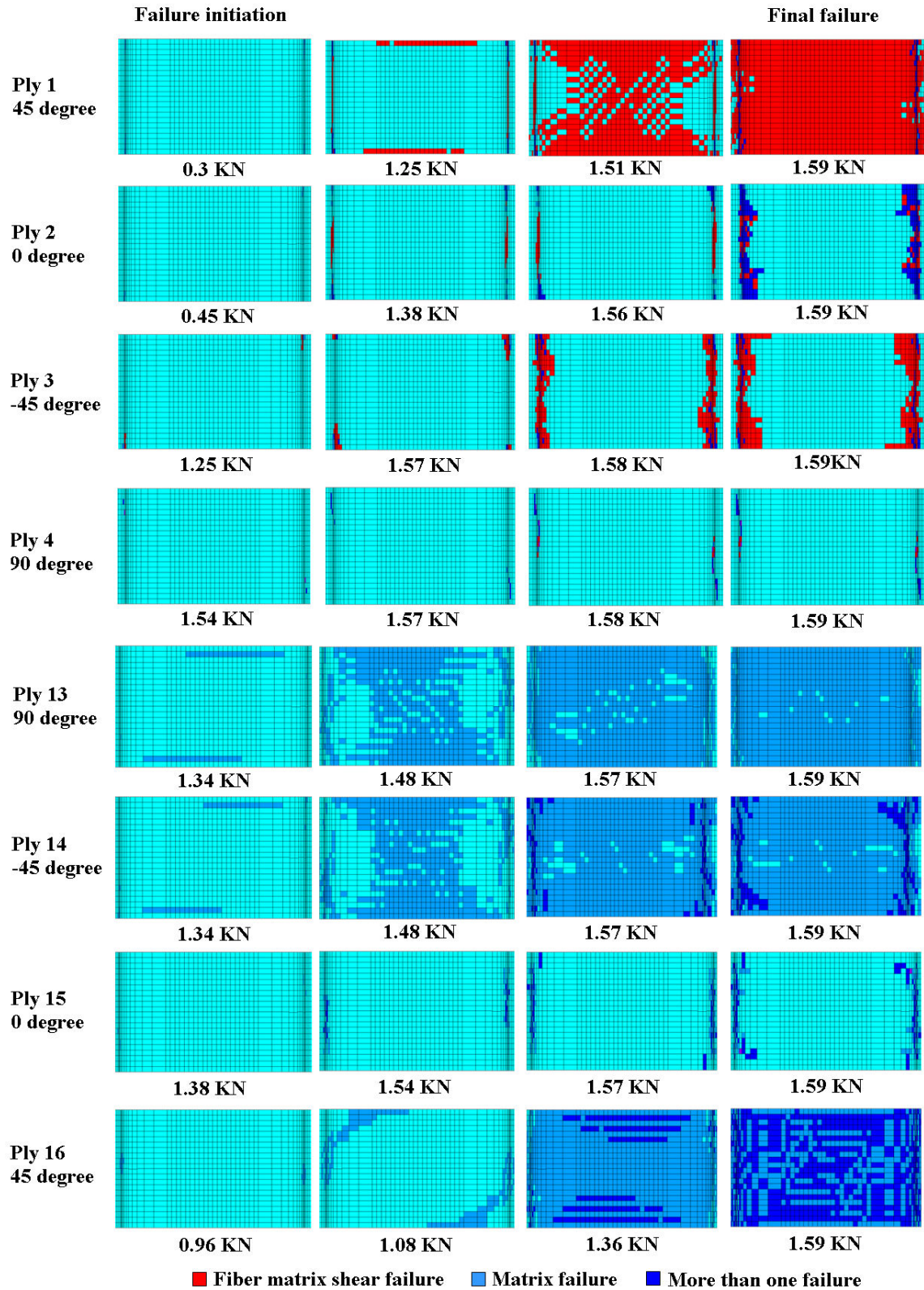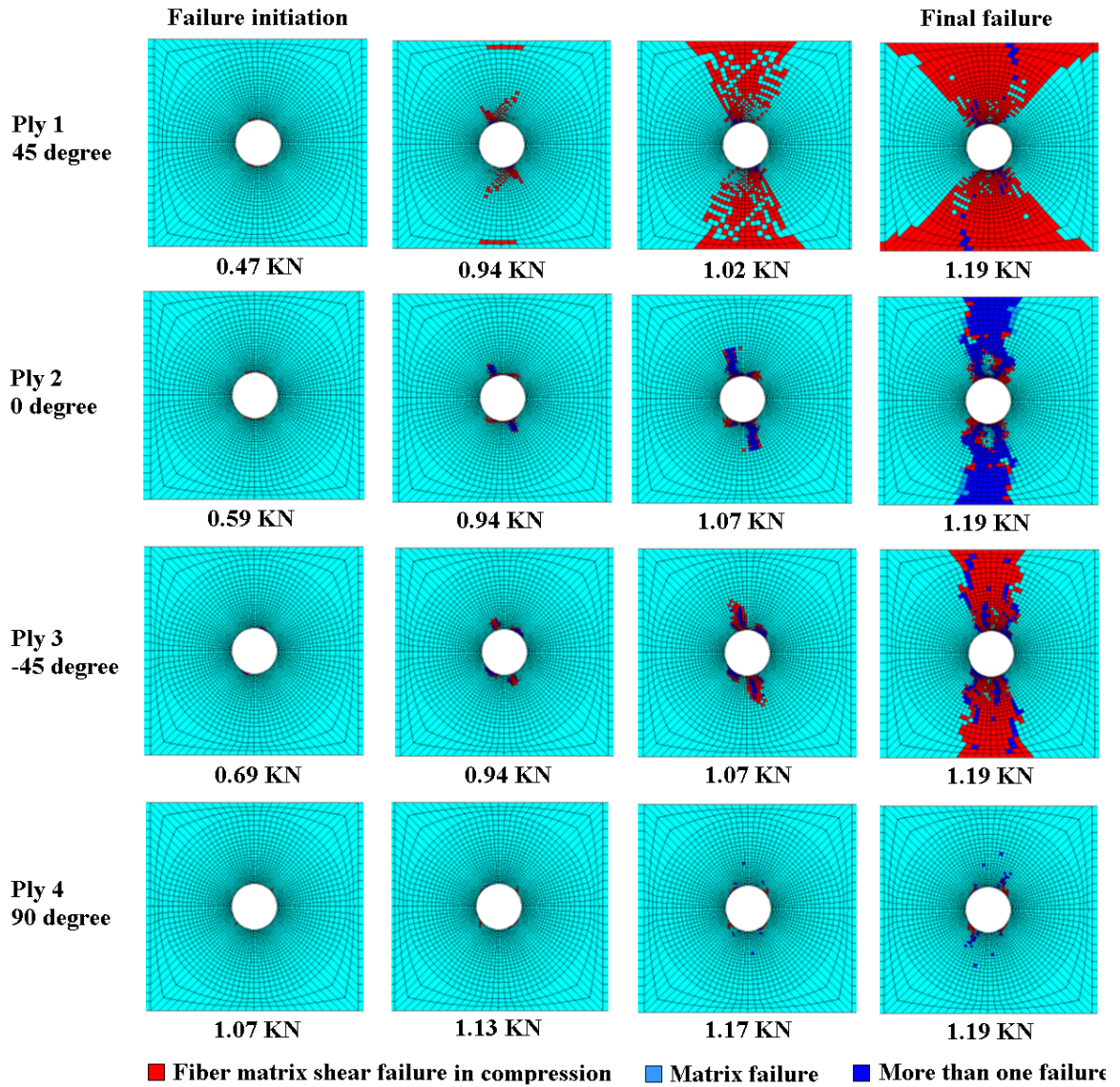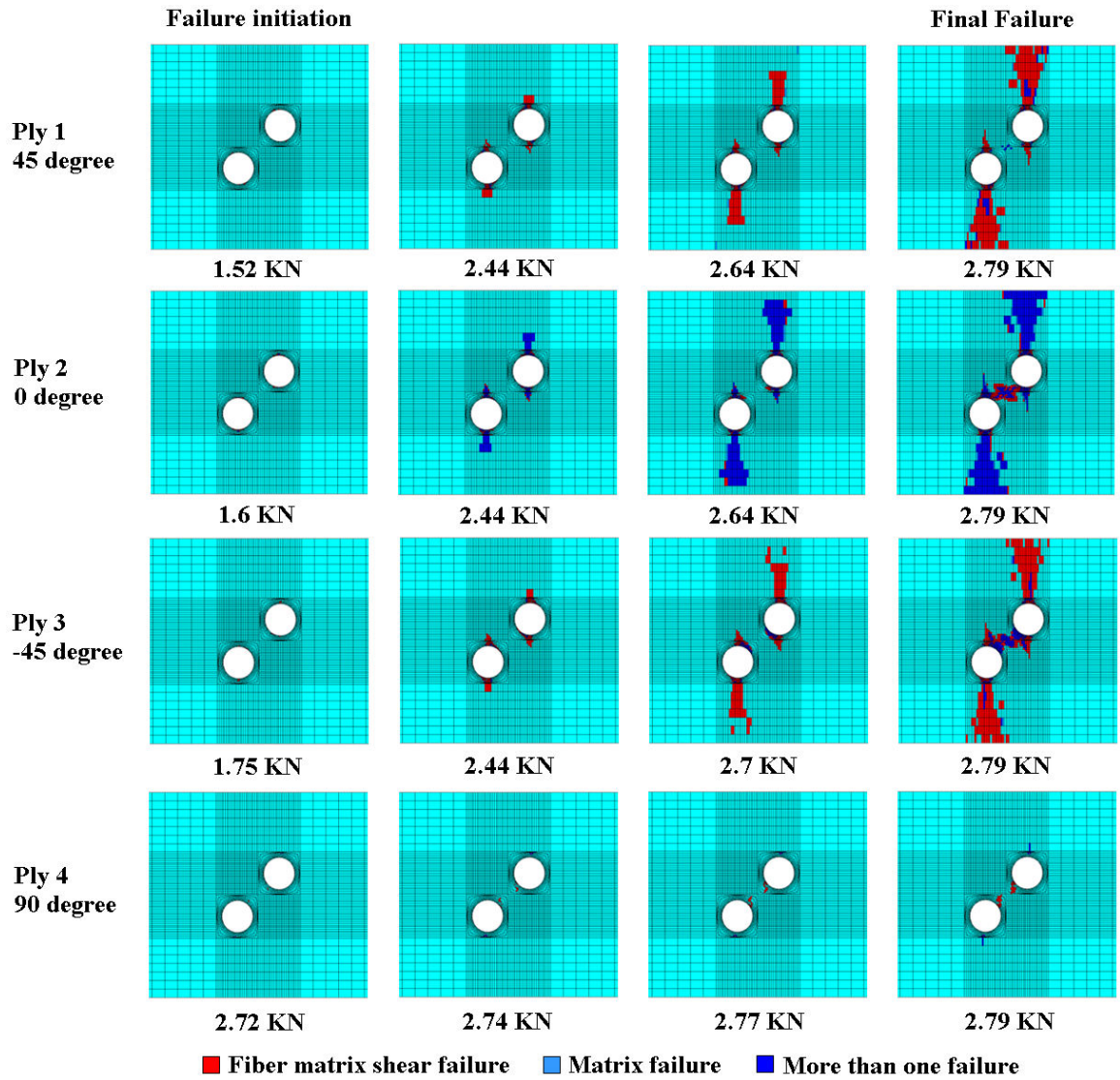
Figure 3.25: Illustration of damage propagation predicted by PDM with increasing load for Quasi-isotropic specimen having 2HD configuration on compressive side

59

**Failure initiation** ... **Final Failure**

Ply 13
90 degree

1.52 KN     2.44 KN     2.74 KN     2.79 KN

Ply 14
-45 degree

1.52 KN     2.64 KN     2.74 KN     2.79 KN

Ply 15
0 degree

1.52 KN     2.64 KN     2.74 KN     2.79 KN

Ply 16
45 degree

1.48 KN     2.44 KN     2.39 KN     2.79 KN

■ **Fiber matrix shear failure**     ■ **Matrix failure**     ■ **More than one failure**
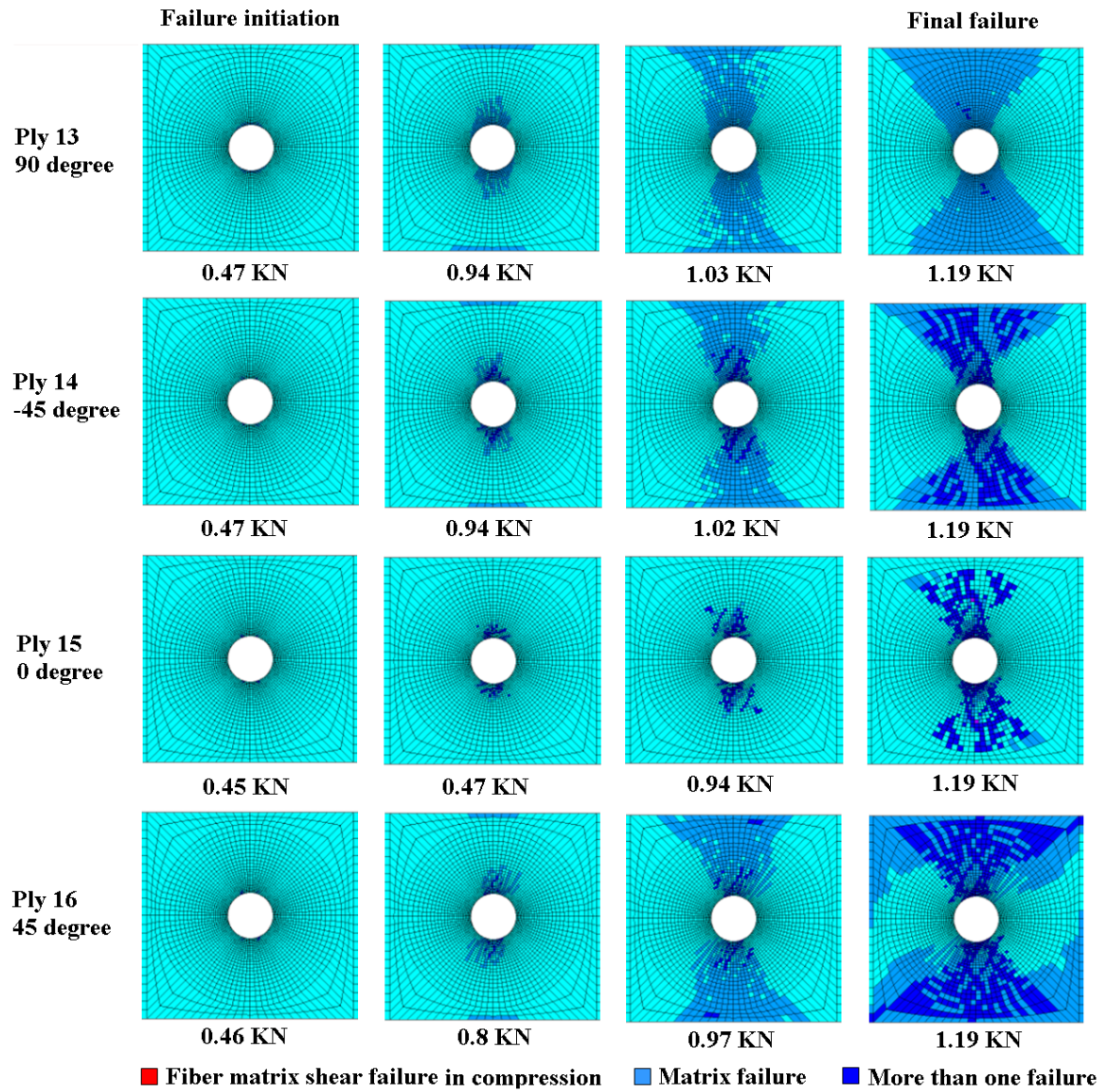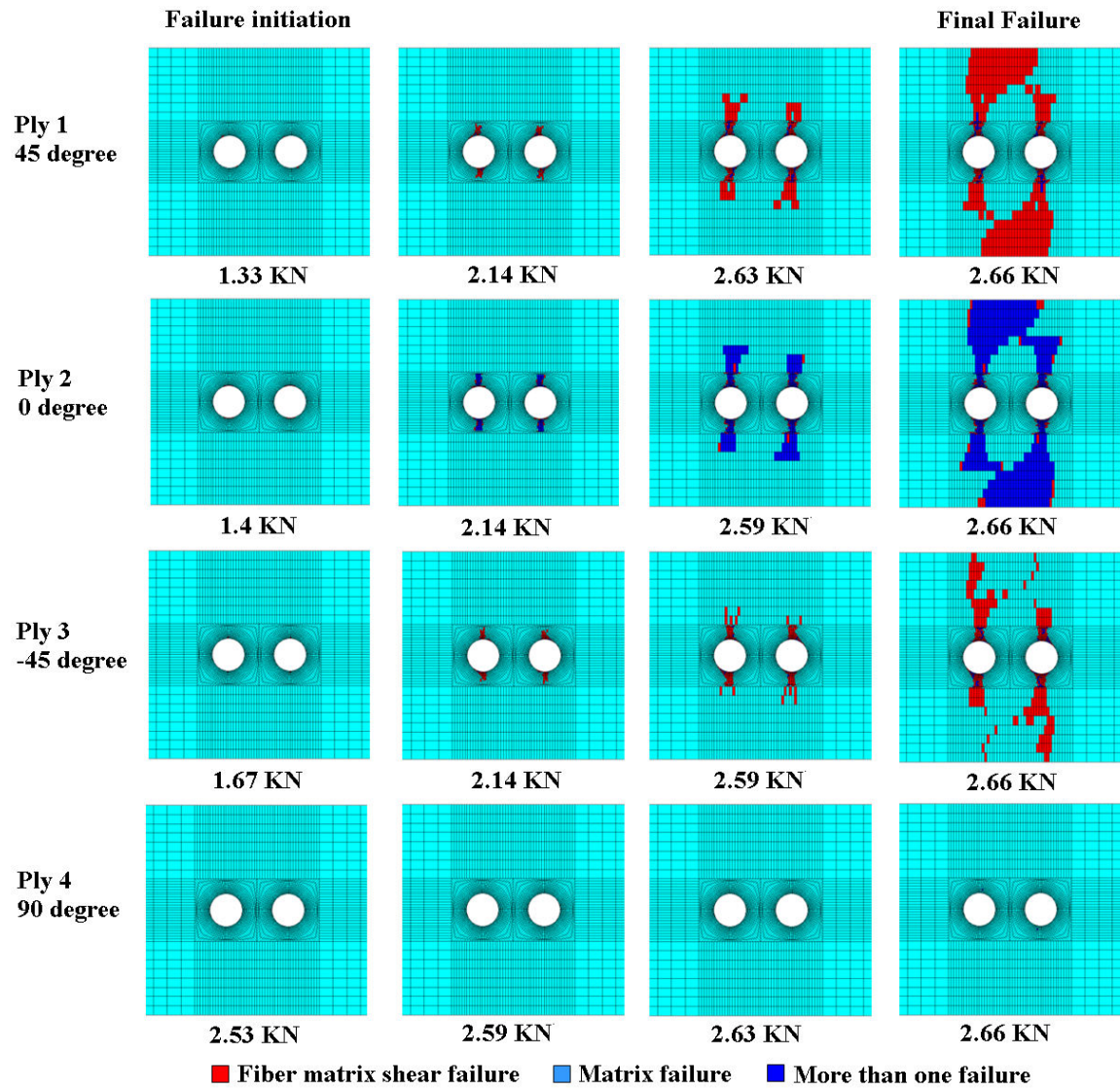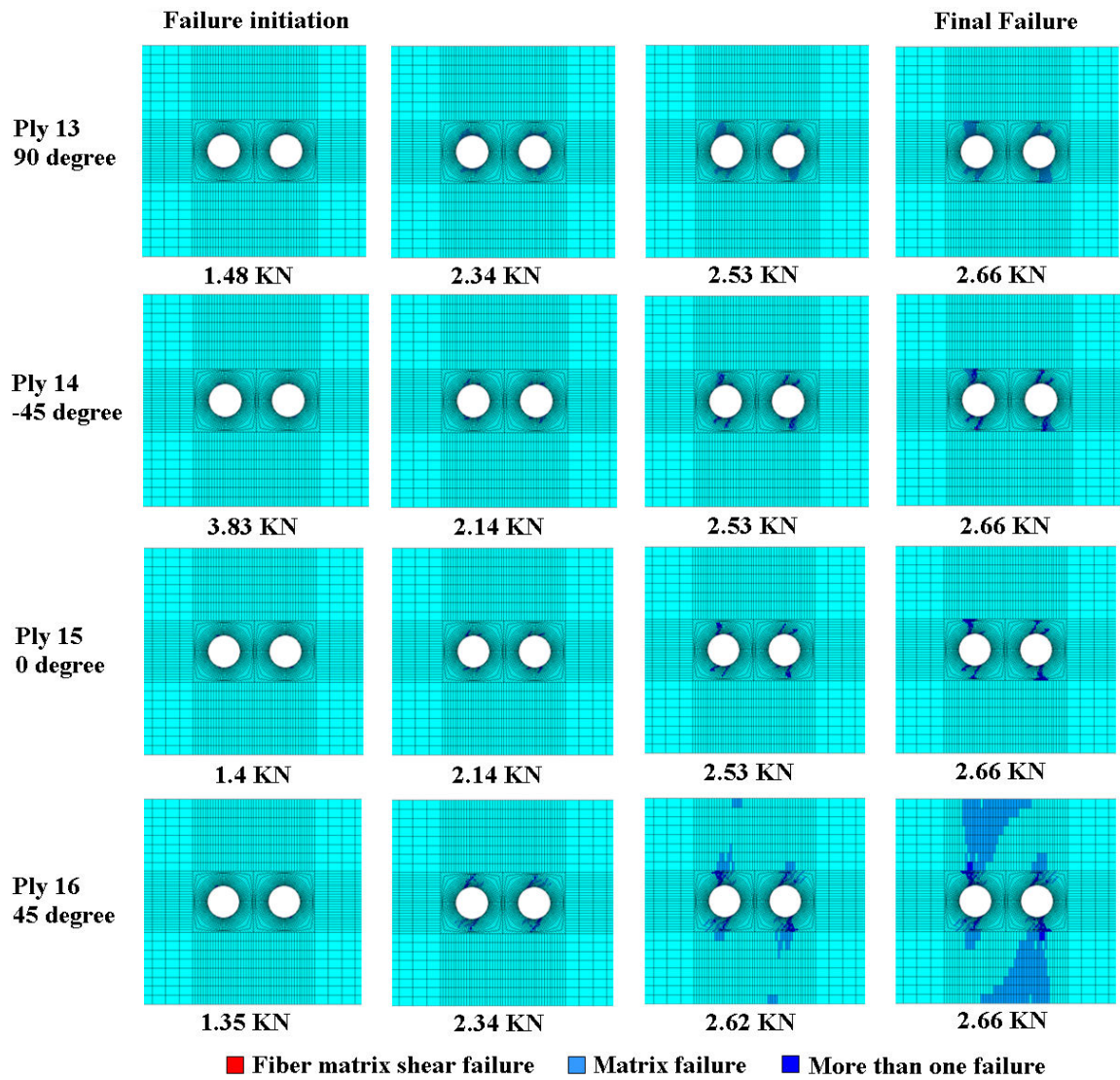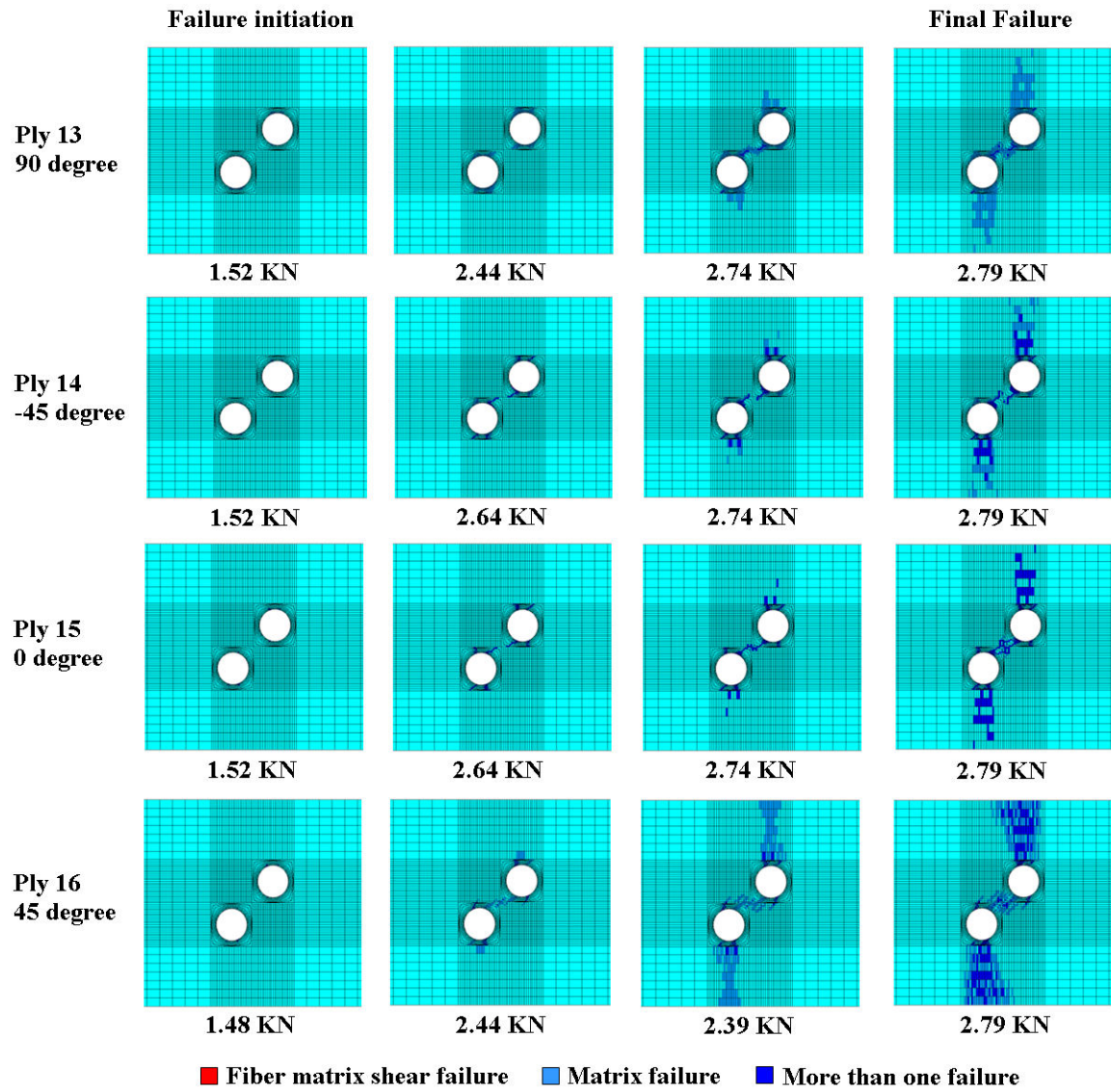
Figure 3.26: Illustration of damage propagation predicted by PDM with increasing load for Quasi-isotropic specimen having 2HD configuration on tensile side

**PDM**          **Experiment**

w/o hole

1H

2HL

2HT

2HD

■ **Fiber matrix shear failure**　■ **Matrix failure**　■ **More than one failure**
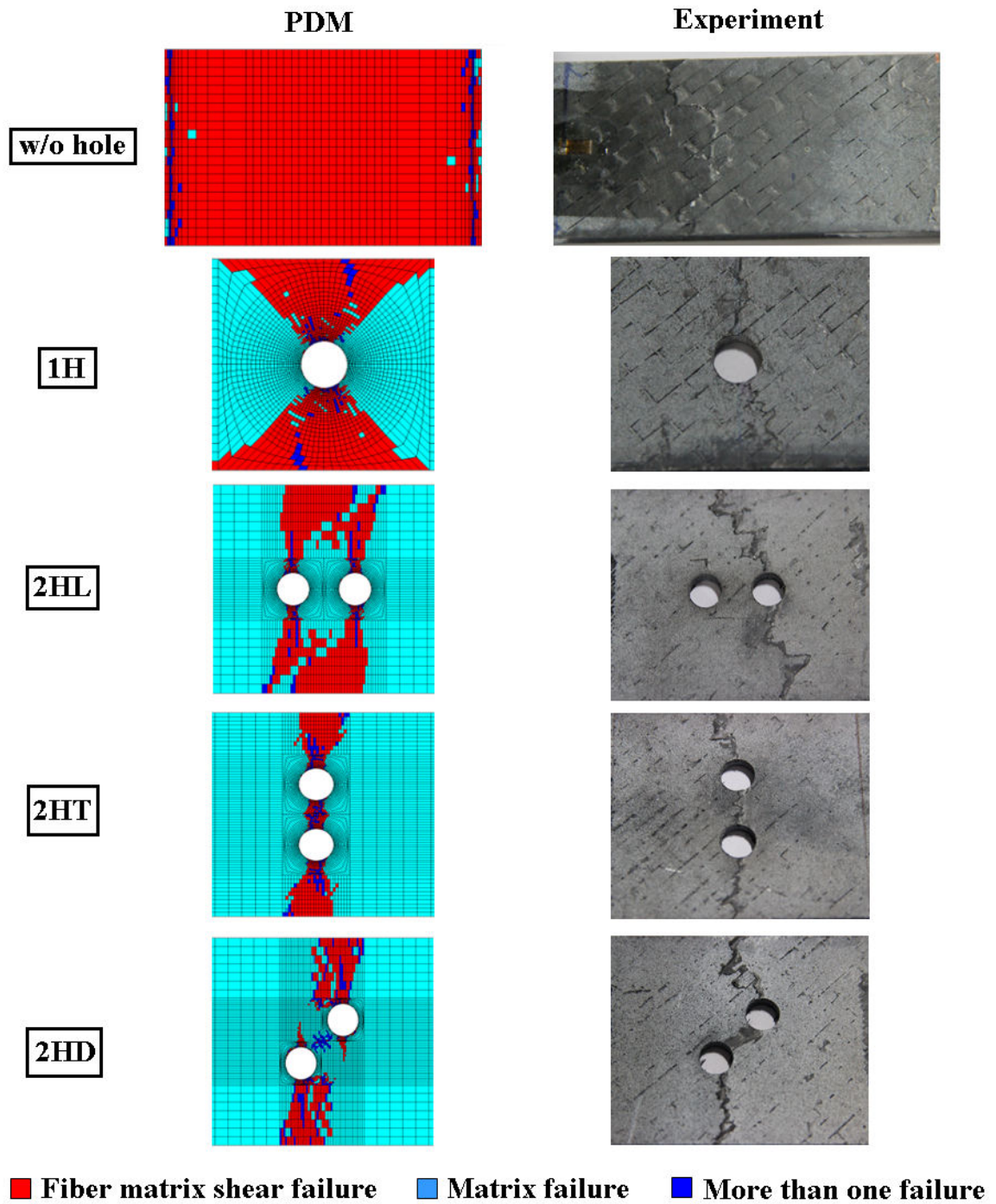
Figure 3.27: Final failure of Quasi-isotropic specimens on compressive side

|  | PDM | Experiment |
| --- | --- | --- |
| w/o hole | | |
| 1H | | |
| 2HL | | |
| 2HT | | |
| 2HD | | |

■ Fiber matrix shear failure     ■ Matrix failure     ■ More than one failure

Figure 3.28: Final failure of Quasi-isotropic specimens on tensile side

## 3.8    Closure

Progressive damage analysis was performed for CFRP specimens without hole, with single hole(1H) and with multiple holes of three different configurations which include 2HL, 2HT and 2HD by implementing a 3D Progressive damage model(PDM) in Finite element simulation.Firstly the 3D models were created in ANSYS 18 commercial FEA package and meshing was done and required boundary conditions were applied to the model. In PDM, Hashin's failure criteria was employed for predicting damage initiation in a lamina at fiber and matrix level, Material property degradation model(MPDM) was employed for predicting damage evolution and Cohesive zone model(CZM) was employed to predict delamination between layers of the specimen. For unidirectional CFRP specimen without hole, it was found that damage initiated at the top most layer on the compressive side at the position of support rollers in the form of fiber matrix shear failure. Then with increase in load this more of failure increased and more than one mode of failure occurred in the specimen near the support rollers.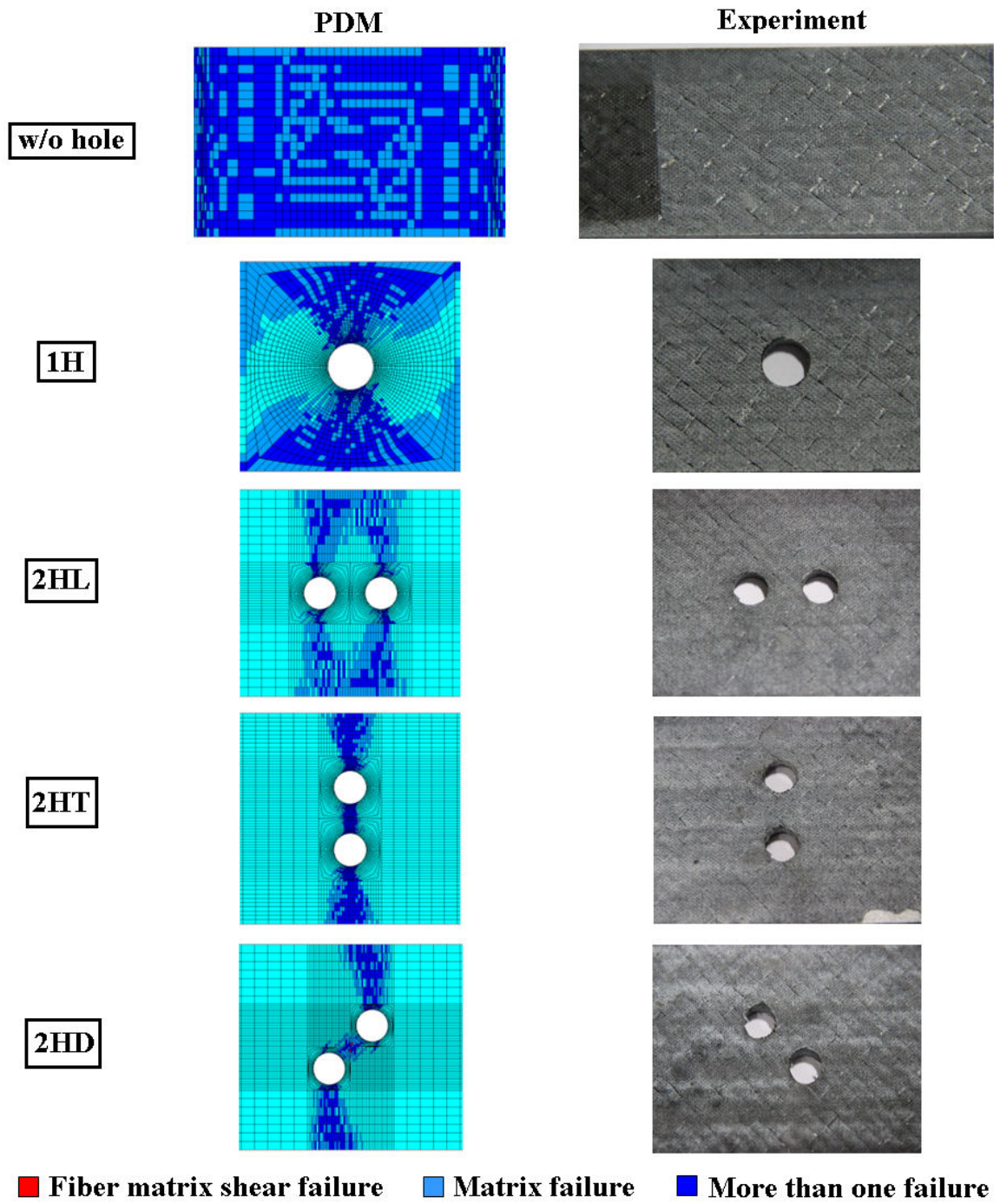 On the tensile side, damage initiated at the same location but in the form of matrix failure and with increase in load, more than one mode of failure occurred in the specimen.For quasi-isotropic specimen without hole, damage initiated on the compressive side at the top most layer in compression whose fiber orientation is 45 degrees in the form of fiber matrix shear failure and with increase in load, this mode of damage propagated throughout the specimen in the region between support rollers and remained the dominant mode of failure in this ply and -45 degree ply. In the 0 degree ply, more than one mode of failure occurred with increase in load near the support rollers and there was very less damage observed in 90 degree ply as it was closest to the neutral axis. On the tensile side, damage propagated throughout the specimen in region between support rollers for 90 degree, -45 degree and 45 degree plies except that matrix failure remained the dominant mode of failure in 90 degree ply and both matrix failure and more than one failure occurred in 45 and -45 degree ply. In 0 degree ply, more than one mode of failure occurred near the support rollers. For specimen having single and multiple cutouts, the damage mechanisms which occurred remained the same compared to specimen without hole but the damage initiated near hole and propagated in the transverse direction and slightly in longitudinal direction. Also there was interaction of holes observed in 2HT and 2HD specimens. The load-displacement plots from FEA showed a decent agreement with that obtained from experiment but Hashin's failure criteria predicted the final failure load and corresponding displacement in few cases, overpredicted them in some cases and unpredicted them in the remaining cases.The longitudinal strain contours and plots obtained from FEA showed good agreement with DIC and there was a linear variation of strain observed along the thickness of the specimen from one particular negative value to around positive of that value with strain at the neutral axis being close to zero.

# Chapter 4

# Conclusions and Recommendations for future work

## 4.1 Conclusion

The current thesis work is focused the on study of damage behavior of CFRP specimen with single hole and multiple holes of three different configurations (two hole longitudinal(2HL), two hole transverse (2HT) and two hole diagonal(2HD)) both experimentally and numerically. The damage behavior of pristine CFRP specimen was studied first and its failure strength was compared with CFRP specimen with single hole. The study was done for two different lay-up sequences for each of the previously mentioned specimen configurations which include Unidirectional whose lay-up sequence is $[0]_{16}$ and Quasi whose lay-up sequence is $[45/0/-45/90]_{2s}$. In the experimental study, the specimens were prepared through vacuum bagging process and tested with four-point bending test. 2D DIC was employed to capture the in-plane displacements and strains across the thickness of specimen. For CFRP specimen without hole, it was observed in both Unidirectional and Quasi-Isotropic specimen that damage initiated on the compressive side at the position of support rollers and propagated in the transverse direction. For CFRP specimen with single and multiple holes, damage initiated on the compressive side near hole and propagated in the transverse direction. There was no damage observed on the tensile side for all configurations of specimens. Delamination was found to occur on the compressive side in all the specimens and in single and multiple holes, it occurred close to the top most ply in compression. Delamination occured after the final failure of the specimen in Unidirectional specimens thereby having a post failure effect on the specimen and it occurred before the final failure of specimen in case of quasi-isotropic specimens thereby having a pre-failure effect on the specimen. For multiple hole specimens having 2HT and 2HD configuration, interaction between holes was also observed. Unidirectional specimen was found to have more stiffness and sustained higher failure load compared to Quasi-isotropic specimen.

Numerically, progressive damage analysis was done by implementing a 3D progressive damage model in a finite element simulation. In this PDM, Hashin's failure criteria was employed for damage initiation, Material property degradation model for damage evolution and cohesive zone model for delamination. In Unidirectional specimen, it was observed that damage initiates in the form of fiber matrix shear failure and with increase in load more than one mode failure occurred. In specimen

without hole, damage initiation occurred at the top most ply on the compressive side at the support rollers and propagated around this region whereas in specimen with hole, damage initiated near hole and propagated in the transverse direction.On the tensile side, damage initiated in the form of matrix failure and with increase in load, more than one mode of failure occurred. In specimen without hole, damage initiated at the support rollers propagated around this whereas in specimen with single and multiple holes, damage initiated near hole and propagated in transverse direction and slightly in longitudinal direction. In Quasi-isotropic specimen, damage initiated at the top most layer at 45 degree fiber orientation in the form of fiber matrix shear failure and it remained the dominant mode of failure in this ply and -45 degree ply. In 0 degree ply, more than one mode of failure occurred with increasing load and there was negligible failure observed in 90 degree ply. In the tensile side, matrix failure was the dominant mode of failure in 90 degree ply and both matrix failure and more than one mode of failure occurred in 45 and -45 degree ply. In 0 degree ply, one than one failure was the dominant mode of failure. In specimen without hole, damage initiated at the support rollers propagated throughout the specimen whereas in specimen with single and multiple hole, damage initiated near hole and propagated in transverse direction. The plot of load versus displacement obtained from PDM showed a decent validation with that obtained from experiment. Hashin's failure criteria predicted the final failure load and corresponding displacement in PDM close to the experiment in few cases, overpredicted them in some cases and underpredicted them in the remaining cases. The longitudinal strain contours and plots obtained from FEA showed a good agreement of that obtained from DIC.

## 4.2   Recommendations for future work

In the present study, Hashin's failure criteria was used to predict damage initiation and it overpredicted the final failure load and corresponding displacement in some cases and underpredicted them in the remaining cases thereby confirming the model is not very much accurate. Recently developed failure criteria like LaCrO3 and LaCrO4 criteria can be employed instead of Hashin's failure criteria to get more accurate predictions of initiations of damage. Also in this study, Material Property Degradation model was used for predicting damage evolution. But in this model, the selective elastic properties were reduced instantaneously to five percent of its original value after initiation of damage depending on the mode of damage. Since the stiffness was reduced instantaneously, damage evolution could not be studied properly. Therefore better models like Continuum Damage model(CDM) can be implemented where stiffness is reduced gradually and thereby the study of damage evolution can be done properly.

# References

[1] J. Chen, D. Tu, and H. Chin. Elastic-plastic analysis of interlaminar stresses in composite laminates due to bending and torsion. *Computers & structures* 33, (1989) 385–393.

[2] P. Copp, J. Dendis, and S. Mall. Failure analysis and damage initiation in carbon-carbon composite materials under three-point bending. *Journal of composite materials* 25, (1991) 593–608.

[3] Y. Reddy and J. Reddy. Linear and non-linear failure analysis of composite laminates with transverse shear. *Composites Science and Technology* 44, (1992) 227–255.

[4] S. Liu, Z. Kutlu, and F.-K. Chang. Matrix cracking and delamination in laminated composite beams subjected to a transverse concentrated line load. *Journal of Composite Materials* 27, (1993) 436–470.

[5] T. Kam and H. Sher. Nonlinear and first-ply failure analyses of laminated composite cross-ply plates. *Journal of Composite Materials* 29, (1995) 463–482.

[6] G. Padhi, R. Shenoi, S. Moy, and G. Hawkins. Progressive failure and ultimate collapse of laminated composite plates in bending. *Composite structures* 40, (1997) 277–291.

[7] L. Dufort, M. Grédiac, and Y. Surrel. Experimental evidence of the cross-section warping in short composite beams under three point bending. *Composite Structures* 51, (2001) 37–47.

[8] P. Feraboli and K. Kedward. Four-point bend interlaminar shear testing of uni-and multi-directional carbon/epoxy composite systems. *Composites Part A: Applied Science and Manufacturing* 34, (2003) 1265–1271.

[9] F. Bosia, M. Facchini, J. Botsis, T. Gmür, and D. de'Sena. Through-the-thickness distribution of strains in laminated composite plates subjected to bending. *Composites science and technology* 64, (2004) 71–82.

[10] A. Turon, P. P. Camanho, J. Costa, and C. Dávila. A damage model for the simulation of delamination in advanced composites under variable-mode loading. *Mechanics of Materials* 38, (2006) 1072–1089.

[11] M. Mulle, R. Zitoune, F. Collombet, L. Robert, and Y.-H. Grunevald. Embedded FBGs and 3-D DIC for the stress analysis of a structural specimen subjected to bending. *Composite Structures* 91, (2009) 48–55.

[12] H. Zhou, L. Mishnaevsky, P. Brøndsted, J. Tan, and L. Gui. SEM in situ laboratory investigations on damage growth in GFRP composite under three-point bending tests. *Chinese Science Bulletin* 55, (2010) 1199–1208.

[13] D. LUCA MOTOC, N. DADIRLAT, and H. TEODORESCU DRAGHICESCU. A COMPARATIVE STUDY ON THE POLYMERIC MULTIPHASE COMPOSITE FAILURE IN 3-POINTS BENDING TESTS .

[14] E. Nelson, A. Hansen, T.-E. Tay, and D. Kenik. Delamination and damage progression in a composite laminate subjected to bending using multicontinuum theory. In 52nd AIAA/ASME/ASCE/AHS/ASC Structures, Structural Dynamics and Materials Conference 19th AIAA/ASME/AHS Adaptive Structures Conference 13t. 2011 1860.

[15] H. Ullah, A. R. Harland, T. Lucas, D. Price, and V. V. Silberschmidt. Finite-element modelling of bending of CFRP laminates: Multiple delaminations. *Computational Materials Science* 52, (2012) 147–156.

[16] M. Allel, A. Mohamed, and B. Ahmed. Stability condition for the evaluation of damage in three-point bending of a laminated composite. *Steel and Composite Structures* 15, (2013) 203–220.

[17] P. Liu, J. Yang, B. Wang, Z. Zhou, and J. Zheng. A study on the intralaminar damage and interlaminar delamination of carbon fiber composite laminates under three-point bending using acoustic emission. *Journal of Failure Analysis and Prevention* 15, (2015) 101–121.

[18] M. Meng, H. Le, M. Rizvi, and S. Grove. 3D FEA modelling of laminated composites in bending and their failure mechanisms. *Composite Structures* 119, (2015) 693–708.

[19] W. Gong, J. Chen, and E. A. Patterson. An experimental study of the behaviour of delaminations in composite panels subjected to bending. *Composite Structures* 123, (2015) 9–18.

[20] C. Marsden, M. Biernacki, C. Li, and S. Carnegie. 4-POINT BENDING FATIGUE TESTING OF THIN CARBONEPOXY LAMINATES. *Composite materials* .

[21] M. Koc, F. O. Sonmez, N. Ersoy, and K. Cinar. Failure behavior of composite laminates under four-point bending. *Journal of Composite Materials* 50, (2016) 3679–3697.

[22] J. Kim, S. Lee, J. Bae, and J. Roh. A study on the failure prediction of composite laminates in bending .

[23] C. Prasad and M. Shuart. Moment distributions around holes in symmetric composite laminates subjected to bending moments. *AIAA journal* 28, (1990) 877–882.

[24] R. D. Bradshaw and S. Pang. Failure analysis of composite laminated plates with circular holes under bending. In Composite Material Technology-1991. 1991 125–135.

[25] Y. Kwon and S. Yang. Bending failure of laminated fibrous composite plates with a hole. Technical Report, American Society of Mechanical Engineers, New York, NY (United States) 1995.

[26] T. Paul and K. Rao. Flexural analysis of laminated composite plates containing two elliptical holes using higher-order shear deformation theory. *Computers & structures* 55, (1995) 279–285.

[27] Y. Zhao, A. K. Tripathy, and S.-S. Pang. Bending strength of composite laminates with an elliptical hole. *Polymer composites* 16, (1995) 60–69.

[28] H. Chen and H. Chen. Bending of laminated composite plates with cutouts. In 38th Structures, Structural Dynamics, and Materials Conference. 1997 1388.

[29] K. S. Ram and T. S. Babu. Study of bending of laminated composite shells. Part II: shells with a cutout. *Composite structures* 51, (2001) 117–126.

[30] Ş. Temiz, A. Özel, and M. D. Aydin. FE stress analysis of thick composite laminates with a hole in bending. *Applied Composite Materials* 10, (2003) 103–117.

[31] N. YAHNİOĞLU and A. Hakan. AN EFFECT OF GEOMETRIC NONLINEARITY ON THE STRESS CONCENTRATION IN A BENDING COMPOSITE STRIP WITH A RECTANGU-LAR HOLE. *Sigma* 2.

[32] S. Akbarov, N. Yahnioglu, and U. B. Yesil. A 3D FEM analysis of stress concentrations around two neighboring cylindrical holes in a prestressed rectangular composite plate under bending. *Mechanics of Composite Materials* 48, (2012) 499–510.

[33] C. Mao and X. Xu. Bending problem of a finite composite laminated plate weakened by multiple elliptical holes. *Acta Mechanica Solida Sinica* 26, (2013) 419–426.

[34] N. P. Patel and D. S. Sharma. Bending of composite plate weakened by square hole. *International Journal of Mechanical Sciences* 94, (2015) 131–139.

[35] J. Ubaid, M. Kashfuddoja, and M. Ramji. Strength prediction and progressive failure analysis of carbon fiber reinforced polymer laminate with multiple interacting holes involving three dimensional finite element analysis and digital image correlation. *International Journal of Damage Mechanics* 23, (2014) 609–635.

[36] M. Kashfuddoja, R. Prasath, and M. Ramji. Study on experimental characterization of carbon fiber reinforced polymer panel using digital image correlation: A sensitivity analysis. *Optics and Lasers in Engineering* 62, (2014) 17–30.

[37] Z. Hashin. Failure criteria for unidirectional fiber composites. *Journal of applied mechanics* 47, (1980) 329–334.

[38] M. Kashfuddoja and M. Ramji. An experimental and numerical investigation of progressive damage analysis in bonded patch repaired CFRP laminates. *Journal of Composite materials* 49, (2015) 439–456.

[39] D. S. Dugdale. Yielding of steel sheets containing slits. *Journal of the Mechanics and Physics of Solids* 8, (1960) 100–104.

[40] G. I. Barenblatt. The mathematical theory of equilibrium cracks in brittle fracture. In Advances in applied mechanics, volume 7, 55–129. Elsevier, 1962.

[41] A. Hillerborg, M. Modéer, and P.-E. Petersson. Analysis of crack formation and crack growth in concrete by means of fracture mechanics and finite elements. *Cement and concrete research* 6, (1976) 773–781.

[42] V. Tvergaard and J. W. Hutchinson. The relation between crack growth resistance and fracture process parameters in elastic-plastic solids. *Journal of the Mechanics and Physics of Solids* 40, (1992) 1377–1397.

[43] X.-P. Xu and A. Needleman. Numerical simulations of fast crack growth in brittle solids. *Journal of the Mechanics and Physics of Solids* 42, (1994) 1397–1434.

[44] S. Matta, V. Chinthapenta, and M. Ramji. A novel approach to analyse adhesive layer strain field in a stepped lap repaired carbon fiber reinforced polymer panel using digital image correlation. *Journal of Adhesion Science and Technology* 31, (2017) 2180–2201.